microwave JOURNAL

contents

VOLUME 25, NUMBER 9
USPS 396-250
SEPTEMBER 1982

BUSINESS/SPECIAL REPORTS

TECHNICAL/APPLICATIONS SECTION

MILITARY MICROWAVES 1982 CONFERENCE

DEPARTMENTS

*Euro-Global Edition Only.

Press run for this issue is 46,003 copies.

ON THE COVER: M/A-COM MPD's fully solid state 1 kw 1750-1850 MHz uplink transmitter subsystem communicates with an orbiting satellite in the Space Ground Link Systems (SGLS) program. Cover art courtesy of M/A-COM MPD Inc. The cover story is on p. 158.

EXECUTIVE EDITORIAL OFFICE
610 Washington Street, Dedham, MA 02026
Tel: 617 326-8220 710 348-0481
TELEX: 951-659
MICROSOL DEDM

EUROPEAN EDITORIAL OFFICE
25 Victoria Street London SW1H OEH England
Tel: 01-222-0466 **TELEX:** 885744

Microwave Journal is issued without charge upon written request to qualified persons working in that portion of the electronics industry including governmental and university installation that deal with VHF through light frequencies. Other subscriptions; domestic, $36 per year, two year subscriptions $65; foreign, $48 per year, two year subscriptions $85: back issues (if available) and single copies $5.00.

POSTMASTER: send address corrections to Microwave Journal, 610 Washington Street, Dedham MA 02026.

BPA

Horizon House also publishes Telecommunications and Journal of Electronic Defense

Passive Direction Finding and Signal Location

A.R. Baron, K.P. Davis, C.P. Hofmann
Amecom Division – Litton Systems, Inc.

Introduction

This paper addresses 3 types of passive location of stationary, ground based emitters from airborne platforms (Figure 1):

- the azimuth/elevation (AZ/EL) location technique which yields single pulse instantaneous emitter location,
- conventional triangulation,
- multiple aircraft time difference of arrival (TDOA), an extension of phase interferometry with spacing between antenna elements of miles, not inches.

Not considered in this paper are comparisons of received signal power with estimates of effective radiated power (ERP) and measurement of TDOA between direct and reflected waves because of their sensitivities to propagation anomalies.

Value of Passive Intercept

Passive intercept systems provide the military with critically important data which can influence the outcome of a military engagement as highlighted by recent events in Lebanon and the Falkland Islands. Israeli success in eliminating the Syrian surface-to-air missile sites was due in part to information derived from passive Electronic Warfare (EW) systems. Similarly the success of the Exocet missile in destroying the British ship HMS Sheffield underscores the need for early detection, identification, and location of radiating hostile missile threats.

—Emitter Identification

Emitter ID requires identifying and associating consecutive pulses produced by the same emitter from a contemporaneous population of pulses in the IF receiver passband. Once a signal is isolated the single pulse parameters are combined with the derived pulse repetition interval (PRI) and the emitter's scan rate (derived by processing the pulse amplitude measurements) to identify the emitter by matching measured parameters with a previously stored listing.

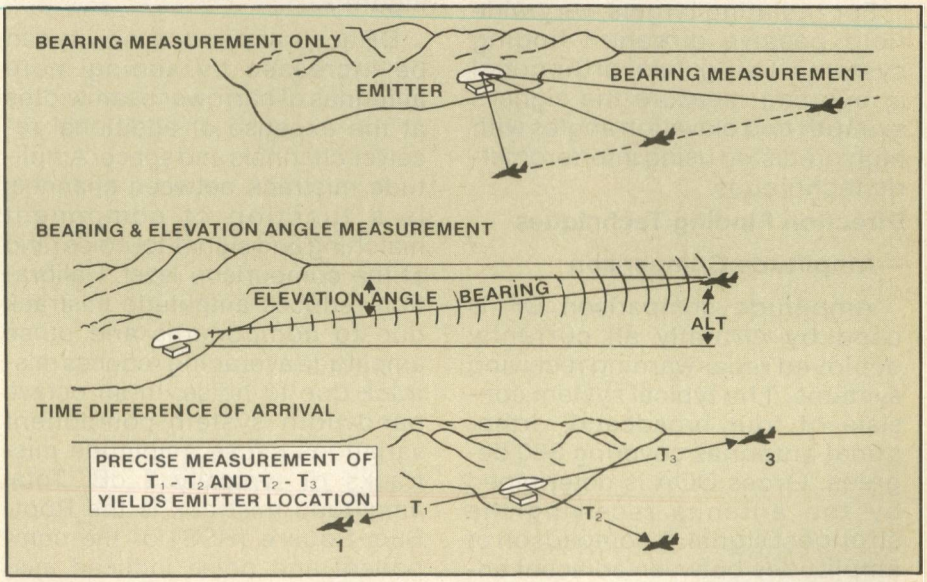

Fig. 1 Passive location.

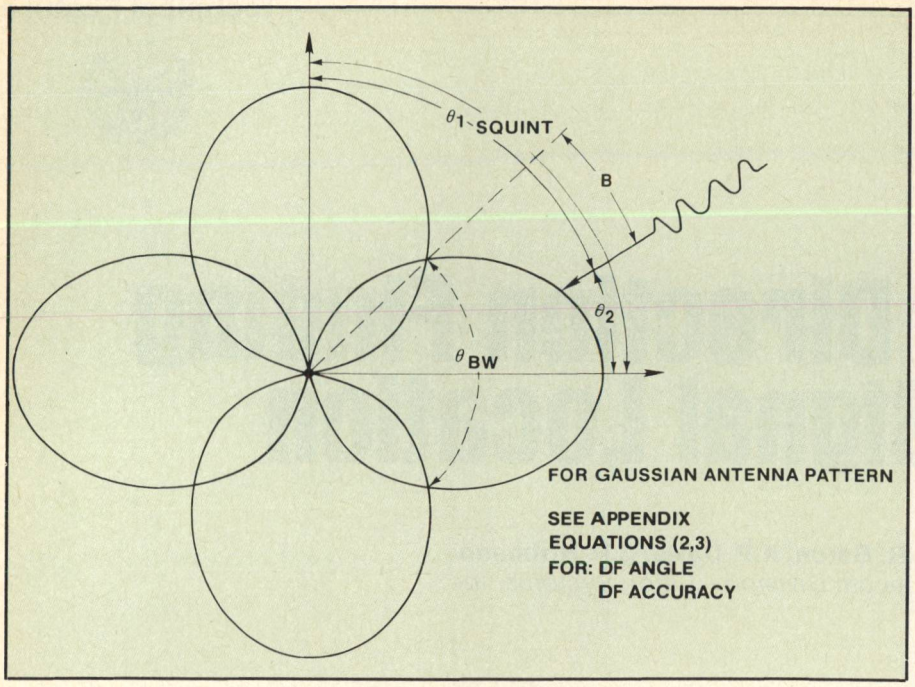

Fig. 2 Amplitude DF concept.

— Precision Direction of Arrival (DOA)

The emitter's DOA is not easily varied so it is a very reliable monopulse sorting parameter for both emitter identification and location. In addition precise DOA information can be used to point highly directional jamming antennas to increase effective jamming power and better screen penetrating aircraft. This data can also be used to steer narrow field of view systems such as infrared missile seekers, laser range finders and TV.

For radiating targets, very wide field passive direction finding systems using two orthogonal arrays can measure the signal's azimuth and elevation angles with high precision using interferometric techniques.

Direction Finding Techniques

—Amplitude Comparison

Amplitude comparison DF is used by virtually all currently deployed radar warning receiving systems. The typical system consists of four broadband, orthogonal antennas covering 360 degrees. Gross DOA is determined by the antenna receiving the strongest signal. A comparison of amplitudes between adjacent antennas provides fine DF. If each antenna has its own dedicated receiver, these amplitudes can be measured simultaneously, providing monopulse DF to accuracies of 3 to 10 degrees.

Fine amplitude comparison is based on the ratio of amplitudes of antenna patterns of known shapes. An example in Figure 2 uses four antennas squinted at 90 degrees to cover 360 degrees. Gain patterns of broad bandwidth spiral antennas, commonly used in such systems closely approximate Gaussian and the DF angle can be expressed as shown in Figure 2.

DF accuracy and sensitivity can be increased by adding more antennas of narrower beamwidths at the expense of additional receiver channels and space. Amplitude mistrack between channels is a function of component matching and signal-to-noise ratio at the comparison level. Calibration reduces amplitude mistrack due to components and pulse amplitude averaging reduces mistrack due to noise. In an octave bandwidth system component variations cause amplitude mistracks of typically 3 dB. Total amplitude mistrack is the Root-Sum-Square (RSS) of the component and noise induced mistrack.

Figure 3 shows requirements for different DF accuracies.

— Phase Interferometry - Single Baseline Theory

In the phase interferometer of Figure 4 a plane wave arriving at an angle is received by one antenna earlier than the other, due to the difference in path length. This time difference can be expressed as a phase difference between the RF signals at each antenna as shown in the figure.

On small fighter aircraft d=1 to 2 feet so the time difference is usually less than one nanosecond. Direct measurement of time requires a very wide band receiver, highly precise clock, and very high speed logic. Consequently the time difference of arrival technique is used only when the antennas are on separate platforms separated by several miles. The phase difference between the signals at each antenna is preserved for the duration of the pulse and can be readily measured. The video bandwidth need be wide enough only for the minimum pulsewidth to be processed (5 MHz) for a 100 ns pulse appropriate to modern ESM systems.

The interferometer antennas typically have 90 degree beams. DF accuracy and resolution are achieved by IF or RF processing.

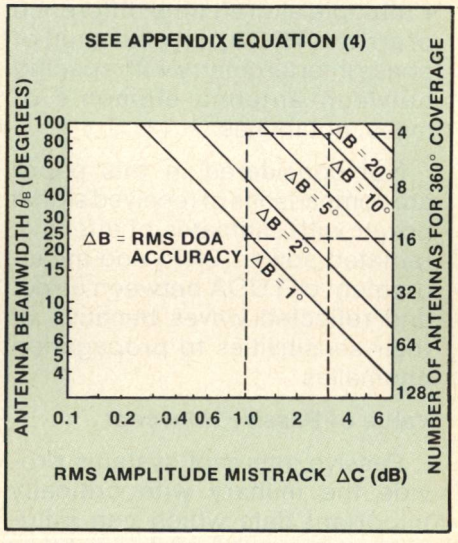

Fig. 3 Amplitude mistrack and beamwidth requirements for various DOA accuracies.

[Continued on page 62]

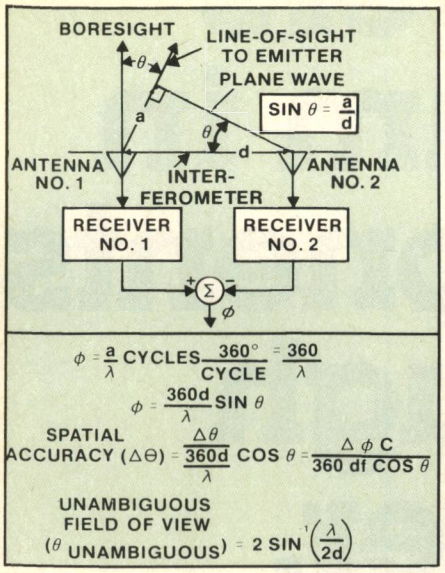

Fig. 4 Basic phase interferometer.

This is an advantage in high probability of signal intercept, but it is a disadvantage in that approximately equal amplitude time coincident pulsed signals within the IF passband from different DOAs will cause large errors in indicated DOA. In most cases, the simultaneous signals eventually separate in time, permitting precise DF on both signals.

In an interferometer the locus of points that produces the same time or phase delay forms a cone. The indicated angle is the true azimuth angle multiplied by the cosine of the elevation angle - the error in assuming the incident angle to be the azimuth angle is negligible for signals from near azimuth and elevation angle boresight. At 45 degrees azimuth and 10 degrees elevation angle the error is less than 1 degree, increasing to 15 degrees for both at 45 degrees, independent of instrumentation errors.

Two orthogonal arrays, one measuring the azimuth angle and the other the elevation angle can eliminate this error. Any two linearly independent measurements are sufficient since there are only two unknowns. For applications to targets near the horizon, the depression angle is small, needing only horizontal arrays.

For the unambiguous field of view of a two element interferometer to be ±90 degrees the spacing between antennas must be half wavelength or less, but the ratio of angular error to phase error decreases with increasing spacing (see appendix).

—Multiple Baseline Theory

The multiple baseline interferometer combines high accuracy with a wide unambiguous field of view (Figure 5). As the baseline increases the phase difference of a plane wave with respect to the reference antenna increases. The phase difference is measured by a phase discriminator in the receiver. Phase quantization up to eight bits has been achieved.

Figure 5 illustrates four-bit phase quantization for both harmonic and nonharmonic multiple baseline interferometers.

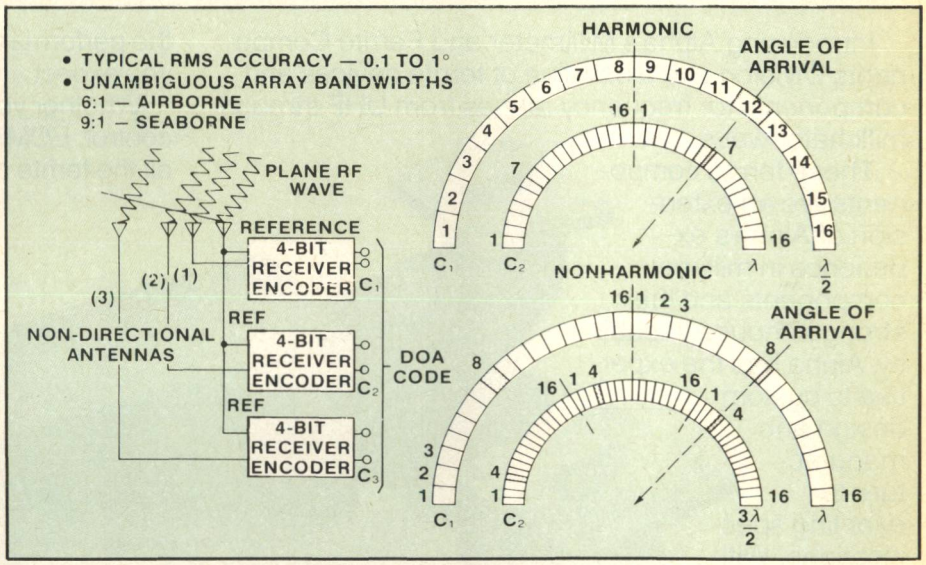

Fig. 5 Multiple-baseline interferometer.

An error made in resolving interferometer ambiguities is called a gross error. Immunity to gross errors (phase tolerance) is a function of the antenna spacing ratio and the degree of phase quantization. The gross error rate, however, is a statistical quantity which depends on the relative proportions of bias and noise in the phase errors, as well as on the overall error value. Gross error rates of less than 1% are readily achieved. Pulse to pulse correlation can digitally filter out ambiguities and accomodate even higher gross error rates in a way that is essentially invisible to the ESM processing system.

In the nonharmonic interferometer no pair of antennas provides a completely unambiguous readout over the field of view, rather, the spacing ratios separate ambiguities of each array through a simple truth table. If RF and IF phase mistrack is within the specified tolerance, simple logic can compensate for it by simply manipulating a digital code to select the appropriate wide base line cell. The accuracy of the interferometer is thus determined by the phase error of the widest baseline antenna pair. Nonharmonic interferometers have been implemented over nine to one bandwidths with operational accuracies from 0.1 to 1 degree rms.

The principal advantage of the nonharmonic interferometer over the harmonic is its greatly in-

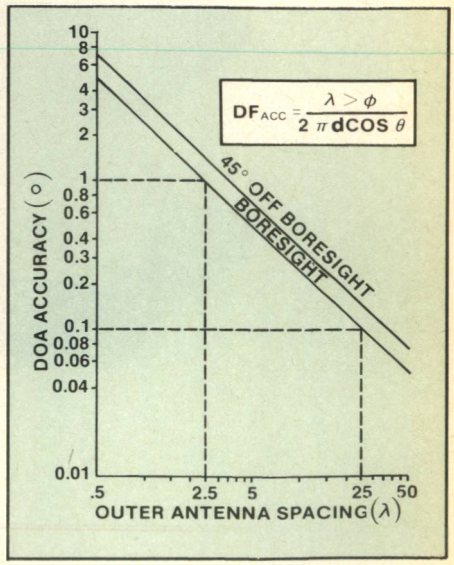

Fig. 6 DOA accuracy at boresight and 45 degrees off boresight as a function of outer antenna spacing ($\Delta\phi$ = 15.7°).

[Continued on page 64]

[From page 62] **PASSIVE DIRECTION**

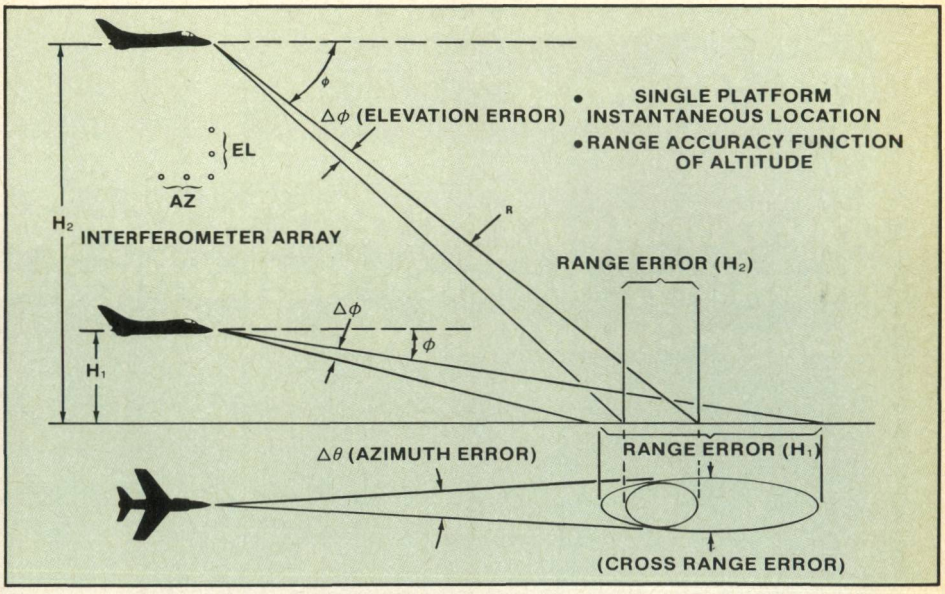

Fig. 7 AZ/EL location technique.

creased bandwidth for nonambiguous coverage. The requirement for no more than half wave spacing at the maximum frequency and one wavelength perimeter at the minimum frequency (to not degrade gain) set the operating bandwidth of the harmonic system at $\pi/2$. Wider band systems can be built to cover narrower angular sectors using auxiliary techniques to locate the sectors, but their characteristics don't approach the nonharmonic systems which have been built to operate over 2 - 18 GHz with no ambiguities over ±90 degrees.

Additional antennas can provide increased accuracy through increased baseline and extend the unambiguous field of view, but at the expense of increased size, weight, and cost.

—DF Accuracy

Interferometer DF accuracy is determined by the widest baseline pair limited by errors due to quantization of the phase difference, phase bias from component mistrack, imperfect frequency correction, and phase bias due to receiver noise. As in the amplitude DF system, pulse averaging reduces the effects of receiver noise at threshold levels.

Typically, multioctave microwave antennas track to six electrical degrees and receivers to nine, a total RMS phase mistrack of 11 electrical degrees. At a typical 16 dB signal to noise ratio the RMS phase noise is nine electrical degrees. The quantization error can be made arbitrarily small. Frequency must be known to determine the electrical spacing of the antenns.

Figure 6 shows error as a function of antenna spacing for a 15.7 electrical degree phase mistrack error.

Location Techniques

—Azimuth/Elevation (AZ/EL)

Emitter location by measuring azimuth angle of arrival of the signal and the slant range to the emitter (AZ/EL) requires only one aircraft and (theoretically) only

TABLE I

	RANGE ERROR (mi)	
R (mi)	ALT = 1 mi	ALT = 4 mi
5	0.43	.07
10	1.75	.4
20	7.0	1.7
30	15.7	3.9
40	—	6.9
50	—	10.9

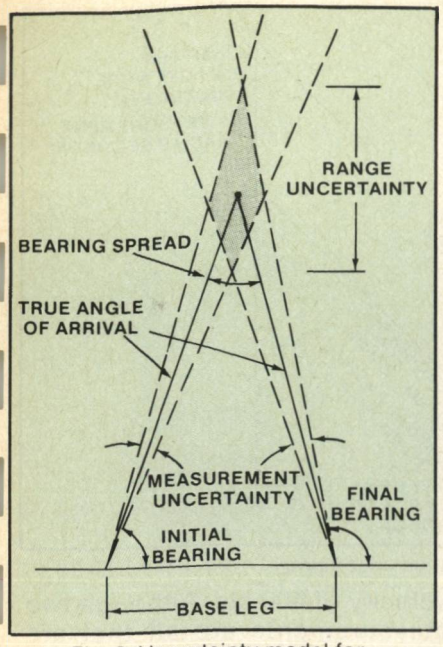

Fig. 8 Uncertainty model for triangulation ranging.

one pulse, and allows measurements to be made while flying directly towards the emitter.

An AZ/EL system defines a ground emitter position by measuring the azimuth and elevations angles of arrival and altitude of the aircraft relative to the emitter. The slant range is inferred by simple geometry. As can be seen in Figure 7, the cross range error is a function of the azimuth angle measurement error and target range. The range error is a function of the elevation angle error, target range, and altitude. For the same elevation angle measurement error (100 feet altitude, 1 degree elevation angle) Table 1 shows AZ/EL location provides better accuracy at high altitudes (large depression angles — see appendix).

Two other sources of error are the effect of altitude difference due to the curvature of the earth and the uncertainty in the target altitude due to topography. Earth curvature errors are slight for typical slant ranges, but the target topography error can be significant, unless a priori knowledge is provided to the data processor.

Multiple baseline phase interferometry is essential to provide the angular accuracy essential to AZ/EL location. Relatively narrow band (10-20 MHz) receivers provide good phase tracking, and multiple channels can measure

[Continued on page 66]

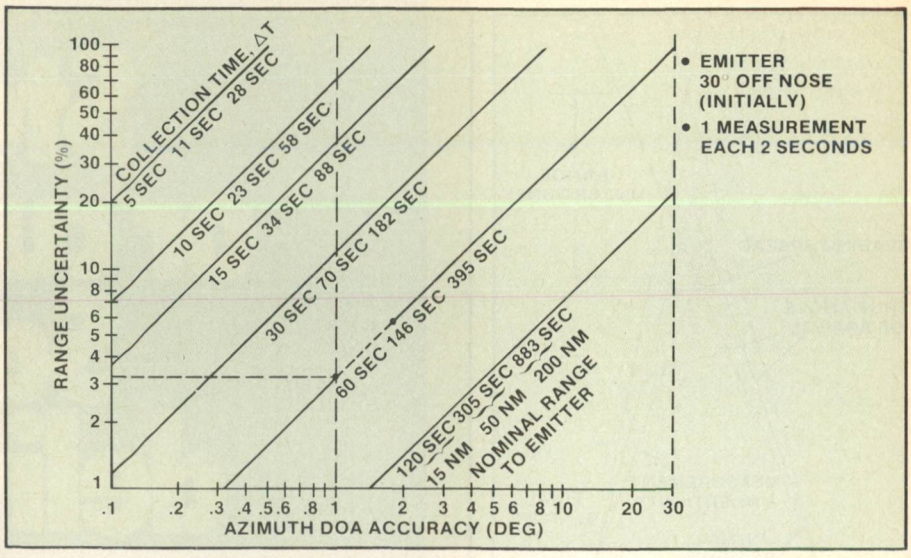

Fig. 9 Triangulation range uncertainty.

both azimuth and elevation simultaneously, providing single pulse emitter location. Normally a number of pulses are measured and averaged to reduce S-N effects.

—Triangulation

Total phase ranging has fully resolved phases as its measurables. For these measurements, the locus of possible emitter positions corresponding to a given measurement is a cone with its axis of symmetry along the baseline of the interferometer. Emitter location is determined by the intersection of two or more such cones. This ranging technique could be used against airborne emitters, but present day systems do not provide the DOA accuracy necessary to achieve useful ranging accuracies. Against surface threats, the DOA cones are projected onto the earth's surface forming triangles (i.e. triangulation).

Figure 8 relates measurement uncertainties, geometric parameters, and resulting range uncertainties. Critical parameters are the measurement uncertainties and the bearing spread, the angle subtended at the emitter by the baseleg flown by the interferometer platform. Bearing spread is largest when the emitter range is small, when the baseleg is large, and when the emitter bearings are close to boresight. Equations are given in the appendix.

Figure 9 shows ranging variation with DOA accuracy, range, and collection time for a platform velocity of 400 kts. Although two measurements are all that are needed to compute a unique emitter location, statistical averaging of many measurements improves accuracy.

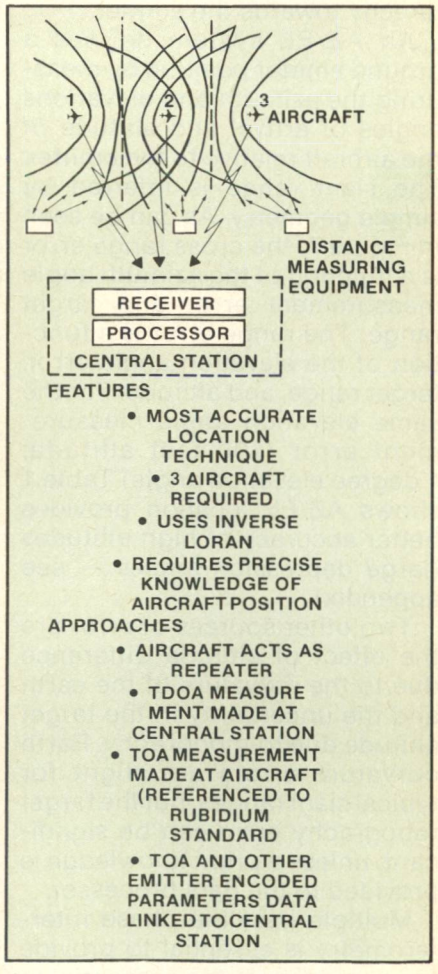

Fig. 10 Time difference of arrival location technique (Pulsed Signals).

—TDOA

Interferometry is a special case

[Continued on page 68]

[From page 66] **PASSIVE DIRECTION**

of TDOA where the distance between receiving antennas is small compared to the distance to the emitter so that incoming electromagnetic waves can be modeled as plane waves and the actual hyperbolic measurement locus approximated by its conical asymptote. TDOA systems, on the other hand, are multi-platform systems where the platform (and antenna) spacing is not small compared to the emitter range. Although two aircraft could be used for a single baseline and ranging with several pulses, TDOA systems are more apt to use three aircraft, and thus two baselines, to range on a single pulse.

The complexities of a multi-platform system are great, but such a system provides the ability to range on a single pulse and thus, range on moving emitters and in all directions.

Perhaps the most significant feature of TDOA is that, as with triangulation, the accuracy depends on the bearing spread, the angle subtended at the emitter by the three aircraft. By spacing the aircraft sufficiently far apart very accurate ranging can be performed at very long ranges.

Although similar in basic concept, interferometer and TDOA ranging systems have several important differences. In TDOA systems, time differences are measured using pulse leading edges rather than relative phase. As a consequence, TDOA systems cannot range on CW signals.

An interferometer measures phase difference essentially by cross correlating two signals whose phase difference is determined (ideally) only by the signal path length difference prior to the antennas, a TDOA system measures time-of-arrival differences between signals arriving at non-colocated receivers. Either a common reference clock must be provided to all the aircraft, or time of arrival information must be

[Continued on page 70]

[From page 68] **PASSIVE DIRECTION**

forwarded in raw form to some central processing location, in which case the distances from the aircraft to the central processing location must also be known and accounted for (Figure 10). Three surface based distance measuring equipment (DME) sites provide the necessary information about the distances from the aircraft to the central processor. These DME sites also take the emitter position relative to the aircraft and translate it to fixed geographic coordinates. For either of the two time difference measurement configurations described above there are new error sources which are not present in interferometer systems, but which ultimately limit the accuracy of TDOA ranging systems.

Because some locations may see mainlobe signals while others see sidelobe signals, TDOA systems must detect and leading edge estimate over a wide received signal power range. Signals must be matched to a particular emitter, and several aircraft and several ground stations must operate simultaneously, which requires high reliability of the individual systems. Even with such potential problems the performance advantages of TDOA systems have justified their development.

TABLE II
DIRECTION OF ARRIVAL MEASUREMENT TECHNIQUES

	Amplitude Comparison	Phase Interferometer
Sensor Configuration	Typically $\measuredangle \leq$ Beamwidth	2 or More RHC or LHC Spirals In Fixed Array
DF Accuracy	$DF_{ACC} \approx \frac{\theta^2_{BW}\,\Delta C}{24_{dB}\,S}$ (Gaussian Antenna Shape)	$DF_{ACC} = \frac{\lambda}{2\pi d \cos\theta}\Delta\theta$
DF Accuracy Improvement	• Decrease Antenna BW • Decrease Amplitude Mistrack • Increase Squint $\measuredangle$	• Increase Spacing of Outer Antennas • Decrease Phase Mistrack
Typical DF Accuracy	3° To 10° RMS	0.1° To 3° RMS
Sensitivity To Multipath/ Reflections	• High Sensitivity • Mistrack of Several dB Can Cause Large DF Errors	• Relatively Insensitive • Interferometer Can Be Made To Tolerate Large Phase Errors
Platform Constraints	• Locate in Reflection Free area	• Reflection Free Area • Real Estate For Array • Prefers Flat Radome
Applicable Receivers	• Crystal Video • Channelizer • A/O • Compressive • Superhet	Superhet

TABLE III
Emitter Location Techniques

Measurement Technique	Advantages	Disadvantages
Triangulation	• Single Aircraft	• Non Instantaneous Location • Inadequate Accuracy For Remote Targeting • Not Forward Looking
Azimuth/Elevation	• Single Aircraft • Instantaneous Location Possible	• Accuracy Degrades Rapidly At Low Altitude • Function of Range
Time Difference Of Arrival (Pulsed Signals)	• Very High Precision Can Support Bomb By Position Requirements • Very Rapid Can Handle Short On Time Threat	• Very Complex Diverse Systems Required • At Least 3 Aircraft • High Quality Receivers • DME (3 Sites) • Very Wide Band Data Link • Very High Performance Central Processor • Requires Very High Reliability Subsystems

[Continued on page 72]

[From page 70] **PASSIVE DIRECTION**

Conclusion

Of the two key direction finding techniques and three emitter location approaches, no single approach in either category is best for all applications. Their properties are summarized in Tables 2 and 3.

While the amplitude comparison DF approach has been most heavily used in the RWR product area, it does not provide high enough DF accuracy to support either weapon control systems or accurate emitter range measurement, and is sensitive to reflections and multipath effects. Phase interferometers, on the other hand, provide 10:1 better DF accuracy for the same frequency range, but are more elaborate, so are confined to those ESM systems with very demanding requirements. They use superheterodyne receivers almost exclusively.

Rotating, high gain antennas can be used with centroiding or monopulse, but flexibility is limited and wide open receivers must be used to minimize time to intercept, a disadvantage in a dense signal environment.

Future development of broadband phased arrays will permit noncontiguous sampling and adaptive revisit of the spatial environment and provide the flexibility that mechanical systems lack.

Amplitude and phase comparison systems have been treated separately, but some ESM systems combine both, either as two separate systems or combined at RF of IF as in the Rotman lens which provides full array gain at many ports simultaneously. A phase interferometer dual of this type combines a circular array with a variant of a Butler matrix in which one output port provides 360 degrees electrical phase for 360 degrees azimuth, while additional ports provide multiples of 360 degrees electrical phase for 360 degrees azimuth, similar to a multiple element linear interferometer.

Of the three location techniques, two can be implemented with a single platform, while TDOA requires multiple platforms. As a result it is less widely deployed

[Continued on page 74]

[From page 72] **PASSIVE DIRECTION** than triangulation and AZ/EL systems, but offers the significant advantage that it can provide accurate target coordinates to attack weapon systems while remaining safely behind the forward edge of the battle area.

Conformal antenna design, miniaturization of receivers, and the explosive improvement in high speed/VLSI processing will greatly improve passive signal location systems but single platform passive ranging systems will still have to be optimized for the specific application by balancing data rate and accuracy against reliability, cost, and size.

APPENDIX

$$C = \text{Log}\ \frac{G_2(\theta_2)}{G_1(\theta_1)} \qquad (1)$$

$G_n(\theta_n)$ is gain of antenna n at angle θ_n from boresight.

The measured DF angle is given by:

$$B = \frac{\theta^2_{BW}\, C}{48.1\ (S/2)} \qquad (2)$$

where

θ_{BW} = Beamwidth of the Antenna in Degrees
C = Amplitude Comparison Ratio in dB
S = Squint Angle in Degrees

DF accuracy (ΔB) is

$$\Delta B = \frac{\theta^2_{BW}\, \Delta C}{48.1\ (S/2)} \qquad (3)$$

If $S = \theta$, then the amplitude mistrack equation reduces to

$$\Delta B = \frac{\theta^2_{BW}\, \Delta C}{24.05} \qquad (4)$$

noise induced mistrack. The single channel amplitude error due to receiver noise is given by

$$\Delta A = \frac{6.14\text{dB}}{\sqrt{\text{SNR}}} \qquad (5)$$

$$\phi = \frac{360\ d}{\lambda} \sin\theta \qquad (6)$$

where

ϕ is phase difference between signals received at each antenna
d is antenna spacing
θ is angle of arrival of signal
λ is wavelength of signal

The unambiguous field of view, θ_u, of the two element interferometer is

$$\theta_u = 2 \sin^{-1} \left\{ \frac{\lambda}{2d} \right\} \qquad (7)$$

The spatial angular error, $\Delta\theta$, as a function of the electrical phase error, $\Delta\phi$, is readily derived by differentiating equation 6 to obtain:

$$\Delta\phi = \frac{\Delta\phi}{(360d/\lambda)\ (\cos\theta)} = \frac{\Delta\phi}{360\ df}\ \frac{c}{\cos\theta} \qquad (8)$$

where

$\Delta\theta$ = spatial angular error
$\Delta\phi$ = electrical phase error
θ = spatial angle of arrival
d = end element spacing
f = frequency
c = speed of light

$$\text{Error}_{(\text{Degrees})} = \frac{(\Delta f)}{f}\ \frac{57.3}{\sqrt{3}}\ \tan\theta \qquad (9)$$

Δf = frequency error
f = frequency
θ = angle of signal arrival

θ, is azimuth angle of arrival, ϕ, is elevation angle of arrival, h, is altitude of the aircraft, with respect to the emitter.

$$\text{Slant Range } R = \frac{h}{\sin\phi} \qquad (10)$$

Percent range accuracy is

$$\frac{\delta R}{R} = \left\{ \left(\frac{\delta h}{h}\right)^2 + \left(\frac{\delta\phi}{\tan\phi}\right)^2 \right\}^{1/2} \qquad (11)$$

where

δh = Altitude Error
$\delta\phi$ = Depression Angle Measurement Error
δR = Slant Range Error
h = Altitude between Platform and Emitter
R = Slant Range
ϕ = Depression Angle

Triangulation Ranging Error σ_R

$$\frac{\delta_R}{R} = \sqrt{\frac{12}{N}}\ \frac{\delta_\theta}{\Delta\theta} \qquad (12)$$

R is nominal range, $\Delta\theta$ is bearing spread, N is number of intercepts and σ_θ is the angular measurement error.

$$\delta_\theta = \frac{\sigma_\phi \lambda}{2\pi d \cos\theta_o} \qquad (13)$$

angular measurement error, σ_θ, the nominal emitter bearing, θ_o, and the measurement system's electrical phase error, σ_ϕ.

[Continued on page 76]

[From page 74] **PASSIVE DIRECTION**

Charles B. Hofmann *has been engaged in the development of electronic warfare systems for 18 years. He is presently Vice President of Engineering at the Amecom Division of Litton Systems, Inc., where he has been employed for the past 12 years. He is responsible for all engineering technical and administrative activities for Amecom's entire project line that includes electronic warfare, communications, telecommunications and radio navigation systems. Previously, at Amecom, Mr. Hofmann was Program Manager for the development of the Passive Detection System [AN/ALR-59] for the Navy's E-2C Aircraft. He was Engineering Program Director for the development of the Terminal Control Voice Switching System presently operational at the Dallas/Fort Worth Airport. Mr. Hofmann was also Director of the Engineering Product Development Directorate, responsible for the design of all electronic subsystems. Mr. Hofmann received a B.S.E.E. from Lehigh University in 1961 and an M.B.A. from the Columbia University Graduate School of Business in 1963.*

Allan R. Baron *has been engaged in the development of electronic warfare systems for 23 years. He is presently Director of Electronic Warfare Systems Engineering at the Amecom Division of Litton Systems, Inc., where he has been employed for the past 12 years. While at Amecom he was responsible for programs that demonstrated the feasibility of the Binary Beam Precision Direction of Arrival and Instantaneous Frequency Measurement Interferometer Techniques. He played a key role in the acquisition and development of a number of major electronic warfare systems including the Passive Detection System [AN/ALR-59] for the Navy's E-2C Airborne Early Warning Aircraft, and the AN/ALQ-125 Tactical Electronic Reconnaissance Sensor [TEREC] for the Air Force's RF-4C fighter aircraft. He has also directed Amecom's Independent Research & Development [IRAD] program and helped transition its products into DoD-sponsored exploratory development projects. Mr. Baron received a B.E.E. from the City College of New York in 1956 and an M.S.E.E. from the Polytechnic Institute of Brooklyn in 1962. His graduate studies emphasized communication and control systems.*

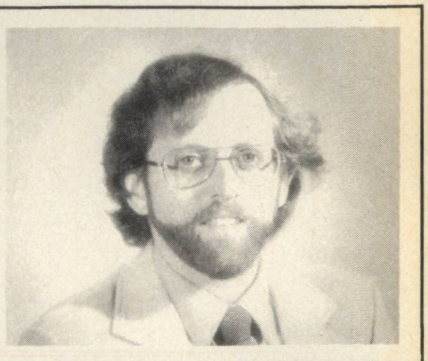

Kenneth P. Davis *has worked in the areas of radar and ESM for five years. He is presently a Senior Member of the Technical Staff at the Amecom Division of Litton Systems, Inc., where he has been employed for the past 2½ years. He has worked with interferometers and with location techniques for several projects, including developing the passive ranging algorithm for the AN/ALR-73, an update of the Passive Detection System for the Navy's E-2C aircraft. He received BS degrees in Mathematics [1975] and Electrical Engineering [1977] from MIT and is currently completing an MSEE from the University of Maryland in College Park.* ■

Phased Arrays for ECM Applications

Irwin Bardash
Sedco Systems, Inc.
Melville, NY

Introduction

The phased array antenna has been applied to just about every radar application ranging from large multifunction radars to tactical missile control systems. This is a result of the development of high speed, low loss phase shifters and control circuitry. Recently, the phased array antenna has been applied to electronic countermeasures. The primary reasons for the adaptation of phased arrays to ECM systems are:

- Higher effective radiated power
- Flexible angular coverage
- Broad bandwidth
- High switching speed and rate
- New techniques

It is in the area of the last feature, new techniques, that the phased array probably contributes its most significant upgrade for ECM applications. By providing capabilities such as polarization diversity and microsecond beam shaping and modulation, the phased array has added new dimensions to the ECM system. High effective radiated power is always a requirement for radar and/or ECM applications. Size, weight, and power consumption are often limitations on the thermal power that can be generated by an ECM transmitter subsystem. Traditional omnidirectional antennas do not provide sufficient gain or angular discrimination. Larger mechanically rotated antennas may have required gain but can not provide rapid angular coverage. Switched horns suffer from high cross-over losses and require excessive real estate. The phased array overcomes these deficiencies and provides the high gain and rapid scanning over a large coverage sector needed for present and future high ERP ECM systems.

The flexible angular coverage available with a phased array provides rapid scanning from a single antenna in both the azimuth and elevation axes. The phased array antenna easily provides coverage over an octant ($\pm 45°$ in both azimuth and elevation) and, in many cases, coverage well beyond that range. Matching techniques have been developed which enable greater than octave array performance over these scan ranges. Hence, one of the fundamental requirements for ECM applications, namely broad bandwidth, can be provided by the phased array. Octave bandwidth operation is relatively straightforward to achieve; bandwidths of 2.5:1 have recently been developed. And, in the not too distant future, two-octave performance from a phased array aperture will become available.

The high switching speed provided by the latching ferrite phase shifter and/or diode phase shifter (or switch) is ideally suited for ECM applications. The ferrite device can change phase states in 200 nanoseconds to 5 microseconds and provide low loss, broad bandwidth performance relatively easily. The diode device can also be made broadband and has exceptionally good switching speed but has higher insertion loss.

Receive Array Considerations

The use of a high gain, narrow beam transmit phased array in an ECM system requires that the location of the threat emitter must be determined to an accuracy related to the beamwidth of the transmit aperture. Several different techniques may be used for this direction-finding application. These include: (1) an instantaneous DF multibeam subsystem; (2) a monopulse DF array subsystem; and (3) an interferometer subsystem. In some cases the same aperture can be used for DF purposes as well as for high gain jamming. On the other hand, there are certain advantages to locating the receive DF subsystem remotely from the transmit phased array, primarily being able to simultaneously receive and transmit. Figure 1 illustrates simplified schematic diagrams of the three receiver subsystems mentioned above.

The *IDF multibeam subsystem* shown in Figure 1a uses an array

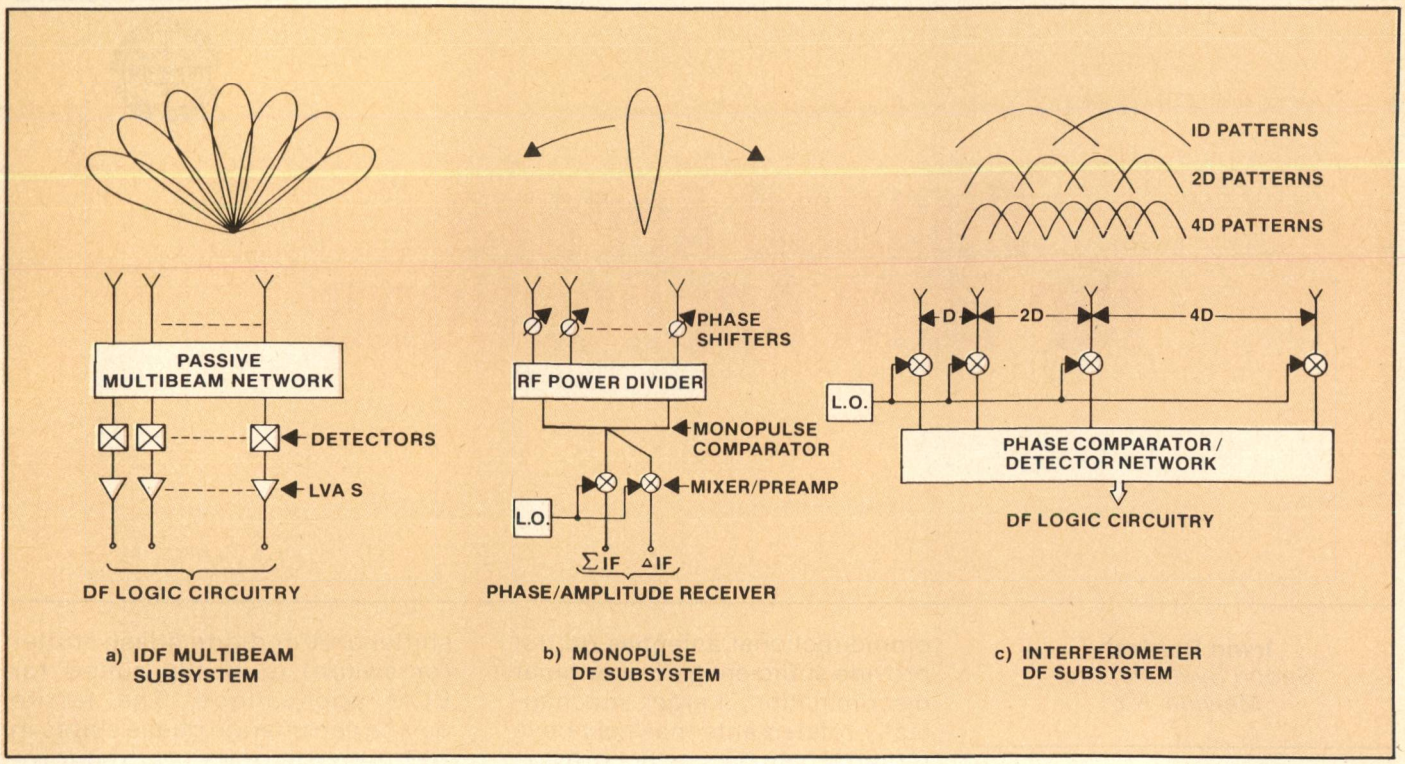

Fig. 1 ECM receiver subsystems block diagrams.

of elements which feed into a passive multibeam network. Required precision determines the number of radiating elements needed for properly pointing the transmit antenna. For example, if a large, narrow beamwidth transmit array is used, then a relatively large receive array must be used. Conversely, a smaller, broader beamwidth receive aperture may be used if a lower gain, broader beamwidth transmit antenna is employed.

The multibeam network may be a Butler matrix or a multibeam lens. The Butler matrix produces a number of spatial beams using an assortment of quadrature couplers and fixed phase shifters. Each output port has a unique antenna pattern and beam-pointing direction created by an associated phase taper within the Butler matrix. As such, the beam-pointing direction scans with frequency similar to all phased arrays. The multibeam lens also produces a number of spatial beams but employs optical properties. Since differential path lengths create the individual antenna patterns and pointing directions, the beam angle remains stationary with frequency. In general, for ECM applications, a Butler matrix is used when a phased array transmit antenna is used and a multibeam lens is used when a lens transmit antenna is employed.

Each output port of the multibeam network contains a detector and a log-video-amplifier. The outputs of the log-video-amplifiers are fed to DF logic circuitry which codes the actual beam of direction-of-arrival of all incoming RF signals. This is done with relatively straightforward "greatest-of" logic circuitry. The application of additional amplitude comparison computations between adjacent beams provides finer DF accuracy. It is possible to achieve between 1/4 and 1/8 beamwidth accuracies using this technique.

The receive sensitivity of the IDF subsystem is determined basically by the gain of the receive antenna and the tangential sensitivity of the detectors. Nominal values ranging from -35 to -45 dBm are readily achievable. Better sensitivity can be obtained using solid-state amplifier devices but with attendant increases in complexity and cost. The primary function of the IDF subsystem is, by definition, to determine instantaneously the direction-of-arrival of all incoming signals over a very broad frequency range. Its success in doing this has resulted in its widespread use in many operational systems.

The *monopulse DF array subsystem* as shown in Figure 1b uses a conventional phased array and determines the direction-of-arrival of an emitter by scanning through the emitter location. This requires a receive sequence involving several pulses before the position of the emitter is accurately determined. By using a monopulse RF comparator followed by sum-and-difference phase and amplitude comparison circuitry, the accuracy of an emitter location can be determined, nominally, to better than 1/20 of a beamwidth. The receive sensitivity of the monopulse DF array subsystem is determined primarily by the mixer-preamp characteristics and is generally in the range between -65 to

[Continued on page 84]

-75 dBm. In this type of subsystem, the same radiating aperture is generally used for both the receive and transmit functions. This minimizes the amount of hardware required in the overall system but, even more significantly, eliminates array DF errors caused by installation effects or parallax associated with separately located receive and transmit apertures. The monopulse DF array subsystem is generally used when high sensitivity, precision angle-of-arrival information is required. For many ECM applications this is highly desirable, particularly if other onboard systems provide initial emitter identification data.

The *interferometer DF subsystem* approach is illustrated in Figure 1c. For this example, four unequally spaced elements are used to create a multiplicity of equivalent beams in space. The broadest beams are created by the closest spaced pair of elements while the narrowest beams are created by the widest spaced pair of elements. Comparator circuitry is used to combine the energy from each pair of elements and, for the case shown in the figure, this is done at the subsystem IF frequency. This enables the system sensitivity to be determined to a large extent by the mixer characteristics. Simple, two-element array theory may be used to calculate the spatial patterns for each pair of elements. The antenna pattern characteristics arise from the phase difference as a function of angle-or-arrival between the two incoming RF signals in each pair of elements. This is the amplitude comparison interferometer technique. A phase interferometer approach is also possible.

For a given coverage sector, the broadest beams (generated by elements spaced at 1 D) split the sector into two parts which may be labelled "left" and "right". The next narrower beams (generated by elements spaced at 2 D) split the sector into four parts which unto themselves are not unambiguous. However, these narrower beams are unambiguous in the "left" and "right" parts of the broader patterns. Simple logic circuitry can then be used to split the coverage sector into four unambiguous zones. Similarly, the next narrower beams can be used to split the coverage sector into eight unambiguous zones and so on. The required angle-of-arrival precision determines how many elements and "sector-splits" must be implemented. It should be noted that the inter-element spacing used for this example was chosen for purposes of explanation and not to suggest an optimum configuration.

The system sensitivity provided by the interferometer DF subsystem is determined by the mixer front-end and the antenna/comparator losses. Because of the power splitting required for the comparator and the lack of antenna gain, system sensitivity will be nominally between -50 and -60 dBm. Subsystem accuracy is affected by multipath, installation configuration, and internal component phase errors. The first two effects are caused by the large field-of-view of each element in the antenna, effects which do not impact the performance of the previously described receive subsystems since their antenna beams are focused by their total apertures. The major advantage of the interferometer receive subsystem is that it is relatively simple and inexpensive, and can provide angle-of-arrival information on a single received RF pulse with fairly attractive system sensitivity.

We have seen that a number of receive array approaches may be used to determine the direction-of-arrival of incoming RF signals for ECM system applications. No single approach can be designated as optimum. The appropriate subsystem is determined after all performance requirements and trade-off analyses have been completed. The primary factors that influence the final selection are: required system receive sensitivity; and required DF precision for properly redirecting the transmit phased array.

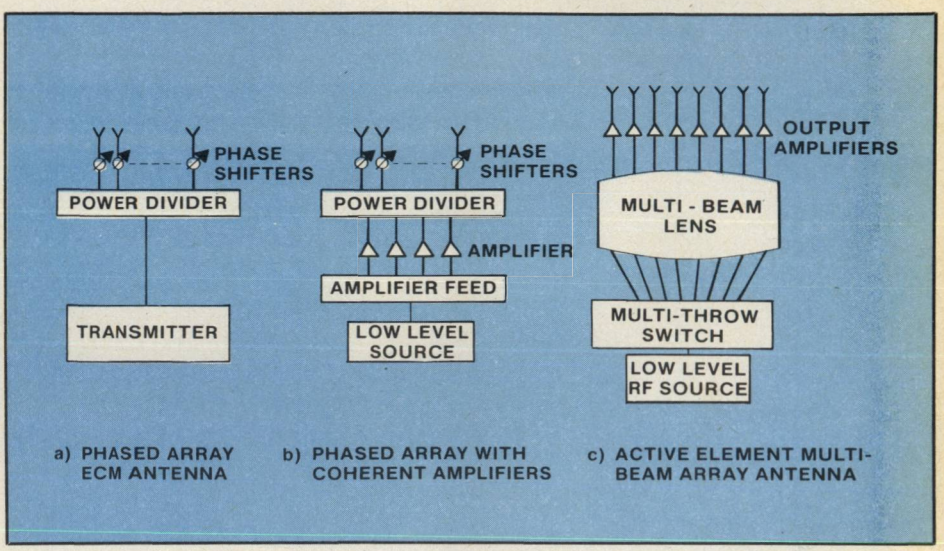

Fig. 2 Transmit phased array configurations.

Transmit Array Considerations

Several different array configurations can be used to generate high gain and high ERP for ECM system applications. Figure 2 shows simplified block diagrams of three different basic array approaches.

The conventional *ECM phased array antenna* is illustrated in Figure 2a and consists of a single input from the high power transmitter into a power divider which feeds a number of phase shifters and radiating elements. Linear arrays using this configuration

[Continued on page 86]

[From page 84] **PHASED ARRAYS**

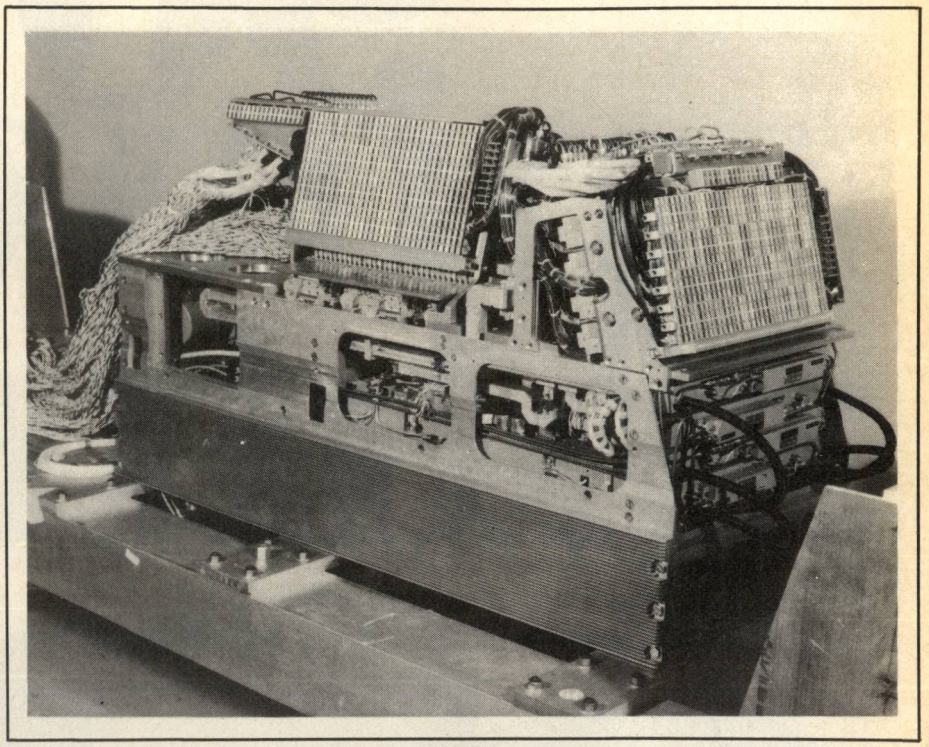

Fig. 3 Phased array and transmitter portion of high ERP ECM system.

provide from 10 to 20 dB of gain. A specific gain level is obviously determined by the number of elements used. The frequency coverage available with this type of array is greater than an octave which is well suited for ECM applications. Reduction of deleterious mutual coupling and resonance effects is responsible for providing required performance over wide frequency and scan angle ranges. The latching ferrite phase shifter provides excellent phase control with nominal loss (less than 1dB) over very wide bandwidths.

Recent improvements in diode phase shifter performance such as increased bandwidth and lower loss performance now make these devices applicable to ECM applications.

Since the ECM phased array is generally much smaller than the radar phased array, the per element power is generally higher. Hence, phase shifters, radiating elements, and power dividers must be designed with sufficient margins of safety to insure reliability in an operational environment. The ferrite phase shifter has been demonstrated to be exceptionally reliable and capable of handling very high power levels, more than ever encountered on a per-element basis. The diode phase shifter may provide adequate power handling capacity but has not been proven operationally. The switching speed of the ferrite device, when operated in a latching mode, is about 200 nanoseconds while diode phase shifters can switch under 100 nanoseconds.

Figure 2b illustrates a *phased array with coherent amplifiers* used to generate very high ERP. The configuration incorporates a number of high power amplifiers within the array feed. The output from a low-level source is divided by a simple feed which provides RF to each of the high power amplifiers. Traveling-wave-tube amplifiers are ideally suited for this application since they operate over broad bands and can generate substantial power per tube. Using this approach

[Continued on page 88]

[From page 86] **PHASED ARRAYS**

it is relatively easy to generate in excess of 1000 watts of thermal power with four traveling-wave tubes to cover more than an octave bandwidth. The second feed within the array is used to sub-divide the output power of each TWT for application to the phase shifter located behind each radiating element. These phase shifters perform beam-steering for the array. The full ERP of this subsystem is obtained by the coherent addition in space of the power radiated from each element.

A typical example of this phased array subsystem is shown in Figure 3 which is a photograph of a system developed and built by Sedco for the Air Force Wright Avionics Laboratory. Two phased arrays are used in this system. Note the presence of two line arrays on the side or on top of each of the planar arrays. These line arrays provide the DF receive information for determining the azimuth and elevation coordinates of an emitter. The TWT transmitter modules are located underneath the phased array apertures. Figure 4 is a composite of antenna patterns covering a $\pm 45^\circ$ azimuthal sector. This system is capable of providing ERP in excess of 500 kilowatts. Four TWT dual-type modules generate 1600 watts of thermal power while the antenna provides more than 25 dB of gain.

A more detailed description of this system may be found in Reference 1.

The *active element multibeam antenna* is shown in Figure 2c. This subsystem employs an amplifier behind each radiator in the array. Mini-TWTs have been developed for this application and provide nominally 30 to 40 watts per device across bandwidths in excess of an octave. The input from a low-level r.f. source is applied to any one of the lens input ports with a multi-throw diode switch. This switch is capable of providing switching speeds of less than 50 nanoseconds which means that beam switching from one angle to another is extremely fast. The multiple beam lens optically creates the required phase and amplitude at each output port to generate a different transmit beam for each input port. There is a fixed beam-pointing angle associated with each input port of the multiple beam lens. Each amplifier must operate coherently at saturation in order for the system to function properly. One of the features of this approach is that r.f. losses in those components located on the input side of the TWT amplifiers do not reduce the output radiated power and therefore the system is very efficient for producing very high ERP for ECM applications.

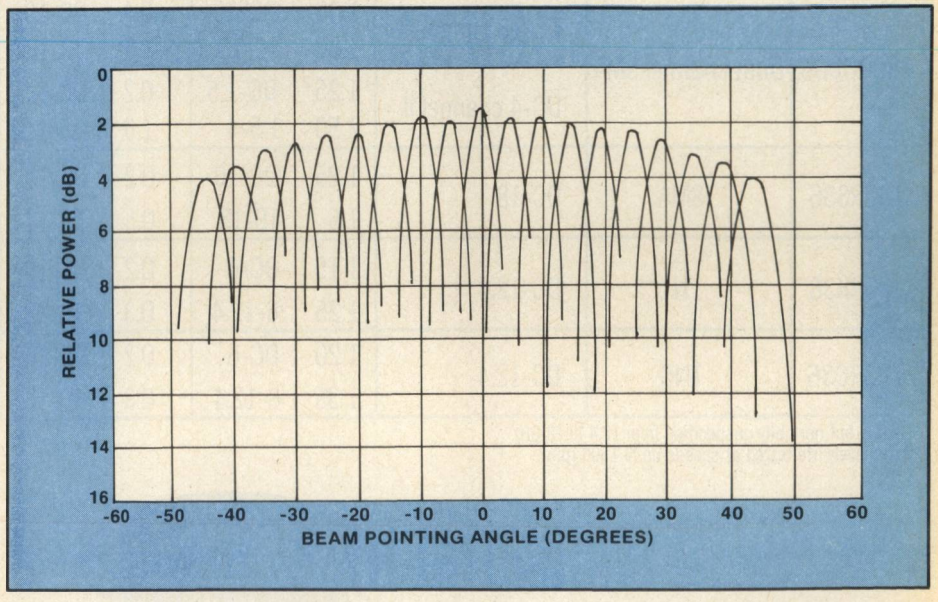

Fig. 4 High ERP system azimuth scan sector composite antenna patterns.

[Continued on page 90]

Another attractive characteristic of the Active Element Multibeam Antenna is that the lens characteristics are frequency insensitive and therefore cause no beam steering across the band. A complete description of this antenna and its application to an operational system may be found in Reference 2.

Recent Concepts

Polarization has recently become a significant parameter for ECM applications. Instantaneously, every radar system radiates a specific polarization and its antenna characteristics may be affected by receive r.f. polarization. If the ECM system can sense the instantaneous polarization of a threat system, it may take advantage of certain polarization- related error factors. As an example, all curved dish antennas have Condon lobes. These lobes appear on the intercardinal axes of the dish and are cross-polarized relative to the antenna's primary polarization Excitation of these Condon lobes with the appropriate polarization can cause a radar tracking system to produce error signals within its detection subsystem.

Another polarization ECM technique involves the sidelobe characteristics of a threat radar antenna. The co-polarized sidelobes of a radar antenna are suppressed by the use of a reference or "guard" antenna. This antenna is a broad-beam device with a gain level set slightly above the maximum sidelobe of the primary antenna. Primary antenna sidelobes are suppressed with simple logic circuitry whenever the guard antenna received signals exceed those of the primary antenna. The cross-polarized characteristics of the primary antenna relative to the polarization characteristics of the guard antenna are essentially random. Hence, false targets can be generated in the threat system by illuminating its sidelobes with cross-polarized RF signals.

Bipolarized phased arrays have been developed for sensing and transmitting arbitrary polarizations. Relatively simple polarization control networks may be used to measure incoming polarization and to generate an appropriate response. Figure 5 is a block diagram of such a Polarization Controller that contains an amplitude control unit and two phasers. Each phase shifter is connected to the vertical and horizontal elements in a bipolar array. The amplitude control unit is used to vary the tangent γ function and the phase shifters are used to control the ϕ factor. (γ and ϕ are defined in the figure.) By sensing the phase and amplitude of r.f. signals received at the input side of the amplitude control unit, the polarization of the received signal can be uniquely determined. Conversely, these same controls can be used to establish any arbitrary transmit polarization. The bipolar phased array with a polarization controller can be used to generate the totally polarization-diverse phased array ECM system.

Radar cross-section of ECM antennas is becoming more significant as the RCS of operational aircraft is reduced. It is therefore important to design an ECM antenna with a minimum RCS. One of the advantages of using nonreciprocal ferrite phase shifters in an ECM phased array system is its nonreciprocal behavior. This causes the receive and transmit patterns of an array using these devices to point in different directions except at boresight. Hence, when a phased array with ferrite phase shifters is transmit-

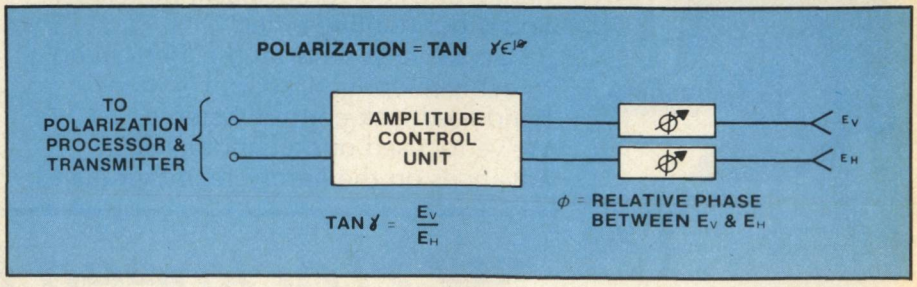

Fig. 5 Polarization controller block diagram.

[Continued on page 92]

[From page 90] **PHASED ARRAYS**

ting in a given direction, its receive RCS is reduced by a factor associated with its sidelobe level. Figure 6 is a graph illustrating the array cross-section for a 12 square inch aperture. The VSWR at its input port is arbitrarily chosen as 2.5:1 and its array sidelobe level has been arbitrarily chosen as -16 dB. The cross-section of this array would range from 0.15 to 0.60

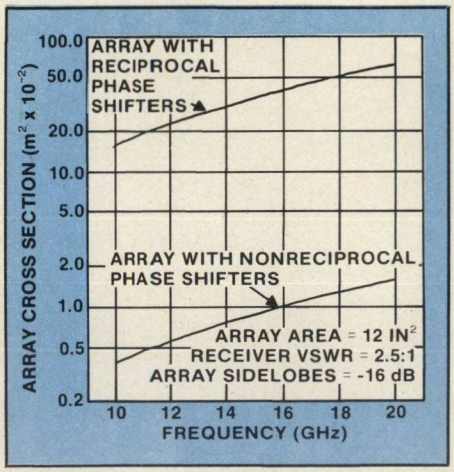

Fig. 6 Array cross section vs frequency.

square meters over the frequency range of 10 to 20 GHz if it employed reciprocal phase shifters, whereas its cross-section would range from .004 to .015 square meters if it contained nonreciprocal phase shifters. This is a very important design consideration in today's environment where antenna RCS is becoming increasingly significant.

Conclusion

The phased array provides an optimum link from the ECM system to the environment as required to counter modern threat scenarios, and, therefore, it is not surprising that virtually all new ECM systems are being designed with phased array antennas. The SLQ-32 ECM system, being built by Raytheon ESD and presently installed on a number of surface ships, is a prime example of an operational system which uses several lens array antennas to provide wide-angle coverage and high ERP. The ALQ-161 ECM system built by the Eaton Corporation AIL Division for the B1-B Bomber contains a number of phased array receive and transmit antennas. The ALQ-172 system, in its final stages of development by ITT Avionics Division, contains phased arrays and will be installed in the B-52 Bomber in the not-too-distant future.

As phased array components are made smaller, lighter, and less expensive, the phased array antenna will be used more and more in airborne and ground-based ECM systems. In anticipation of the deployment of millimeter threat systems, ECM phased arrays are being developed at higher and higher frequencies. Multi-megawatt and higher ERP ECM systems will become a reality using phased array technology. It is safe to say that all future sophisticated ECM systems needed to meet the demands of existing and anticipated threat environments will rely on the phased array antenna to provide required ERP, coverage, bandwidth, speed, and new techniques.

REFERENCES

1. "High ERP phased array ECM systems" by Murray Simpson, p. 41, *Journal of Electronic Defense*, March, 1982.
2. "Higher ERP with lens fed multibeam arrays" by D.H. Archer and A.A. Black, p. 51, *Journal of Electronic Defense*, March, 1982.

Irwin Bardash, *as director of Advanced Programs at Sedco, is responsible for all independent research and development programs and technical proposal efforts. His present focus is on the adaptation of phased array technology to high ERP, polarization diverse ECM systems. He participated in developing the concepts and designs of the phased array subsystems for the ALQ-161, ALQ-172, and the ALQ-131 upgrade systems. Previously Mr. Bardash was the Program Manager of the B-52 ESAS ECM Program which involved the design and development of a two-octave, 360°, receive-transmit high ERP phased array systems. His earlier r.f. technical activities centered on the research and development of ferrite phase shifters and circulators for which he has written a number of papers and holds several patents. Prior to his affiliation with Sedco he worked at the RCA and M&SR Division where he was a member of the Antenna Group and was responsible for the design and development of ferrite devices. Mr. Bardash received his BEE degree from Cornell University and his MSEE degree from the University of Pennsylvania. He is a registered professional engineer in the State of New Jersey. He is a member of the Association of Old Crows, the IEEE and a past chairman of the Long Island Section PTGMTT Group.* ■

Miniature 1-Watt 7-15 GHz FET Amplifier

S. A. McOwen and A. J. Stein

Raytheon Electromagnetic Systems Division
6380 Hollister Avenue
Goleta, California 93117

Introduction

Wideband, 1-watt C.W. power amplifiers that operate above 8 GHz have been developed using circuit power combining techniques [1,2]. However, many systems applications do not allow sufficient physical size to use these power combining hardware techniques, therefore, the use of large gate periphery FET's are a necessary alternative.

This paper presents data on four miniature (48.00 x 10.67 x 5.5 mm) amplifiers consisting of three cascaded balanced modules incorporating six FET's (3 pairs) whose gate peripheries are respectively 500, 800 and 1600 μm, see Figure 1. The 500 μm FET is an AVANTEK AT8251 with an I_{DSS} of 130 mA. The 800 and 1600 μm FET's are Raytheon, via-hole FET's with 380 and 500 mA I_{DSS} respectively. All FET's were mounted in common source configuration using separate gate and drain bias supplies.

Phased array and lens fed type applications require very good phase and gain tracking from amplifier to amplifier. This design gave primary consideration to output power while maintaining phase and gain tracking over the full 7 - 15 GHz band. The performance of the amplifiers was very satisfactory allowing a successful set of system tests. Table I summarized the goals for this project and compares them to the actual achieved performance. Small signal S-parameters, suitably modified, were successfully used for design of these high power amplifiers.

The design procedure can be divided into five major steps:

- FET Characterization
- Computer Aided Design
- Fabricate and Test Single-Ended Modules
- Fabricate and Test Balanced Modules
- Fabricate and Test Multiple Stage Amplifiers

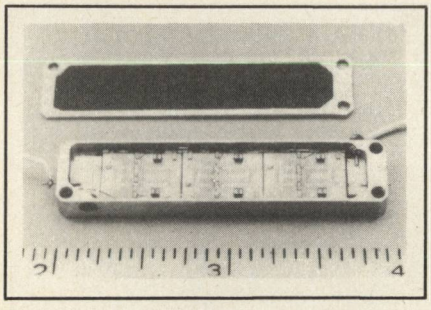

Fig. 1 Miniature 1 watt amplifier.

FET Characterization

This consists of dc and small signal S-parameter measurements as well as optimum output impedance measurements for maximum output power. The dc data is used to set the operating bias level. The S-parameters and output impedance data are used for RF matching.

Each FET type was evaluated. At least two FET's from each wafer used were chosen for evaluation. Table II summarizes the S-parameters for three different gate peripheries. The S-parameter reference plane is at the edge of the rib upon which the FET's are mounted. As can be seen, as the gate periphery increases, the S_{11} and S_{22} become more difficult to match and the Gumax (maximum unilateral transducer power gain) decreases. It was found that the Gumax at the high end of the band was the most useful small signal gain figure of merit for large gate periphery FET's. Even so the realizable small signal gain is 1 to 2 dB below Gumax for maximum gain designs. For maximum power designs, the deviation from Gumax can be 2 to 3 dB lower at the high end of the band. Maximum power designs are achieved when the FET is matched for best power out, not best gain.

The optimum output impedance for maximum power was obtained by an approximate method. This method is to assume that the large signal S_{22} is equal to the small signal value of S_{22} at the knee of the I_{DS} versus V_{DS} curve. This assumption was tested a number of times using various gate periphery FET's and the easily tunable circuits discussed below. In all cases the circuit based on the approximate large signal S_{22} gave maximum output power across the band. While approximate, this method has the obvious advantage of reduced design time when compared with the various large signal measurement techniques discussed in the literature. We found it to be very satisfactory as demonstrated by the results of this work.

Comparative Evaluation of Circuits

Computer aided design makes use of the small signal S-parameters to determine the RF input and output matching circuits. Optimun output impedance for maximum power is also considered here.

TABLE I
SUMMARY OF SIZE AND ELECTRICAL PERFORMANCE OF ALL FOUR AMPLIFIERS.

	PERFORMANCE	GOALS
Size	48 x 10.67 x 5.5 mm	48 x 10.67 x 5.5 mm
Weight	13 grams	13 grams
Frequency	7 - 15 GHz	7 - 15 GHz
Small Signal Gain (Nominal)	11.5 dB	12 dB
Small Signal Gain (Tracking) (Worst Case)	±1.5 dB	±1 dB
SAT Power @ 11GHz	30.5 dBm	32 dBm
SAT Power Tracking (Worst Case)	±.85 dB	±1 dB
SAT Power (Max)	31.5 dBm	31 dBm
1dB Compression Power @11GHz	30 dBm	30 dBm
1dB Compression Power Tracking (Worst Case)	±1.05 dB	±1 db
Phase Tracking	±25° Full Band ±19° for 85% of Band	±15°
Power Added Efficiency (Nominal)	12.5%	13%
Power Added Efficiency (Best)	17%	13%

TABLE II
MEASURED S-PARAMETERS AND CALCULATED GUMAX.

FREQ (GHz)	S_{11} 0°	S_{21} 0° (dB)	S_{12} 0° (dB)	S_{22} 0°	GUMAX
AVANTEK 500μm FET STAGE 1					
7	.79/-120	7.2/ 81	-23.5/23	.57/- 45	13.2
9	.77/-132	5.9/ 68	-22.5/27	.58/- 50	11.5
11	.77/-140	4.3/ 50	-22 /25	.56/- 81	9.8
13	.75/-150	4.5/ 45	-21 /27	.56/- 76	8.7
15	.77/-170	7.5/ 90	-25 /15	.55/- 90	7.9
18	.78/-180	1.5/ 27	-25 /40	.65/-116	7.8
RAYTHEON 800μm FET STAGE 2					
7	.87/-123	2.98/ 66	-32 /28	.71/- 58	12.2
9	.88/-137	1.51/ 44	-28.6/35	.77/- 76	14.6
11	.87/-149	- .92/ 24	-25 /38	.80/- 98	9.7
13	.88/-157	-1.62/ 10	-26.7/24	.84/- 98	10.2
15	.88/-169	-3.22/- 3	-28.4/36	.82/-130	8.1
18	.88/-180	-6.74/-22	-30.5/17	.94/-142	8.8
RAYTHEON 1600μm FET STAGE 5					
7	.90/-148	.83/ 45	-32.8/34	.69/- 96	10.7
9	.91/-157	-1.62/ 24	-30.5/50	.78/-110	10.0
11	.90/-164	-4.15/ 13	-24.7/48	.82/-124	7.9
13	.90/-164	-5.04/- 6	-26 /37	.84/-126	7.4
15	.90/-172	-7.94/-18	-29 /44	.86/-148	5.0
18	.90/-176	-12.04/-33	-34 /28	.94/-156	4.5

The first step in a CAD circuit design is to choose a topology and three candidates considered during this program are shown in Figure 2. The circuit in Figure 2b uses shorted stubs and consists of series transformers and open and shorted stubs. This circuit is discussed by K. Niclas[3]. The major drawback arises from the short circuited stubs which are found to be larger and more difficult to tune than the shunt lumped indicators of the circuit in Figure 2a, the one chosen

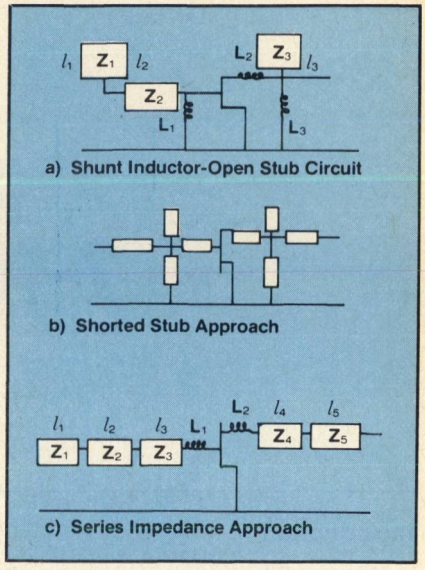

Fig. 2 RF circuit topologies investigated during this program.

for this program. Both of these types of circuits were built and tested.

The high/low series impedance circuit shown in Figure 2c was not fabricated, but an analytic comparison conducted with the shunt inductor-open stub circuit. Figure 3 summarizes the results of this comparison. Small signal S-parameters from a Texas Instrument π gate 600 μm FET were used for the comparison of the two circuits. CAD was used with identical optimization goals for both circuits. As can be seen, the optimized results are essentially identical. The advantages for the shunt inductor-open stub circuit include:

- Fewer tuning elements, 6 compared to 7
- Tuning elements are easier to build, all lines are 50 ohms.
- Easier to tune because positions and values of stubs and inductors can be varied independently.
- Smaller size. The high/low series impedance circuit is 5 to 6 times longer.
- dc bias circuitry can be incorporated within the RF circuit elements. The high/low series impedance circuit has no shunt elements to bring the bias to the FET's.

On the other hand, the high/low impedance seems to have two advantages:

- Wider bandwidth at lower frequencies. Since the bias circuit is optimized separately from the

[Continued on page 100]

RF circuit, it could be designed so that very little low-end roll-off in gain occurs. The shunt inductors cause sharp gain roll-off at the low edge of the frequency band. Very wide bandwidths have been reported using the high/low impedance circuit, for example see references (4) and (5).

- Positioning the gate of the FET very close to the RF circuit is less critical.

In view of these considerations, the shunt inductor-open stub circuit was selected. This could be expanded to include series transformers, but such action was not found to be necessary to meet the program goals.

— Specific Design Procedure

The value of the S_{22} that gave maximum output power was used to obtain a circuit that gave a good RF match to 50 ohms across the frequency band. This output circuit was then fixed and the input circuit optimized for flat gain across the band.

The circuits are very versatile and lend themselves to ease of tuning. The stubs were realized by small pads so placed that, when attached using bonding wire, they form open circuited stubs. The position (distance from the FET), length and characteristic impedance of the stubs is varied by attaching various combinations of the pads. CAD used to model the bonding wires to the pads revealed that any effect they introduced could be compensated by using somewhat shorter lengths of open stubs than would otherwise be used.

The shunt inductors are formed by 0.7 mil wires which are RF grounded thru 27 pF capacitors attached to the rib on which the FET's are mounted. The inductance of these wires can be varied by changing their length, which in turn can be varied by changing the FET attachment position on the 50 Ω line. It was found that two parallel wires the same length did not reduce inductance to one-half and a third wire did not further reduce the inductance at all. The same inductor wires were used to bring the gate and drain bias to the FET's, no further bias network being needed.

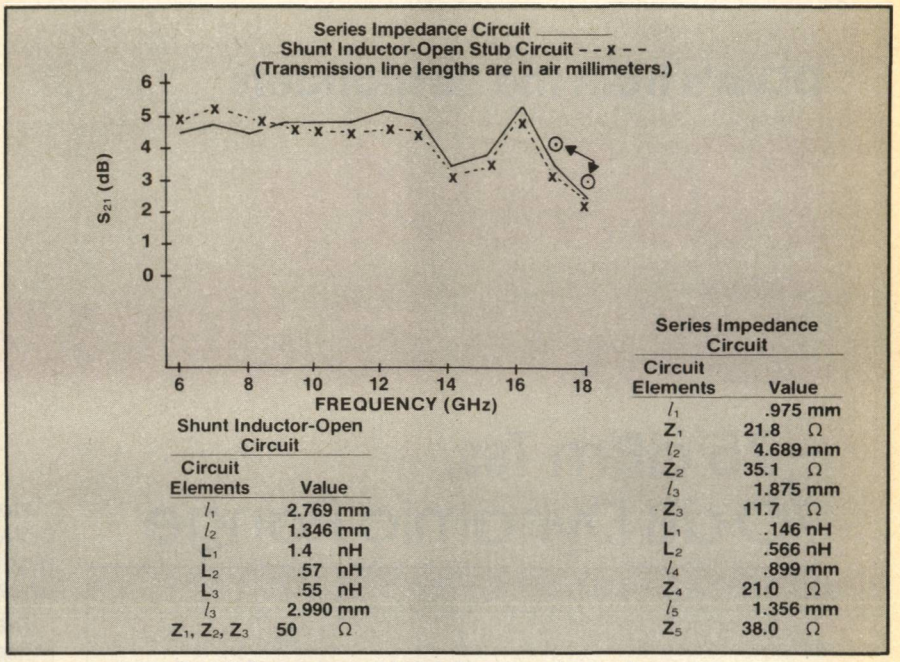

Shunt Inductor-Open Circuit

Circuit Elements	Value
l_1	2.769 mm
l_2	1.346 mm
L_1	1.4 nH
L_2	.57 nH
L_3	.55 nH
l_3	2.990 mm
Z_1, Z_2, Z_3	50 Ω

Series Impedance Circuit

Circuit Elements	Value
l_1	.975 mm
Z_1	21.8 Ω
l_2	4.689 mm
Z_2	35.1 Ω
l_3	1.875 mm
Z_3	11.7 Ω
L_1	.146 nH
L_2	.566 nH
l_4	.899 mm
Z_4	21.0 Ω
l_5	1.356 mm
Z_5	38.0 Ω

Fig. 3 Comparison of high/low — series and shunt inductor — open stub circuits.

The versatility of this circuit can be appreciated from the following features:

- A common circuit layout was useable for both the gate drain circuits. The same two layouts were used throughout the program for all FET evaluation (S-parameters and power tests), circuit design verification and final realization of the amplifier stages, various tuning requirements for the three gate periphery FET's being accomodated by attaching different combinations of open-stub tuning pads and lengths of inductors.
- The FET evaluation was accomplished using a single-ended version of the two circuits, whereby no pads or inductor wires were used, bias was applied with external bias T's. This provided a representative 50 Ω system for S-parameter measurements. Thereafter, the circuit could be tested immediately by attaching tuning pads and inductor wires. In fact, tuning elements could be applied one at a time to evaluate their separate effects. Considerable time was saved because no new circuits were required to be etched, no additional FET's mounted or test fixtures fabricated.
- Another advantage was that the low-end of the frequency band is primarily affected by the shunt inductors and the high-end affected by the open stubs. The middle of the band is affected by both. Thus, once an approximate circuit optimization has been generally realized in which one portion of the frequency band is slightly out of specification, it is clear which circuit elements are to be modified. This feature allows less experienced personnel to perform the test and tune operations.

Fabricate and Test Single-Ended Modules

A single-ended module consists of one FET, one input, and one output RF matching circuit. As noted already, the single ended tests were performed with the FET's in situ before proceeding to balanced modules so that the effects of the matching circuitry could be monitored concerning input and output impedance. The 3 dB quadrature hybrid couplers prevent the observation of these impedances in the balanced circuit module configuration.

Fabricate and Test Balanced Modules

Based on the single-ended tests, the balanced modules were fine tuned as required.

Figure 4 compares the predicted small signal gain to the measured small signal gain of the four bal-

[Continued on page 102]

[From page 100] **FET AMPLIFIER**

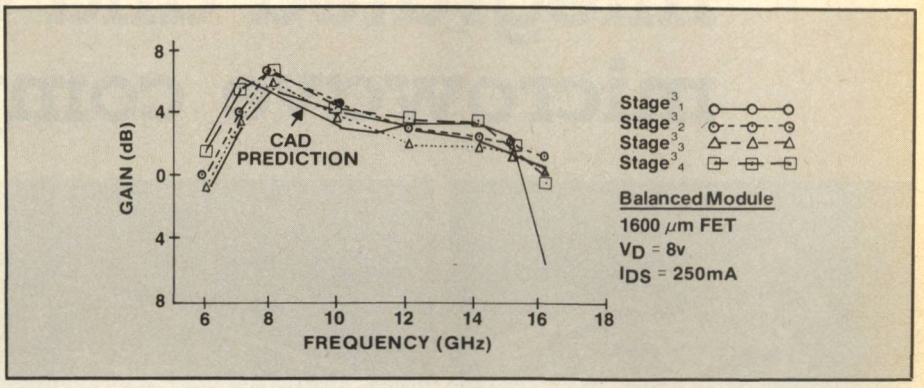

Fig. 4 Predicted gain shows excellent correlation with measured results for output stages.

anced output stages used in the four amplifiers. The gain is within approximately 1 dB of the predicted results. Stages 1 and 2 similarly duplicated predictions, with mid-band gains of approximately 6 and 4 dB respectively. All stages had approximately the same shape to their gain curves, very little effort being needed for gain flattening. Approximately 75% of the gain variation is due to individual FET variations, particularly true of the 800 and 1600 μm gate periphery FET's, the remaining 25% is attributable to circuit variations.

Two major difficulties were encountered, the first, inherent low gain of large gate periphery FET's at 12 GHz and above, and the second, FET to FET parameter variation for the 800 μm and 1600 μm FET's. The latter no doubt due to the fact that these FET's were among the first wafers of this type to be produced.

Future programs should encounter fewer problems and closer tracking between amplifiers and a closer match bewtween predictions and measurements, because the FET fabrication technology should improve. Also, circuit reproducibility will be improved by such techniques as automatic wire bonding.

Fabricate and Test Multiple Stage Amplifiers

The final step is to fabricate and test multiple stage amplifiers. This consists of checking each balanced module for proper gain and power and then cascading the balanced modules. To obtain optimum tracking and power performance, our primary goals, the various stages were "mixed and matched", to find the optimum combination of stages 1, 2, and 3 for the four amplifiers that provided optimum tracking and power-output. Presumably, this need will be reduced in future programs as FET and circuit improvements are made.

Structural Considerations

The amplifier consists of three microwave circuit stages mounted inside an aluminum housing with cover and 50 ohm RF coaxial feedthroughs for the input and output. Two dc supply voltages of -5V and +7V are required and enter the housing from each end. Both the RF and dc voltages share a common alumina substrate to which gold circuits are plated 5.1 and 6.4 microns thick. This circuit provides interconnections between external voltages and RF power into the internal microwave amplifier circuit stages. The circuit stages are made from alumina ceramic and bonded to a molybdenum carrier for thermal expansion compatibility and high thermal conductivity. The FET is attached to a central rib of the carrier using a gold-tin solder preform to ensure a good electrical ground and high heat transfer from FET to mounting surface. Each stage is independently mounted to the housing with two screws at the center of the carrier and rib. An indium shim is clamped and compressed between the carrier and housing to absorb surface roughness and eliminate gaps.

Thermal modeling and computer analysis was used to predict FET channel temperatures. The calculated temperature rise of 54° C gives a device temperature of 134° C for a 90° C mounting surface. The thermal design goal was to prevent the maximum channel temperature from exceeding 150° C for proper

[Continued on page 104]

[From page 102] **FET AMPLIFIER**

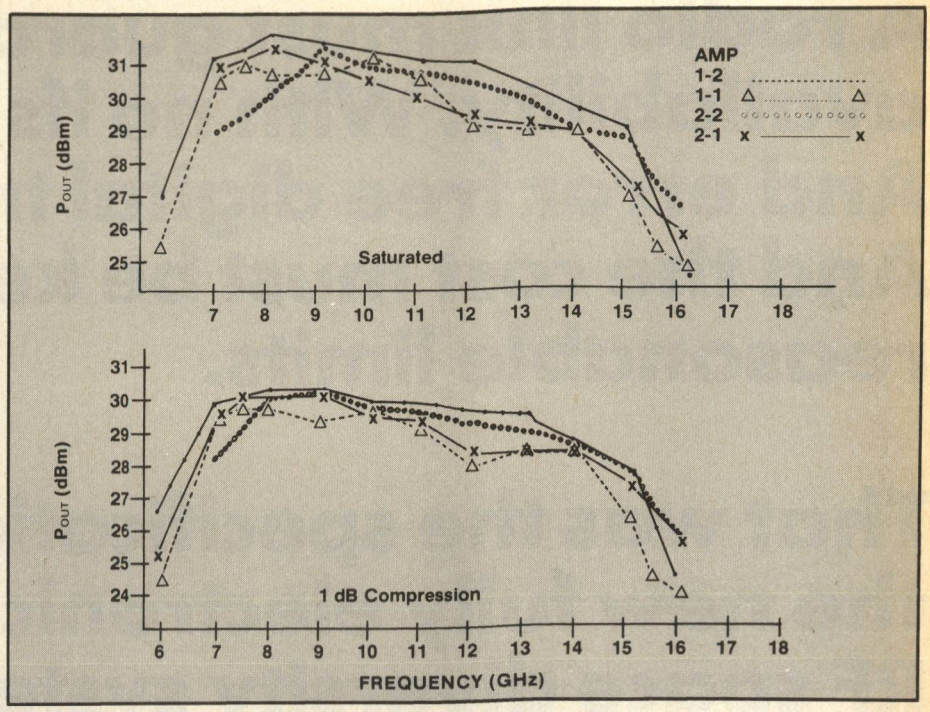

Fig. 5 3 stage 1-watt FET amplifier.
All amplifiers gave excellent power-out.

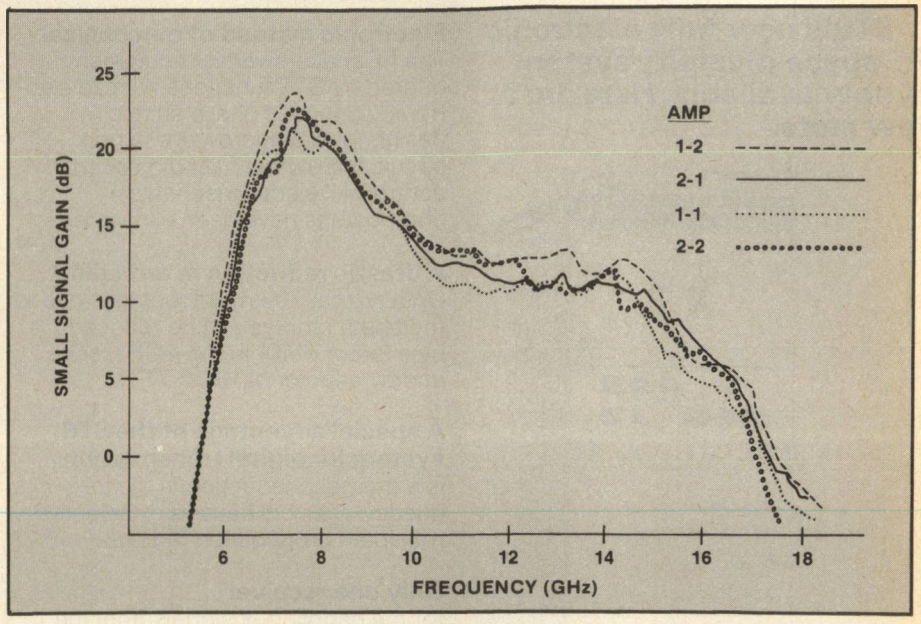

Fig. 6 3 stage 1-watt FET amplifiers
Good gain tracking was exhibited.

reliability. Theoretically the design goal was met but tests were not performed to verify this.

Future amplifiers will have a stiffness requirement for all parts of the stages and housing which will preclude resonant characteristics below 2800 Hz to ensure reliability within MIL-Spec environments.

Test Results

Figure 5 shows the saturated power and the 1 dB compression power for all four amplifiers. Within the 7.0 to 15 GHz bandwidth, the worst case spread in power is 1.7 dB for the saturated case, and 2.1 dB for the 1 dB compression case. These data were obtained using a power divider at the input to the amplifier and separate power meters for input and output power.

Figure 6 shows the small signal gain for each amplifier, the maximum spread being ±1.5 dB. The gain over the band is not flat but this was not considered an important design criteria for the present amplifiers. Future designs will

[Continued on page 106]

[From page 104] **FET AMPLIFIER**

require flat gain.

Figure 7 shows the phase response for each amplifier, within ±25° C at 14 GHz. Up to 13 GHz the spread drops to ±19° C. With amplifier 1 - 2 eliminated the phase spread is ±10° C up to 15 GHz. On the other hand, amplifier 1 - 2 is best in gain and power over most of the band. The output stage of amplifier 1 - 2 seemed to have very good FET's but significantly different tuning when compared to the other amplifiers. Presumably, with additional tuning the phase tracking of these amplifiers could be improved. As FET technology advances, the typical performance will likely approximate amplifier 1 - 2. It is very significant that no tuning was performed after the amplifier stages were assembled into the amplifier housing and that the phase variation with input drive was tested and found to be insignificant.

Figure 8 illustrates the power added efficiency for the four amplifiers, amplifier 1 - 2 being significantly better than the others.

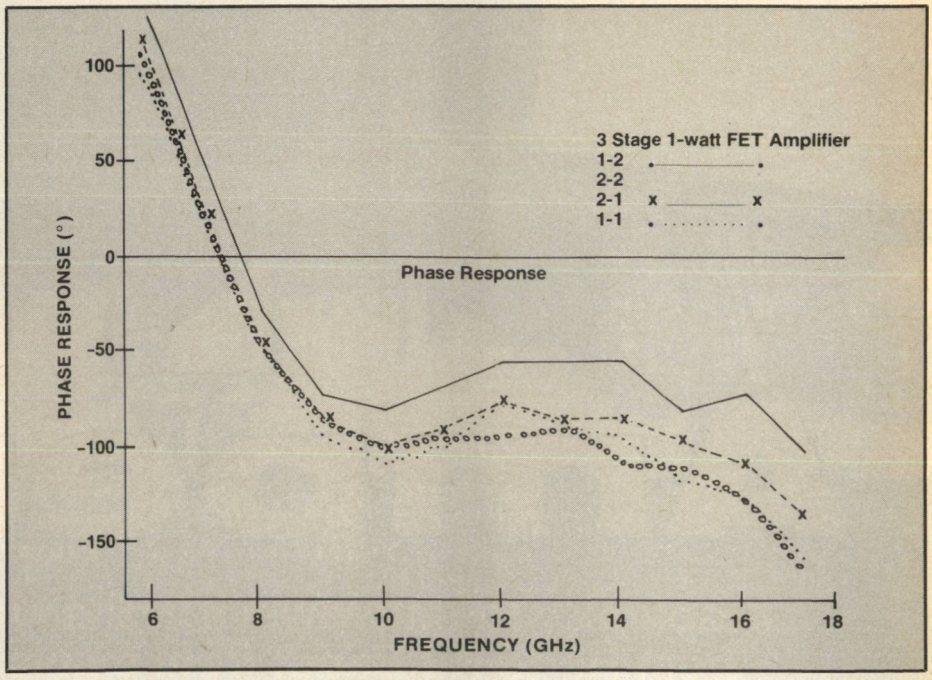

Fig. 7 Amplifier design provides excellent phase tracking.

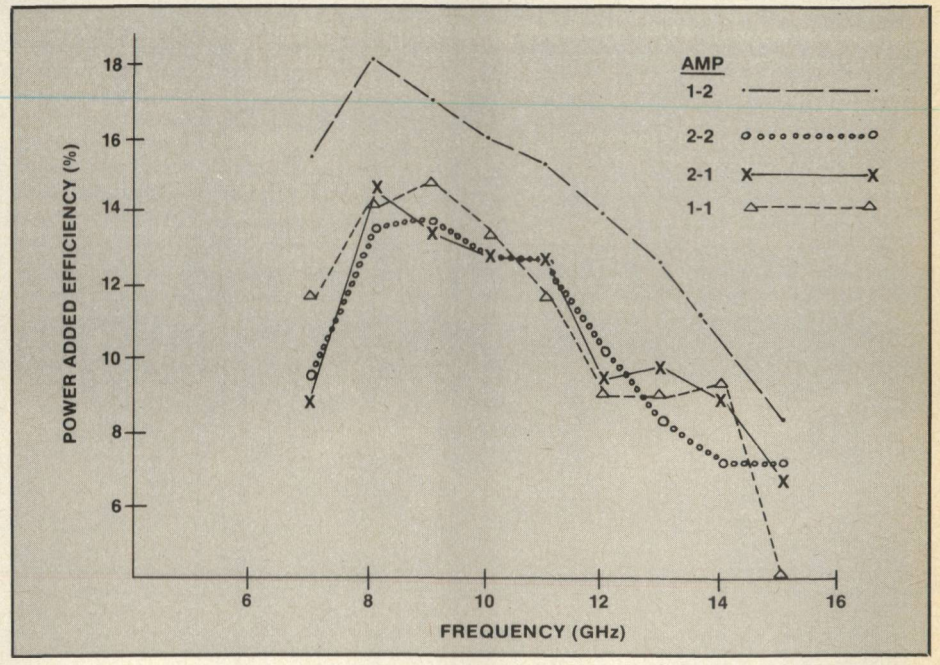

Fig. 8 Power added efficiency vs frequency.

[Continued on page 108]

[From page 106] **FET AMPLIFIER**

Recommendations, Predictions and Conclusions

It is recommended that future designs use four stages of amplification, which can be accomplished in the same length amplifier. This is practical because the length of the matching circuits used herein were intentionally much longer than necessary since these same circuit layouts were used for many purposes. The fourth stage option should provide higher gain, as well as the flexibility to flatten the gain versus frequency.

Based on the performance of amplifier 1 - 2, the performance of future designs can be expected to achieve this behavior routinely, as FET technology improves.

Also, future designs should allow phase tracking to approximately ±10° for the 7 - 15 GHz band, based on 2 factors, first, three out of four amplifiers built tracked within ±10° without any tuning after amplifier assembly, and, second, preliminary calculations show that with slight phase tuning on the present amplifiers they can all be brought to within ±15°. Improved FET reproducibility should reduce this to ±10°.

Four 1-watt miniature amplifiers with instantaneous bandwidths of 7 - 15 GHz have been demonstrated which closely follow theoretical prediction of performance.

It is concluded that very small, light weight and reliable 1-watt, wideband amplifiers presently can be produced. Measured data suggests that future designs will provide gain and phase tracking to within ±1 dB and ±10° respectively.

Acknowledgements

The authors wish to thank Don Sharpe and Toshikazu Tsukii for their encouragement and guidance. The authors are also indebted to Tom Hall for amplifier assembly and Tom Schmidt and Don Holm for testing. Appreciation is given Raytheon's Special Microwave Device Operation for providing the power FET's.

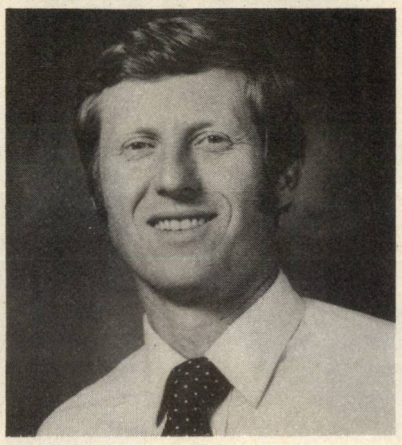

Sherwood A. McOwen joined Raytheon in 1967. He is currently responsible for the microwave analysis design and development of wideband FET amplifiers. Previously, his responsibilities were the design of varactor tuned Impatt and Gunn Oscillators. Also, he has had experience with various types of antenna designs. His work has resulted in two (2) patents. He received his BSEE in 1966 and MSEE in 1967 from the University of California at Santa Barbara.

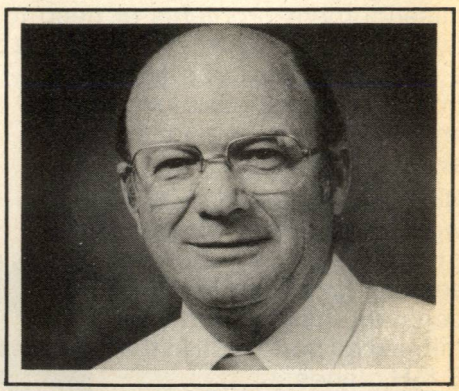

A. Joseph Stein joined Raytheon, ESD, Santa Barbara, California in 1969. He is currently a Principal Engineer responsible for Mechanical Design, Thermal and Structural Analysis of Development and Productized Microelectronics. Previously, he was lead engineer in Product Assurance responsible for thermal management and structural integrity of ESD's Shipboard and Airborne ECM Systems. He received his BSME in 1965 from West Coast University at Los Angeles.

REFERENCES

1. R. L. Comisa, et al., "Broadband Lumped-Element GaAs FET Power Amplifiers," 1981 IEEE MTT-S International Microwave Symposium Digest.
2. V. Sokolov and R. C. Bennett, "A 4.5 W 26 dB Gain FET Power Amplifier at Ku-Bond", 1981 IEEE MTT-S International Microwave Symposium Digest.
3. K. Niclas, et at., "A 12-18 Medium-Power GaAs MESFET Amplifier", IEEE Journal of Solid-State Circuits, Vol. SC-13, No. 4, August 1978.
4. Hua Quen Tserng. et al., "Ultra-Wideband Medium-Power GaAS MESFET Amplifier", 1980 IEEE International Solid-Sate Circuits Conferences Digest, page 166.
5. R. Neidert, et al., "Wide-Band Gallium Arsenide Power MESFET Amplifiers", IEEE Transactions on Microwave Theory and Techniques, Vol. MTT-24, No. 6, June 1976. ■

Open Guiding Structures for mmW Integrated Circuits

Tatsuo Itoh
Dept. of Electrical Engineering
University of Texas
Austin, TX

This paper reviews development, describes potential advantages and discusses problems to be solved in the areas of open guided wave techniques as applied to millimeter-wave integrated circuits. Several waveguide structures are first described with some new insight into the waveguiding mechanism. The construction of passive components, integrated antennas, active components and nonreciprocal devices with open guide structures is then explained in some detail. Discussion will include hybrid approaches where more than one type of waveguide structures are used, such as a combination of dielectric waveguides and printed transmission lines. Also discussed are possible use of unconventional materials such as $LiNbO_3$ and YIG films to realize controlling and nonreciprocal devices based on distributed interactions. Feasiblities of monolithic approaches in which devices and circuits are fabricated in-situ in a semi-conductor material are also discussed.

Introduction

One of the key requirements for the realization of full potentials of millimeterwave systems is the development of low cost integrated circuits.

The millimeter-wave spectrum extending from 30 GHz to 300 GHz lies between the microwave and optical frequency bands. At the lower side of this spectrum, a number of techniques originally developed for microwaves have been extended and applied. Components and circuit arrangement of this type resemble those of microwave circuits. Although rectangular waveguides are still being used, a preferred way is the millimeterwave integrated circuit based upon printed transmission lines and solid state devices such as beam lead diodes. These printed lines include suspended microstrips,[1] fin-lines[2] and even microstrip lines.[3] As the operating frequencies become higher, these "low frequency" techniques face increasing challenge as the performance of the transmission lines and the solid state components generally degrades. It is natural to think if there are alternative approaches to circumvent these problems based on those used in optical circuits. As such, these approaches are more suited at higher millimeter-wave frequencies.

There exist two basic approaches. One is the "quasi-optical" structure which is the millimeter-wave counterpart of the beam optics in which mirrors, polarizers and lenses are used in the free space optical path. This approach is particularly favored for low noise receiver development used for radio astronomy. Many low loss passive components have been developed,[4] and a number of mixers are available including monolithic ones.[5]

The other approach is to form integrated cirucits by means of dielectric waveguides, and is considered as a millimeter-wave replica of integrated optics structure. Dielectric waveguides used in this scheme are desired to be the ones convenient to realize various functional components. Low attenuation constants should not be the sole criterion for selecting waveguides.

In this paper, we focus our attention to the dielectric waveguide technology. Some of the recent progress as well as the problems to be solved will be described. In addition, important problems of interfacing dielectric waveguides with other transmission line structures and solid state devices will be addressed. It is also attempted to compare some accomplishments with those attained with more conventional techniques. Before going into the topics of different components, it should be helpful to briefly describe the wave propagation characteristics in some of the dielectric waveguides.

Waveguiding Phenomena

Many printed circuit transmission lines have characteristics inherent to open structures such as coupling, dispersion and radiation. However, these characteristics are predominantly observed in dielectric waveguides which will be focused in this section. For strongly guided rectangular dielectric rods or image guides (figure 1a), the method developed by Marcatili is the simplest and yet quite accurate for many applications.[7] To improve the accuracy especially near the cutoff, the effective dielectric constant (EDC) method was introduced.[8] Basically, this method provides the EDC to replace Region I in Figure 1a so that we only need to solve the eigenvalue equation for a hyppthetical vertical slab of thickness equal to that of Region I. This technique can be applied to a weakly guiding structure such as the inverted strip dielectric waveguide (Figure 1c).[9] A number of methods have been introduced to further improve the accuracy of analytical results.[10, 11]

It was recently pointed out that interesting and potentially useful leakage phenomena exist in a class of dielectric waveguides.[12, 13] The leakage is in the form of a surface wave propagating in Region II away from the central core Region I and is caused by the mode coupling at the interface between I and II. Obviously, this phenomena *could* occur in a waveguide in which Region II consists of a layered structure which supports surface waves (Figures 1b and c, but not in Figures 1a, d and e). In usual circumstances where the attenuation in the waveguide should be minimized, this phenomenon is undesirable as it contributes to the loss. However, this phenomenon can be used to possibly create a new device such as a directional coupler. It is also interesting to note that, since this leakage phenomenon involves coupling of TE and TM waves, a polarization filter or discriminator may be constructed.

One of the most undesirable characteristics of open waveguides is the radiation loss at the bends and discontinuities. Some attempts have been made to alleviate this radiation problem. One possibility is to use a dielectric waveguide made of a high permittivity material to concentrate more electromagnetic field inside the dielectric rod. A trapped image guide (Figure 1d) consists of a dielectric rod placed in a metal trough so that the radiated field at a bend in a horizontal plane is "reflected" back into the rod by a side wall.[14] As much as 10 dB of loss reduction has been attained at a 90° bend in the Ka band. Recently, a nonradiative dielectric waveguide has been introduced.[15] As shown in Figure 1e, this structure resembles that of an H-guide. However, the separation of the top and bottom conducting plate is such that the field is below cutoff in the air region and above cutoff in the dielectric when the

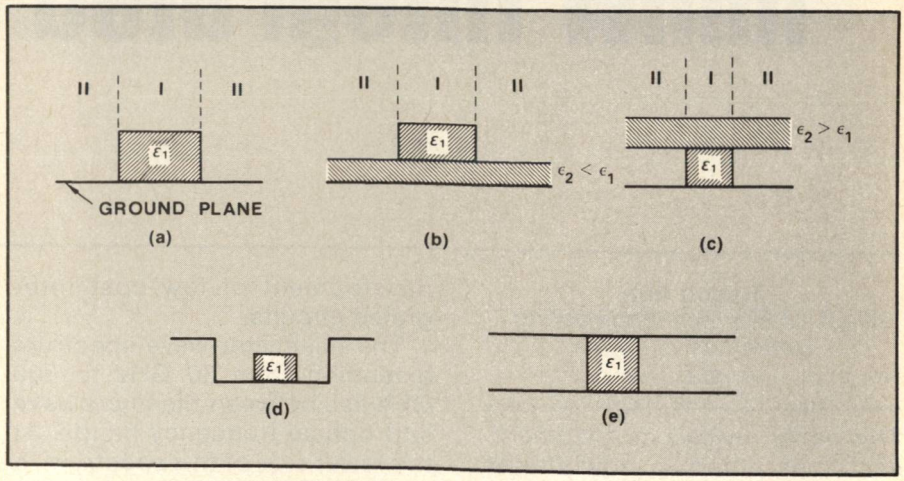

Fig. 1 Cross sections of typical dielectric waveguides.
(a) Image guide, (b) Insulated image guide, (c) Inverted strip dielectric guide, (d) Trapped image guide, (e) Non-radiative dielectric guide.

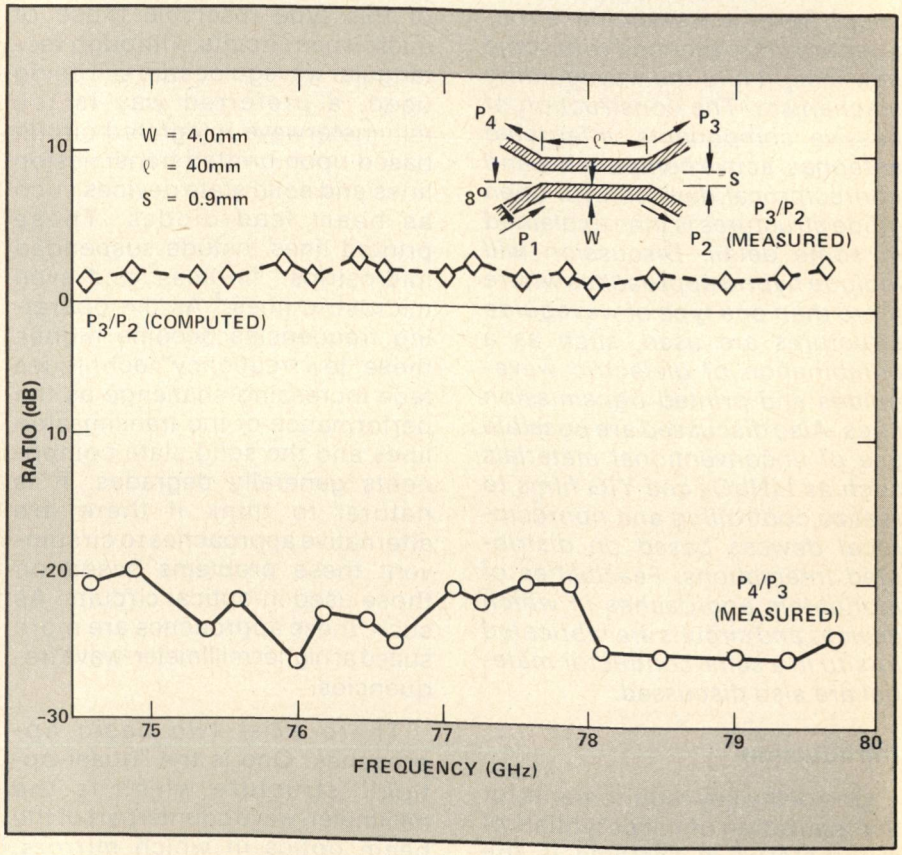

Fig. 2 Computed and measured directional coupler performance.

[Continued on page 116]

guide is excited with its E field parallel to the conducting walls. Because of this below-cutoff nature, no radiation occurs at a bend.

Passive Components

Directional couplers and bandpass filters are examples of passive components developed with dielectric waveguides. A number of works have been done to develop 3 dB hybrid couplers based on distributed coupling principle.[16,17] These couplers are used in many ways including the balanced mixer development. The length L needed for complete power transfer from port 1 to port 3 is given by $L = \pi/B_e - B_o$ where β_e and β_o are respectively the propagation constants of the "even" and "odd" modes in a coupled waveguide. The length required for a 3 dB coupler is one half of L given in this equation. Figure 2 shows a typical example of a 3 db hybrid performance. In general, it is necessary to include coupling effects between the connecting arms for design of these couplers. Therefore, the effective coupling length is longer than that of a parallel coupled portion of the structure.

Bandpass or channel-dropping filters can be constructed with several ring resonators[18] (Figure 3a). Filter characteristics can be tailored by adjusting each ring size and separation between them. The design of ring resonator itself is quite similar to that of a microstrip ring except that the radiation loss is an important consideration for the dielectric ring realized in an image guide type structure. The radiation loss can be substantially reduced in the ring made of the waveguide in Figure 1e. Band reject as high as 30 dB has been attained with this scheme.[19]

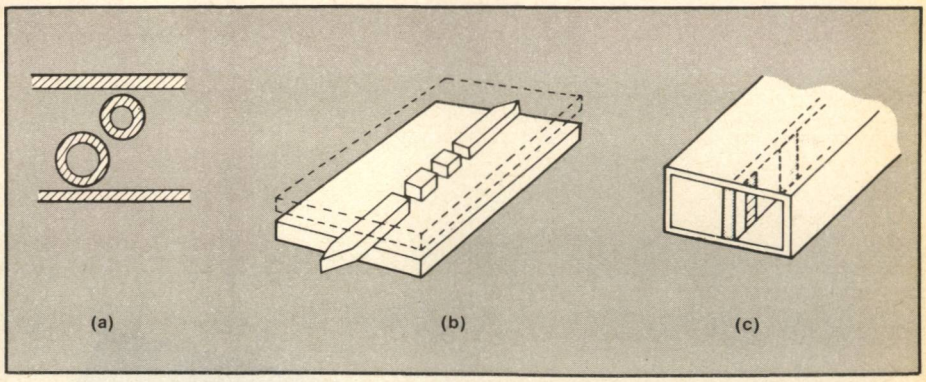

Fig. 3 Filter structures (a) Ring type, (b) Nonradiative dielectric guide type, (c) E-plane filter.

Another interesting structure is a two-pole band pass filter designed at center frequency of 50 GHz using Figure 1e structures (Figure 3b).[19] A pair of dielectric chips is inserted between two radiative dielectric waveguide ports. Since the top and bottom conducting plates are separated by less than half a wavelength, this filter is similar to metal waveguide evanescent mode filters. The reported insertion loss at the center frequency of 50 GHz is 1 dB. It is interesting to compare this filter with fin-line filters made of inductive strips separating resonators (Figure 3c).[20] In this structure, the portions with vertical metal fins are below cutoff. Therefore, the resonators are again connected by way of evanescent fields. The insertion loss at the center frequency was found to be about 0.5 dB at 34 GHz and 1.9 dB at 65 GHz in the case of 3 resonator filters.

In optical structures, a grating can often be used as a frequency selecting device. This idea has also been tried. Figure 4 shows the reflection coefficient of a notch grating created in an inverted strip dielectric guide.[21] Around 15 GHz, a strong reflection appears as the period of the grating was designed to have a stopband there. A more detailed analysis of stopband phenomena in a dielectric waveguide has been performed.[22]

Integrated Antennas

Perhaps one of the most useful features of dielectric waveguide techniques is a possibility of realizing high-performance antennas being integrated with the RF front end. Traveling wave antennas made of dielectric waveguides are especially suited for this purpose. Both surface wave antennas[23] and leaky wave antennas[21, 24] have been developed and tested. The former is essentially a dielectric rod antenna, radiating principally in the endfire direction. The latter is a millimeter-wave replica of the grating coupler used in integrated optics to couple a Gaussian beam into or out of a planar dielectric waveguide. As shown in Figure 5,

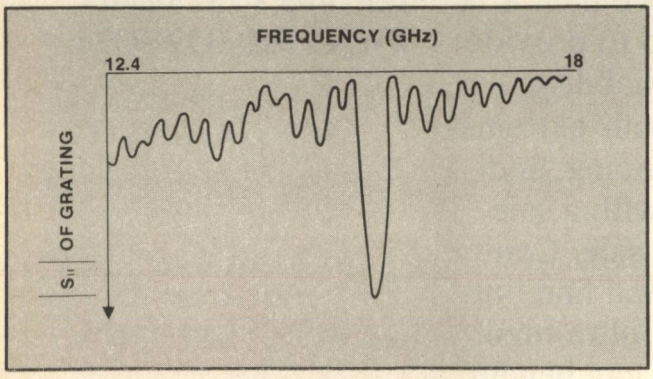

Fig. 4 Input reflection coefficient of a grating.

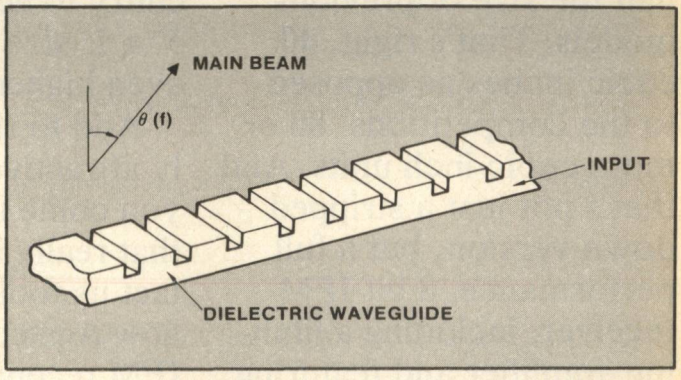

Fig. 5 Typical leaky wave antenna.

[Continued on page 118]

[From page 116] **GUIDING STRUCTURES**

the main beam emerges in a direction by θ from the broadside. Since this angle is a function of the electrical length of the grating period, the beam can be steered by changing this electrical length. The easiest method to accomplish this is to change the frequency. Change in the propagation constant is also possible if a distributed phase shifter is available. (See the section on Nonreciprocal and Control Devices later.) One example is the use of a distributed PIN diode attached on the side wall of the dielectric waveguide grating antenna so that the boundary condition can be modulated by the diode bias.[25] The radiation pattern and the sidelobe level can be controlled by various beam shaping techniques such as the use of tapered section in the first portion of the grating.

An interesting hybrid approach has been taken recently in which an insulated image guide (Figure 1b) is used as a low-loss feeder for a microstrip patch antenna array.[26] As shown in Figure 6, the radiating elements are made of resonant microstrip patches. For a longer array, the feeder loss is much smaller in this scheme than in the conventional microstrip array with microstrip feed structures. Other advantages include a greater flexibility in controlling and shaping the radiation pattern and ease of fabrication of a rather complex array configuration. More attention should be paid to this type of hybrid approach because it may open up new possibilities and provide solutions to the problems which cannot be solved by printed line or dielectric waveguide techniques individually.

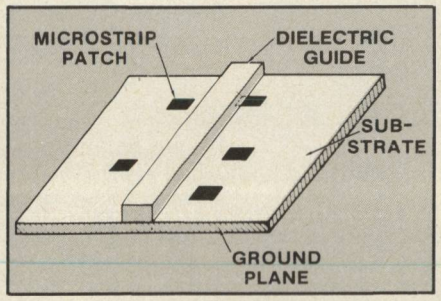

Fig. 6 Microstrip array excited by a dielectric guide.

Active Components

Development of active components is more difficult than other components. This is mainly due to the inherent nature of open waveguide structures. Any discontinuity arising out of implementation of solid state devices causes radiation. Therefore, the device sees an impedance consisting of two resistive parts, one due to radiation and another due to the loading circuit, as well as the reactive part. These junction problems need to be characterized more accurately. Many earlier active component fabrications avoided direct confrontation with this problem by providing a mechanical shield to the device. Gunn oscillators and self-oscillating mixers have been developed with an image guide in which a Gunn diode is inserted vertically and a tuning metal disk is on the top surface to control the radiation loss.[27,28]

The distributed feedback con-

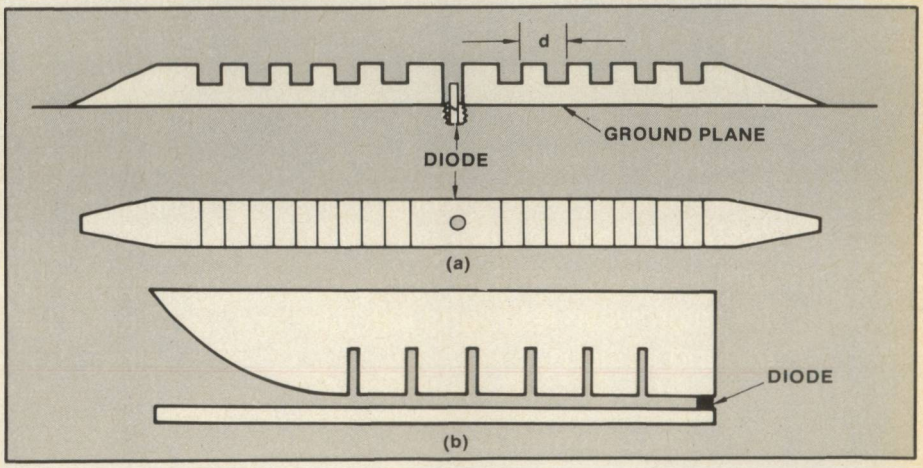

Fig. 7 Distributed reflection oscillator (a) Dielectric guide, (b) Fin-line.

[Continued on page 120]

[From page 118] **GUIDING STRUCTURES**

cept originally employed in semiconductor laser development has been applied to a Ku-band Gunn oscillator in an image guide[29] (Figure 7a). The grating structures on both sides of the diode provide frequency selective feedback so that the diode is provided with a high Q cavity. Although the output was rather low due to radiation loss, the oscillation frequency was fairly stable. The grating structure has also been used as a distributed feedback mechanism for a Gunn oscillator in a fin-line arrangement[30] (Figure 7b). Using a 250 μm RT/Duroid fin-line substrate and an MA Type 49172-138 Gunn diode, the oscillation frequency of the Ka-band oscillator agreed with the theory within 2%.

A balanced mixer has been developed with a 3 dB hybrid made of boron nitride image guides and with GaAs beam lead diodes.[31] Metal strip lines are printed on the top surface of the image guide in order to provide bias input and IF output to the diodes. A typical noise figure at 60 GHz was 13 dB including the IF amplifier noise figure of 3.5 dB. This figure compares reasonably well with the one attainable in a balanced mixer developed with printed circuit techniques. For instance, planar balanced mixers made of fin-lines and suspended microstrip lines on RT/Duriod substrate exhibit the typical conversion loss of 7 dB at Ka-band and 10 dB at w-band.[32]

A hybrid constuction of a quasi-optical detector has been accomplished in which a dielectric surface wave antenna is combined with a planar slot detector.[3] Bismuth bolometers have been installed in dielectric waveguide structures by way of stripline type V-couplers.[34] It is expected that these approaches will eventually allow monolithic construction of reciever front ends with Si or GaAs material.

As discussed in the paragraph concerning Gunn oscillators, direct implementation of devices in a dielectric waveguide may not attempts have been made to develop hybrid structures in which both dielectric waveguides and printed lines are coupled and a device is installed in a planar line environment. Solbach used slots created in an image guide with metallized dielectric substrate for a detector mount.[35] This metalized substrate is used as the ground plane of the image guide and at the same time for accomodating the low frequency coplanar line connecting the slot and the output patch. A detector diode is installed in the slot and the image guide rod is placed on top of it.

Nonreciprocal and Control Devices

Relatively few works have been done in the area of nonreciprocal device development. A Y-junction circulator operating in the dielectric waveguide medium was recently developed at 35 GHz with 8% bandwidth.[36] The device is made of NiZn ferrite as the gyromagnetic material and magnesium titanate as the dielectric waveguide. The latter is physically supported on a Rexolite plate. The insertion loss was less than 1 dB and the isolation more than 15

[Continued on page 122]

dB from 32 to 34.7 GHz.

It is generally recognized that as the frequency increases, performance of ferrite devices deteriorate due to increased material loss and reduced off-diagonal permeability tensor elements. To make maximum use of weak nonreciprocity, use of distributed structure may be a possible solution. A field displacement isolator was tested in which a resistive card is placed near a ferrite loaded dielectric waveguide.[37] When a dc magnetic field is applied, the field displacement occurs. The wave propagating in the direction for which the displacement is toward the resistive card is absorbed more than the wave propagating in the opposite direction for which the shift is away from the card (see Figure 8). The problem of this structure is that the insertion loss increases if an increase in isolation is attempted, because the lossy film affects the waves shifted in either direction.

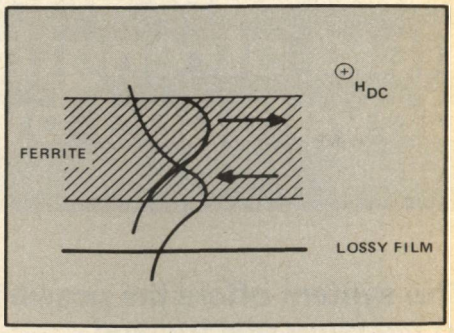

Fig. 8 Field displacement isolator.

Two new types of distributed nonreciprocal devices have been proposed recently.[38, 39] They rely on nonreciprocity of the propagation constants in a ferrite dielectric waveguide with nonsymmetric cross section. In such structures, when the field is displaced by a dc magnetic field, the propagation constants of the guided waves traveling in the opposite directions are different as the fields of these waves are transversely displaced in different directions. When a grating with an appropriate period is created on this nonsymmetric ferrite loaded dielectric guide, it is possible within a certain frequency range to make the wave propagating in one direction leaky, whereas, the one in the opposite direction is still guided as a surface wave. In this way, a distributed isolator can be constructed.[38]

Another structure which looks more promising than the grating type is the one based on nonreciprocal coupling phenomena. As discussed above, the propagation constants of the wave traveling in opposite directions in a nonsymmetric ferrite waveguide are different, say β_f^+ and β_f^-. Suppose we create an isotropic

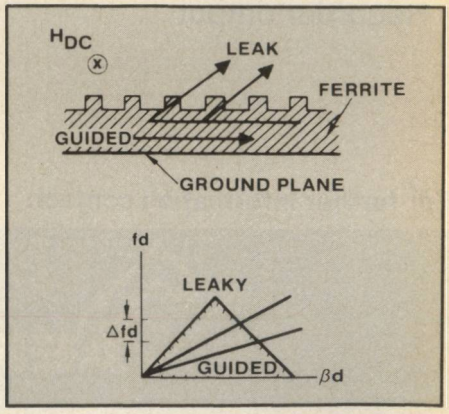

Fig. 9 Nonreciprocal leakage isolator.

[Continued on page 124]

[From page 122] **GUIDING STRUCTURES**

dielectric waveguide with its propagation constant β_d (independent of the direction of propagation) equal to that of one of the waves in the ferrite guide, say β_f^- is chosen, and place this guide near the nonsymmetric ferrite guide. The distributed coupling takes place for only one direction as indicated in Figure 10. Therefore, the wave propagating in one direction in the isotropic guide is diverted into the ferrite guide and absorbed by a termination or by the ferrite loss itself. On the other hand, the wave propagating in the opposite direction does not couple into the ferrite and is little affected. In this manner we can create an isolator or a circulator.[39, 40] A design example for a 200 GHz device indicated the insertion loss of 1 dB and the 15 dB isolation bandwidth of 5 GHz if a metal backed ferrite ($4\pi M_s$ = 5kG, ε = 10-j0.005) layer of 190 μm and a dielectric layer (ε = 10.3-j0.005) of 180 μm are coupled through a low dielectric layer (ε = 2) of 670 μm. The device length of 15 mm was used for calculation.[39] High purity epitaxial YIG films deposited on gadolinium gallium garnet may be used for realization of this distributed isolator.

The surface plasmon effect in a high purity GaAs may be another candidate for distributed nonreciprocal devices. Recent modeling studies indicated sufficient promise for development of such devices.[41]

In the area of control devices, we have already mentioned the distributed PIN diode in conjunction with scannable dielectric antennas.[25] The electrooptic effect in crystals has been used to create modulators and phase shifters in optical circuits. Recently, the feasibility of using $LiNbO_3$ and $LiTaO_3$ at 94 GHz has been studied.[42] Dielectric waveguide structures containing these electrooptic materials may be an interesting topic of study.

Conclusion

In this paper, we reviewed recent advances in open waveguide structures as applied to millimeter-wave integrated circuits by way of illustrating several examples. Here, we try to address some of the important areas of further investigation to make the dielectric waveguide technique more practical.

— Interfacing problems

Hybrid structures in which both dielectric waveguides and printed transmission lines are used may alleviate some of the problems which otherwise are difficult to handle. We have shown several examples in this paper. Investigation of this approach is especially important for active component development, because the device must be supplied with at least two conductors for dc bias or low frequency signals.

— Active devices

Many active devices available today have been developed for metal waveguides and printed circuit structures. It is easier to build dielectric waveguide active components if there are semi-conductor devices created for this technique. Perhaps, the monolithic approach should be looked into as the devices can be created in situ in the dielectric waveguide made of semiconductor.

— Optimization of waveguide structure

As the wave interactions with matters generally become weaker with increasing frequencies, we need to find the waveguide structure which makes the best use of phenomena without significantly increasing the loss. This study is especially important in the area of

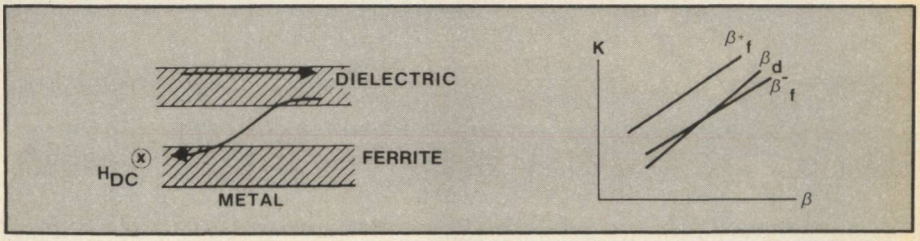

Fig.10 Nonreciprocal coupling isolator.

distributed nonreciprocal and control devices.

— Fabrication techniques

Most of the dielectric waveguide structures require some forms of machining process. For greater accuracy, other fabrication techniques should be adopted. At higher frequencies, the size becomes smaller and non-mechanical fabrication may be more easily applied.

There are other problems including better materials and more accurate solutions for waveguide junction problems.

Finally, it is not intended that this paper comprehensively cover all the works which have appeared in literature. There are many excellent works not referenced here. Also, some opinions expressed in the paper are quite subjective.

REFERENCES

1. Schneider, M. V. "Millimeter-wave, Integrated Circuits," 1973 IEEE MTT-S International Microwave Symposium, Boulder, CO, June 1973.
2. Meier, P. J. "Millimeter Integrated Circuits, Suspended in the E-plane of Rectangular Waveguide," *IEEE Trans. Microwave Theory and Techniques*, Vol. MTT-26, pp. 726-733, October 1978.
3. Scarman, R. E., P. L. Lowbridge and T. H. Oxley, "Hybrid-Microstrip Millimeter Wavelength Mixers," 11th European Microwave Conference, Amsterdam, The Netherlands, September 1981.
4. Nakajima, N. and R. Watanobe, "A Quasioptical Circuit Technology for Short Millimeter-Wavelength Multiplexers," *IEEE Trans. Microwave Theory and Techniques*, Vol. MTT-29, pp. 897-905, September 1981.
5. Clifton, B. J., G. D. Alley, R. A. Murphy, W. J. Piacentini, I. H. Mrockowski and W. Macropoulos, "Cooled Low Noise GaAs Monolithic Mixers at 110 GHz," 1981 IEEE MTT-S International Microwave Symposium, Los Angeles, CA, June 1981.
6. Itoh, T, "Dielectric Waveguide-Type Millimeter-wave Integrated Circuits," *Infrared and Millimeter Waves*, Vol. 4, ed. K. J. Button and J. C. Wiltse, pp. 199-273, Academic Press, New York, NY, 1981.
7. Marcatili, E. A. J., "Dielectric Rectangular Waveguide and Directional Coupler for Integrated Optics," *Bell Syst. Tech. J.*, Vol 48, pp. 2079-2102, September 1969.
8. Knox, R. M. and P. P. Toulios, "Integrated Circuits for the Millimeter through optical Frequency Range," in Proc. Symp. Submillimeter Waves, New York, March 31-April 2, 1970.
9. Itoh, T., "Inverted Strip Dielectric Waveguide for Millimeter-Wave Integrated Circuits," *IEEE Trans. Microwave Theory and Techniques*, Vol. MTT-24, pp. 821-827, November 1976.
10. Solbach, K. and J. Wolff, "The Electromganetic Fields and Phase Constants of Dielectric Image Lines," *IEEE*

[Continued on page 126]

[From page 125] **GUIDING STRUCTURES**

Trans. Microwave Theory and Techniques, Vol. MTT-26, pp. 266-274, April 1978.

11. Mittra, R., Y. L. Hou and V. Tamnejad, "Analysis of Open Dielectric Waveguides Using Mode-Matching Technique and Variational Methods," *IEEE Trans. Microwave Theory and Techniques*, Vol. MTT-28, pp. 36-43, January 1980.
12. Peng, S. T., and A. A. Oliner, "Guidance and Leakage Properties of a Class of Open Dielectric Waveguides," *IEEE Trans. Microwave Theory and Techniques*, Vol. MTT 29, pp. 843-869, September 1981.
13. Ogusu, K. and I. Tanaka, "Optical Strip Waveguide: An Experiment," *Appl. Opt.*, Vol. 19, pp. 3322-3325, Oct. 1, 1980.
14. Itoh, T. and B. Adelseck, "Trapped image guide for milimeter-wave circuits," *IEEE Trans. Microwave Theory and Techniques*, Vol. MTT-28, pp. 1433-1436, December 1980.
15. Yoneyama, T., and S. Nishida, "Nonradiative Dielectric Waveguide for Millimeter-wave Integrated Circuits," *IEEE Trans. Microwave Theory and Techniques*, Vol. MTT-29, pp. 1188-1192, November 1981.
16. Rudokas, R. and T. Itoh, "Passive Millimeter-Wave IC Components Made of Inverted Strip Dielectric Waveguides," *IEEE Trans. Microwave Theory and Techniques*, Vol. MTT-24, pp. 978-981, December 1976.
17. Paul, J. A., and P. C. H. Yen, "Millimeter-Wave Passive Components and Six-Port Network Analyzer in Dielectric Waveguide," *IEEE Trans. Microwave Theory and Techniques*, Vol. MTT-29, pp. 948-953, September 1981.
18. Aylward, M. J. and N. Williams, "The design of Multi-pole Filters for use in Millimeter Wave Image Line Integrated Circuits," 8th European Microwave Conference, Paris, France, September 1978.
19. Yoneyama, T. and S. Nishida, "Nonradiative Dielectric Waveguide Circuit Components," Sixth Int. Conf. Infrared and Millimeter Waves, Miami Beach, FL, December 1981.
20. Arndt, F., J. Bornemann, D. Grauerholz and R. Vahldieck, "Low Insertion Loss Fin-Line Filters for Millimeter-Wave Applications," 11th European Microwave Conf. Amsterdam, The Netherlands, September 1981.
21. Itoh, T. "Applications of Gratings in a Dielectric Waveguide for Leaky-Wave Antennas and Band-Reject Filters," *IEEE Trans. Microwave Theory and Technique*, Vol. MTT-25, pp. 1134-1138, December 1977.
22. Ohira, T., M. Tsutsumi and N. Kumagai, "Perturbation Analysis on the corrugated Dielectric Waveguide with Application to Millimeter-Wave filters," Trans. Inst. Elec. Comm. Eng. of Japan, Vol. J64-B, pp. 659-665, July 1981.
23. Williams, N. and A. W. Rudge, "Millimeter-Wave INSULAR Guide Frequency Scanned Array," 1977 IEEE MTT-S International Microwave Symposium, San Diego, CA, June 1977.
24. Klohn, K. L., R. E. Horn, H. Jacobs and E. Freibergs, "Silicon Waveguide Frequency Scanning Linear Array Antenna," *IEEE Trans. Microwave Theory and Techniques*, Vol. MTT-26 pp. 764-773.
25. Horn, R. E., H. Jacobs, E. Freibergs and K. L. Klohn, "Electronic Modulated Beam-Steerable Silicon Waveguide Array Antenna," *IEEE Trans. Microwave Theory and Techniques*, Vol. MTT-28, pp. 647-653, June 1980.
26. Henderson, A., E. England and J. R. James, "New Low-Loss Millimeter-Wave Hybrid Microstrip Antenna Array," 11th European Microwave Conf., Amsterdam, The Netherlands, September 1981.
27. Jacobs, H., G. Novick, C. M. LoCasico and M. M. Chrepta, "Measurement of Guided Wavelength in Rectangular Dielectric Waveguide," *IEEE Trans. Microwave Theory and Techniques*, Vol. MTT-24, pp. 815-820, November 1976.
28. Dixon, S. and H. Jacobs, "Millimeter-Wave InP Image LIne Self-Mixing Gunn Oscillator," *IEEE Trans. Microwave Theory and Techniques*, Vol. MTT-29, pp. 958-961, September 1981.
29. Song, B. S., and T. Itoh, "Distributed Bragg Reflection Dielectric Waveguide Oscillators," *IEEE Trans. Microwave Theory and Techniques*, Vol. MTT-27, pp. 1019-1022, December 1979.
30. Hofmann, H., "MM-Wave Gunn Oscillator with Distributed Feedback Fin-Line Circuit," 1980 IEEE MTT-S International Microwave Symposium, Washington, D.C, May 1980.
31. Paul, J. A., and Y. W. Chang, "Millimeter-Wave Image-Guide Integrated Passive Devices," *IEEE Trans. Microwave Theory and Techniques*, Vol. MTT-26, pp. 751-754, October 1978.
32. Ball, D. W., L. Q. Bui and C. Warzman, "Low Cost Broadband Integrated Millimeter Receivers," in this Issue.
33. Yen, P., J. A. Paul and T. Itoh, Millimeter-wave Planar Slot Antennas with Dielectric Feeds," 1981 IEEE MTT-S International Microwave Symposium, Los Angeles, CA, June 1981.
34. Rutledge, D. B., S. E. Schwarz, T. L. Hwang, D. J. Angelakos, K. K. Mei and S. Yokota, "Antennas and Waveguides for Far-Infrared Integrated Circuits," *IEEE J. Quantum Electronics*, Vol. QE-16, pp. 508-516.
35. Solbach, K. "Millimeter-wave Dielectric Image Line Detector-Circuit Employing Etched Slot Structure," *IEEE Trans. Microwave Theory and Techniques*, Vol. MTT-29, pp. 953-957, September 1981.
36. Stern, R. A. and R. W. Babbit, "Dielectric Waveguide Circulator," *Int. J. Infrared and Millimeter Waves*, Vol. 3, pp. 11-18, January 1981.
37. Nanda, V. P. "A New Form of Ferrite Device for Millimeter-wave Integrated Circuits," *IEEE Trans. Microwaves Theory and Techniques*, Vol. MTT-24, pp. 876-879, November 1976.
38. Araki, K., B. S. Song and T. Itoh, "Nonreciprocal Effects In An Open Dielectric Waveguide with Grating Structures," 1980 IEEE MTT-S International Microwave Symposium, Washington, D.C., May 1980.
39. Awai, I. and T. Itoh, "Coupled-mode Theory Analysis of Distributed Nonreciprocal Microwave Theory and Techniques, Vol.MTT-29, pp. 1077-1087, October 1981.
40. Muraguchi, M. and Y. Naito, "Nonreciprocal Devices in Open-boundary Structures for Millimeter-wave Integrated Circuits," *Trans. Inst. Elec. Comm. Eng. of Japan*, Vol. J64-B, pp. 604-611, July 1981.
41. Bolle, D. M., and S. H. Talisa, "Fundamental Considerations in Millimeter and Near-Millimeter Component Design Employing Magnetoplasmons," *IEEE Trans. Microwave Theory and Techniques*, Vol. MTT-29, pp. 916-923, Sept. 1981.
42. Klein, M. B., "Phase Shifting at 94 GHz Using the Electrooptic Effect in Bulk Crystals," *Int. J. Infrared and Millimeter Waves*, Vol. 2, pp. 239-246, March 1981.

L-Band Quadriphase Phase Shift Keyed Modulator

R.K. Shoho and M.H. Arain

Collins Communications Systems Division
Defense Electronics Operations
Rockwell International Corporation

Introduction

The Integrated Operational Nuclear Detonation (NUDET) Detection System (IONDS) Global Segment (IGS) is a NUDET detection and digital communication network which provides space surveillance capability for NUDETS. The space related portion of IGS is a part of the Global Positioning System satellite. The L-Band transmitter developed and space qualified for this system incorporates the quadriphase modulator that is the subject of this paper. The paper describes a useful circuit to provide four diode switched quadrature spaced output phase signals depending on the bias applied to the diodes. The important aspect of the design is that unlike a conventional 2-bit phase shifter (which would consist of the cascade combination of a 90 degree bit and a 180 degree bit) this design utilizes 180 degree bit phase shifters which are identical and achieve the 90 degree offset between them by virtue of the inherent 90 degree phase difference (which is frequency insensitive) of the backward wave coupler. In this case the backward wave coupler is realized as a Lange, interdigitated microstrip device. The inherent 3 dB power loss with this configuration is of no consequence since amplitude leveling by an AGC circuit preceding the QPSK modulator is used and is an acceptable tradeoff for phase stability purposes. Figure 1 shows this transmitter and the quadriphase modulator can be seen in the lower right-hand corner.

The quadriphase modulator is designed for high data rate (10 megabit) digital input. It can be used either in the bi-phase shift keyed (BPSK) or quadriphase (QPSK) mode. For BPSK operation, the input carrier at 1.381 GHz is modulated by identical data inputs at the modulation input ports, Data 1 and Data 2. The output carrier phase, relative to the input carrier, is phase shifted by 0 to 180 degrees, depending upon the data input.

For QPSK operation, the input carrier is modulated by two independent data channels at the Data 1 and Data 2 input ports. Each data channel consists of a two-level biphase pulse code. The output carrier phase, relative to the input, is phase shifted by 0, 90, 180 or 270 degrees, depending on the properties of the data input.

In the primary on-orbit operational mode, Data 1 is at 10.23 megabit and Data 2 is at 1.023 megabit.

Basic Design Considerations

The QPSK modulator consists of three dB quadrature hybrids, one Wilkinson power combiner, four PIN diodes and two TTL controlled drivers. Two ports of two of the hybrids are loaded with shunt mounted PIN diodes followed by a shorted quarter wave transmission line. The phase shifting is achieved by switching the diodes "on" and "off."

To clearly understand the operation of the QPSK modulator, the phase shifting effect of the quadrature hybrid loaded with PIN diodes and their relationship with the shorted quarter wave transmission lines is briefly reviewed.

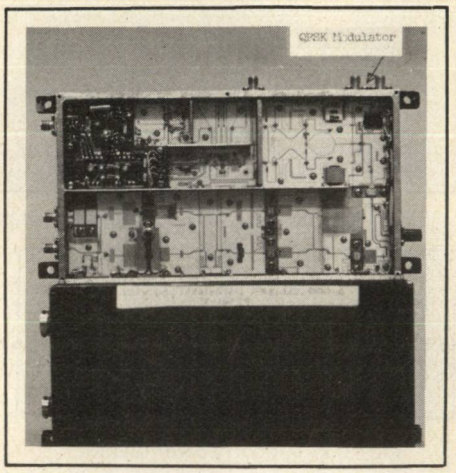

Fig. 1 L_3 transmitter.

Consider the network shown in Figure 2 where an ideal 3 dB quadrature coupler[1] and two identical circuits, each consisting of a shunt mounted PIN diode followed by a $\lambda/4$ shorted stub, connected to Ports 3 and 4. Defining S_{11} as the reflection coefficient of the circuits connected to Port 3 and 4 and under the conditions when the coupling coefficient K of the coupler is .707, the RF output at Port 2 is depicted and summarized in Table 1. That is, when the diodes switch from open to short circuit, the reflection coefficient

TABLE I

DESCRIPTION OF OPERATION OF HYBRID COUPLED PHASE SHIFTER

Diode State	S_{11} Refl. coeff. of Diode Term. Stub	Input Signal at Port 1	Output Signal at Port 2
Diodes ON	$1 \angle 180°$	$1 \angle 0°$	$1 \angle 90°$
Diodes OFF	$1 \angle 0°$	$1 \angle 0°$	$1 \angle -90°$

S_{11} of diode terminated stub transforms from $1\angle 180°$ when the diodes are on, to $1\angle 0°$ when they are off. Viewing from the output (Port 2) S_{11} is transformed to $1\angle 90°$ when the diodes are on, and $1\angle -90°$ when the diodes are off.

The output of the QPSK modulator utilizes a Wilkinson hybrid,[2] a 3-port network of the form shown in Figure 3. Wilkinson hybrid is characterized as follows. An RF input at Port 1 divides equally between Ports 2 and 3 by the virtue of the symmetry. The resulting fields of these two ports are equal in pnase and amplitude. Also, no power is dissipated in resistor R when matched loads are connected to the Ports 2 and 3. An RF input at Port 2 divides equally between Port 1 and the resistor. The halved signal appearing at Port 1 is delayed by 90°, while the other half is lost in the resistor. Correspondingly, an RF input at Port 3 propagates to Port 1 with a phase lag of 90° while the other half is dissipated in the resistor. A table of the amplitude and phase relationship of various ports is shown in Table 2.

Figure 4 shows a schematic of the QPSK modulator. The RF signal out of this modulator is rapidly phase-shifted between one of four orthogonal positions by the binary data word supplied by the logic network to the two TTL controlled drivers.[3]

To clearly follow the phasing of the QPSK modulator, refer to Figure 4 and trace the signal from the input to the output. At the input, assume a signal of normalized unity at zero phase. This signal is divided equally by the 3 dB quadrature hybrid 1 and the signal appearing at Ports A and B are $.707\angle 0°$ and $.707\angle -90°$. Continuing the flow toward the output from the right-hand side (RHS), the signal at Port A is divided equally by hybrid 3. Assume both D3 and D4 are turned "on". The signal component at D4 is $.5\angle 0°$, but upon conversion by the shorted diode termination, it is $.5\angle -180°$. Propagating toward Port C, it is $.353\angle -270°$. At D3, the signal component from A is reduced to $.5\angle -90°$. D3 being a shorted diode termination, adds -180° so that it is $.5\angle -270°$. Propagating toward the output to Port C, it is $.353\angle -270°$. Summing both signal components from D3 and D4, we get $.707\angle -270°$ at Port C. Finally, dividing equally at Port C between the resistor and the output Port E, the signal component from the (RHS) equals $.5<0$.

Following the same procedure through the left-hand side (LHS) except assuming D1 and D2 are "off", the signal output at Port E from the LHS equals $.5\angle -270°$. Summing both signal components from LHS and RHS, we get $.707\angle 45°$.

In the cases where the diodes are biased "off", the shorted ter-

TABLE II

AMPLITUDE AND PHASE RELATIONSHIP AT VARIOUS PORTS

Input Port	Port 1	Port 2	Port 3
Port 1	$1\angle 0°$	$.707\angle -90°$	$.707\angle -90°$
PORT 2	$.707\angle -90°$	$1\angle 0°$	—
PORT 3	$.707\angle -90°$	—	$1\angle 0°$

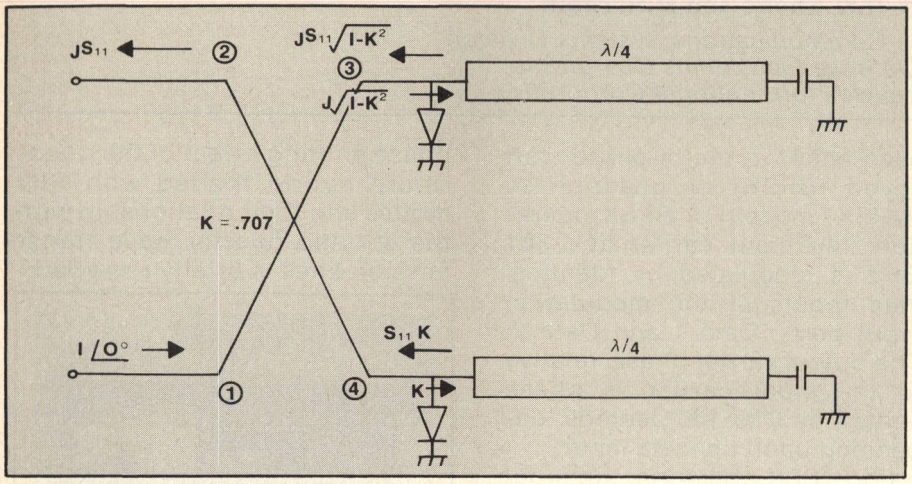

Fig. 2 Block diagram of hybrid coupled phase shifter.

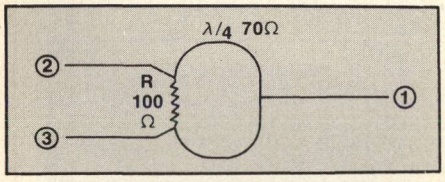

Fig. 3 Wilkinson power divider.

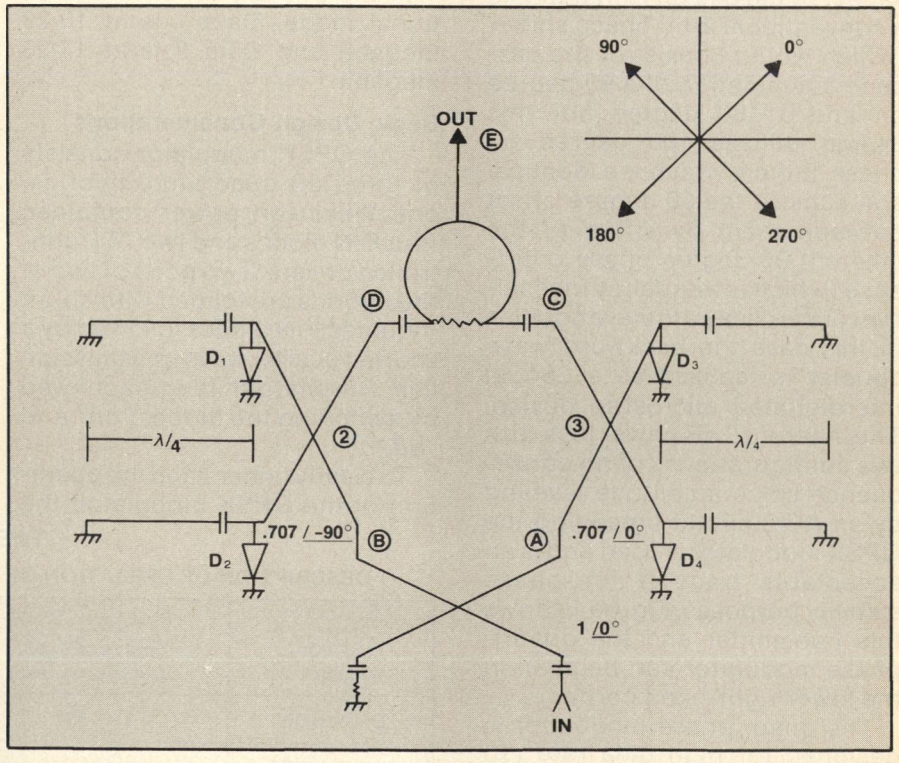

Fig. 4 QPSK modulator block diagram.

[Continued on page 134]

mination is lagged an additional 180°. D1 and D2 are paired, as are D3 and D4, and driven by the TTL controlled driver A1 and A2, respectively, shown in Figure 5. A table of magnitude and phase conditions at various ports is summarized in Table 3.

IGS's QSPK Modulator Circuit

The QSPK modulator shown in Figure 5 was fabricated on microstrip on a 2" x 2" x .025" alumina substrate. The input RF frequency is L-band at +10 dBm level. The PIN diodes are fast switching. HP-3305 ceramic package device requiring low drive current supplied by the ultra high-speed diode drivers at 10.23 MHz bit rate.

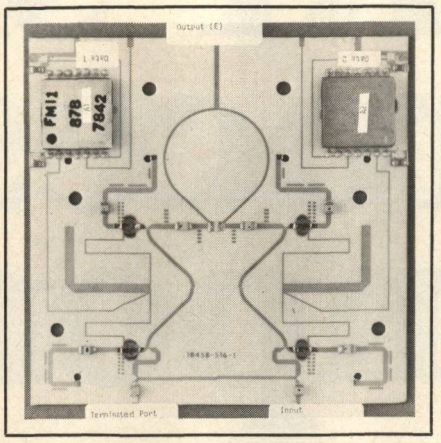

Fig. 5 QPSK modulator fabricated on microstrip of alumina substrate.

TABLE III

DESCRIPTION OF QPSK MODULATOR OPERATION

	Diodes On/Off	Voltage at E From D	Voltage at E From C	Voltage at E
1	All Diodes Off	.5 / -270°	.5 / -180°	.707 / 135°
2	RHS Diodes On	.5 / -270°	.5 / 0°	.707 /45°
3	LHS Diodes On	.5 / -90°	.5 / -180°	.707 / -135°
4	All Diodes On	.5 / - 90°	.5 / 0°	.707 / -45°

QPSK MODULATOR TRANSMITTER
10458-516-1

Freq MHz	Phase 2 Rel 1	Phase 3 Rel 1	Phase 4 Rel 1	RTN Loss Meas 1	RTN Loss Meas 2	RTN Loss Meas 3
1376.050	179.55	91.34	-90.33	17.48	14.27	20.26
1377.050	179.40	91.31	-90.38	17.49	14.25	20.28
1378.050	179.13	91.16	-90.55	17.49	14.26	20.30
1379.050	179.00	91.08	-90.63	17.51	14.25	20.32
1380.050	178.66	90.98	-90.77	17.52	14.26	20.34
1381.050	178.37	90.76	-90.94	17.54	14.27	20.36
1382.050	178.16	90.67	-91.10	17.56	14.28	20.39
1383.050	177.97	90.60	-91.07	17.59	14.29	20.42
1384.050	177.73	90.47	-91.24	17.63	14.31	20.44
1385.050	177.50	90.29	-91.42	17.67	14.32	20.46
1386.050	177.30	90.28	-91.49	17.69	14.34	20.49

Freq MHz	RTN Loss Meas 4	Loss-DB Meas 1	Loss-DB Meas 2	Loss-DB Meas 3	Loss-DB Meas 4
1376.050	16.67	4.37	4.19	4.42	4.33
1377.050	16.62	4.38	4.20	4.41	4.35
1378.050	16.58	4.39	4.21	4.41	4.39
1379.050	16.54	4.40	4.21	4.39	4.40
1380.050	16.52	4.41	4.23	4.38	4.43
1381.050	16.48	4.41	4.22	4.37	4.46
1382.050	16.46	4.41	4.24	4.35	4.49
1383.050	16.43	4.42	4.24	4.34	4.50
1384.050	16.41	4.41	4.25	4.32	4.53
1385.050	16.39	4.42	4.24	4.30	4.54
1386.050	16.37	4.41	4.25	4.28	4.57

REF PLANE EXT (CM): REFL = .00, TRAN = .00

Fig. 6 Quadriphase performance to less than 2° from the desired quad phase.

In the previous analysis, it was assumed that the transmission line, hybrid balance, PIN diodes, $\lambda/4$ line spacing, port match is ideal and lossless. In actuality, the sum total of the losses amounted to 1.3 dB and this added to the theoretical 3.0 dB loss amounted to 4.3 dB loss for the modulator. Actual test data, Figure 6, show the quadriphase performance to less than 2° from the desired quad phase. The unit was tested environmentally from -24° C through +71° C with the quad phase separation virtually unchanged. From the cold to the hot extreme, there was a counterclockwise displacement of ~3°, but all quad phase moved synchronously to maintain the original quadriphase performance.

Besides quadriphase performance, it was also required that the output magnitude of the QPSK modulator remain constant within a small tolerance of 0.3 dB. The reason for this requirement is that in the IGS system, the modulator output feeds a cascade of class C amplifiers. Class C amplifiers, depending on bias level, are extremely sensitive to AM/PM modulation. For minimum insertion phase shift, the class C stages are biased at saturation. Therefore, to maintain the system quadriphase performance, the amplitude variation is controlled to less than 0.3 dB variation between quad states.

Modification For Realization of Production Modulators

The concept of a quarter-wavelength shorted termination from a reference 0° point to achieve 180° phase shift is simple and straightforward. Yet in practice, when biased PIN diodes and blocking chip capacitors are used, the presumption of ideal shorts and lossless blocking does not hold true. Furthermore, tolerance on components contributes to phase differences beyond the accepted 3° tolerance per quad between units. If we can manipulate the quarter wave stub section by adding positive or negative susceptance, this problem is alleviated.

Figure 7a shows a $\lambda/4$ diode terminated stub, where the stub

[Continued on page 136]

has 50 ohm characteristic impedance. In an ideal case this stub will result in a 180° phase shift. However, in practice, due to diode parasitics and/or slight deviation in the short position, the actual phase shift may deviate from 180°. This phase discrepancy can be corrected by adjusting the physical length of the stub if possible. In microwave integrated circuits (MIC), the line is etched and therein lies the problem. However, there are ways to circumvent this problem. Two methods are described which can be used to adjust for phase deviation without actually changing the physical length of this stub.

Figure 7b illustrates the case where the phase deviation can be corrected by varying the impedance of a part of the stub. If the overall phase of the diode terminated stub is greater than 180°, the phase can be corrected by widening the line (i.e., lowering the impedance). On the other hand, if the phase of the diode terminated stub is less than 180°, it can be corrected by narrowing the line width. The amount of correction is restricted to small phase deviation, generally less than 10°, or else other complications, such as mismatch loss, become a factor.

Figure 7c illustrates this method in detail where a phase error of 6° is corrected by changing the impedance of the stub. That is, assume the diode terminated stub measured 186° because of parasitics.

The analysis is as follows. The normalized admittance of a lossless, short-circuited transmission line stub is

$y_{sc} = Y_{sc}/Y_o = -j \cot B1.$

where

Y_{sc} = unnormalized short circuit admittance

Y_o = characteristic admittance

$B = 2\pi/\lambda$

l = length of transmission line section.

In Figure 7b, let $y_{01} = .0222$ and $y_{02} = .02$ with l_1 and $l_2 = \lambda/8$ at 1.381 GHz. On the Smith Chart (admittance), starting at $y = j\infty$, the physical short postion, we traverse CW a distance of $\lambda/8$ to -j1.0. We next renormalize, -j1.0 x .0222/.02 = -j1.11, shown as Point A in figure 7c. Continuing CW for another $\lambda/8$, we reach point B (-j.05). The resultant phase shifts show 174° for these composite $\lambda/8$ sections. Next, add the 6° due to parasitics and we obtain the desired 180° phase shift.

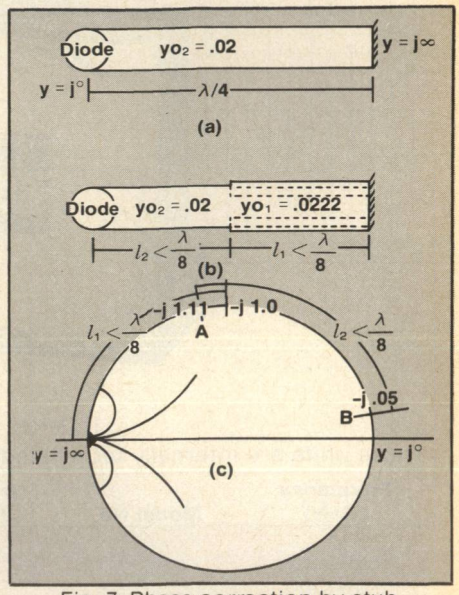

Fig. 7 Phase correction by stub impedance adjustment.

Another way to add small phase compensation is to use open circuit shunt stub. Small sections of islands are etched next to the pin diodes as shown in figure 8a. Assume that l_1 is slightly less than 180° and l_2 is required to compensate for the difference. That is,

$y_{comp} = y_{sc} + y_{oc}$

where

y_{comp} = normalized composite admittances of short circuit and open circuited stubs.

y_{sc} = normalized admittance of short-circuit stub

y_{oc} = j tan B1 = normalized admittance of open-circuit stub

Let $l_2 = \lambda/80$

Then $y_{oc} = j \tan \frac{2\pi}{\lambda} \cdot \frac{\lambda}{80} = j.078,$

Shown in Figure 8b on the Smith Chart, l_1 is less than $\lambda/4$ and l_2 is required to compensate for the difference.

Finally, as mentioned earlier, the magnitude balance between all quad states must be constant to within 0.3 dB at the output. To alleviate this problem we add a provision to selectively mismatch

[Continued on page 138]

[From page 136] **MODULATOR**

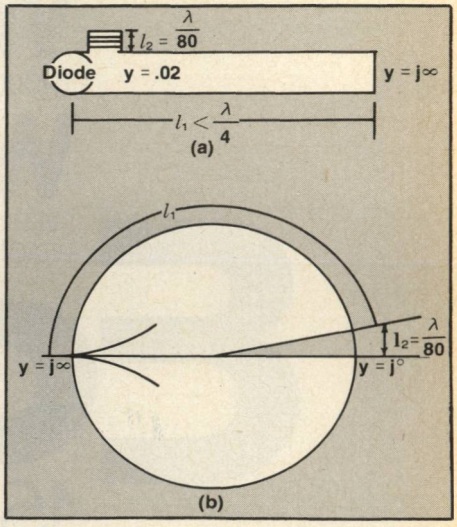

Fig. 8 Phase correction by open circuit shunt stub adjustment.

either of the resistively coupled ports of the Wilkinson power divider. Small islands to add capacitive susceptance are generally sufficient to balance the modulator output to within 0.3 dB for any of the quad states. Actual loss data shown in Figure 6 demonstrates that the magnitude balance achieved for the modulator was less than 0.25 dB.

Acknowledgements

The authors wish to acknowledge personnel of Department 743-030, Rockwell International, for the design, development and test of the modulator, particularly the contributions of D. Ball (Hughes), E. DesRoches (Hughes), D. Jayne, J. Stewart and K. Cooper in publishing this paper. Special thanks to M. Loper (Aerospace Corp.) for his suggestions and helpful discussions in clarifying vague points. This paper reports on a modulator activity of Contract FO4701-78-C-0153.

References

1. Wenzel, Robert J., "A Useful Hybrid Circuit," Lecture Notes, *Microwave Circuit Design* [*UCLA*], pp. 5-13, May 1981.
2. Wilkinson, E.J., "An N-Way Hybrid Power Divider," *T-MTT, v. 9, n. 1,* pp. 116-118, January 1960.
3. Film Microelectronics Inc., DD311 Ultra High Speed Multipurpose Diode Driver.
4. Smith, P.H., "Transmission Line Calculator" *Electronics,* January 1935. ■

Gunn Effect Devices Move Up in Frequency and Become More Versatile

F. B. Fank and J. D. Crowley
Varian Associates, Inc.
Santa Clara, CA

Introduction

For more than twelve years, the Gunn Effect Device (also called the Transferred Electron Device, (TED), has been serving as a useful device for oscillators of all types across the microwave spectrum. Most of the first broadband microwave solid state sweepers used YIG-tuned Gunn oscillators, and many present radar and communication systems use fixed-tuned Gunn oscillators for low noise, local oscillators. The majority of solid state parametric amplifier pumps were, and still are, Gunn Effect oscillators. Thus, Gunn Effect devices have been used in almost every microwave application where low noise, low and medium power performance characteristics are required.

The rapid development of the GaAs FET, as a device for microwave sources and amplifiers, has led to the use of the FET in place of the Gunn diode in many applications where its characteristics are suitable. Primary advantages of the FET over the Gunn devices are ease of characterization and circuit design obtainable with a three-terminal device, lower power drain (i.e., higher efficiency), and compatibility with microstrip circuits. With the present practical upper frequency limit of the GaAs FET at 26 GHz and intense development to push this practical limit higher, what can one say about the future of the Gunn Effect device?

First of all, in the microwave range below 30 GHz, the GaAs Gunn Effect device will continue to be used in oscillator applications where its low FM and AM noise characteristics are essential for system performance. Radars and many communication systems need high sensitivity and, therefore, require low noise local oscillators. However, except for some other special applications, the practical use of the GaAs Gunn device below 30 GHz will be limited to these low noise applications. It is at the frequencies above 30 GHz, where the millimeter-wave growth has spawned many new requirements, that the Gunn Effect device will become a major device in system components. To see more clearly where the Gunn Effect device will be used and its present and future capabilities at millimeter-waves, a discussion of GaAs and InP Gunn characteristics is helpful. This article will discuss the development of Gunn Effect devices above 30 GHz and some specific applications at millimeter-waves. Also, a forecast of where the Gunn device will ultimately be used is also given.

Comparison of GaAs and InP Gunn Characteristics

It is well known that both GaAs and InP materials with proper doping characteristics will exhibit the transferred electron effect. Thus, both GaAs and InP devices can be used in similar applications. However, InP has several properties sufficiently different from those of GaAs that allow its application to a wider group of products. Specifically, the major characteristics of InP relative to GaAs are:

- The transferred electron effect is calculated to be effective to about twice the frequency of GaAs.
- The efficiency of InP is about twice as high as that of GaAs.
- The noise measure of InP is approximately 6 dB lower than GaAs.
- The threshold field in InP is about three times that of GaAs.

Simply speaking, InP is best for high-frequency applications, i.e., millimeter waves, as both an oscillator and an amplifier. The efficiency curves of GaAs and InP versus frequency, shown in Figure 1, summarize the calculated oscillator characteristics. Experimental data to date are in good agreement with these curves.

The optimum noise measure of a practical InP Gunn diode can be expected to be less than 10 db

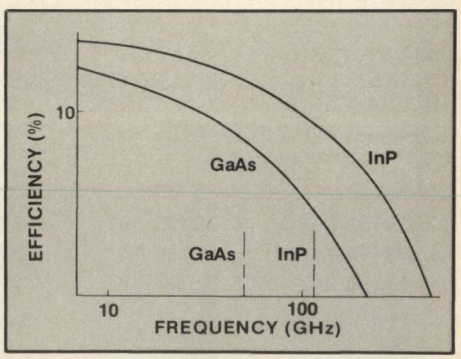

Fig. 1 Predicted transferred electron device efficiency vs frequency.

TABLE 1
RF PERFORMANCE OF FIXED FREQUENCY InP GUNN OSCILLATORS

DEVICE	FREQUENCY (GHz)	OUTPUT POWER (mW)	EFFICIENCY (%)
EE209	56.4	200	6.35
EE210	56.8	157	4.86
EE201	56.8	125	4.50
EE196	66.0	115	4.10

TABLE 2
RF PERFORMANCE OF FIXED FREQUENCY InP GUNN OSCILLATORS

CW InP GUNN DIODES

DEVICE	TYPE	F (GHz)	Po (mW)	η (%)
EE211-1	2L	89.5	125	3.27
EE198-380	2L	89.6	107	3.48
EE198-395	2L	90.1	100	2.80
EE198-380	2L	93.1	91	2.96
EE198-384	2L	93.15	79	2.81
EE198-382	2L	94.48	71	2.48
EE198-390	2L	94.8	68	2.5
EE198-392	2L	94.9	63	2.4
EE198-390	2L	100.5	44	1.52
EE196	2L	89.7	35	4.7

through 100 GHz, making the InP Gunn the only low noise amplifying device for all millimeter wave frequencies through 100 GHz. Because of this, significant emphasis of development work at millimeter-waves has been placed on InP materials, devices, and components in recent years.

Millimeter-wave Oscillators

The development of InP material for oscillator devices over the last several years has been primarily at 60 and 94 GHz. Work has continued on the development of the InP Gunn diode design to increase the efficiency and power output at these frequencies. The effect of the cathode on the "launching" of electrons into the active region has been shown to be the critical design factor in the operation of a Gunn Effect device. Design effort has been concentrating on reliable current limiting cathode contacts and "two-zone" cathodes for highest efficiencies. The best CW results of the development work at 60 GHz are shown in Table 1. The highest CW powers in the 50 to 60 GHz range are also still somewhat limited by thermal considerations as well as skin effect losses and these areas are under development to further increase the efficiency and power of these CW Gunn diodes. Present designs use a 40 μm substrate thickness which is well over the skin depth at both 60 GHz and 94 GHz. Final product designs will require the overall thickness to be 10 μm or less.

Oscillator-type circuits have been developed for both mechanical and electronic tuning at 60 GHz. Mechanical tuning of a CW oscillator is shown in Figure 2. Ten percent tuning bandwidths are achievable with reduced-height waveguide cavities. Electronic tuning of 60 GHz oscillators is achievable over nearly the same bandwidth, but the power output is considerably less due to the power absorbed in the varactor. Best varactor tuning results are shown in Figure 3. Also, work is being undertaken to increase the tuning bandwidth and the power level for a given electronic tuning bandwidth.

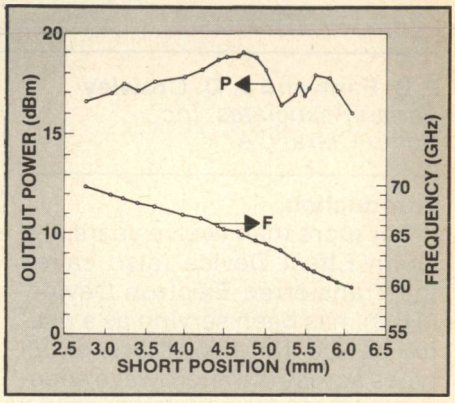

Fig. 2 Output power and frequency vs sliding short position for a mechanically-tuned InP Gunn oscillator.

The development of the InP Gunn diode for operation at 94 GHz has received considerable attention in the last several years and the summary of the best CW efforts of this work are shown in Tables 2 and 3. The highest CW power obtained to date is 125 mW with an efficiency of 3.27%. One of the most promising developments in this area has been the straightforward application of power combining techniques to achieve over a quarter-watt of CW power at 90 GHz as indicated in Table 3. The use of standard in-line half-wavelength spaced diodes allows combining efficiencies well above 90% in every case. The use of the InP Gunn diode in this manner creates a good medium power component which has low-noise properties as well as reasonable efficiencies and good lifetimes. Only a small effort has been devoted to achieving pulse powers at 94 GHz; however, the results to date are encouraging in that typical pulse powers

TABLE 3
RF PERFORMANCE OF 2 AND 4 DIODE COMBINING CIRCUITS

DIODES		F (GHz)	Po (mW)	η (%)	ηcomb (%)
EE198-397	EE198-401	89.55	170	2.89	93
EE198-397	EE198-401	90.25	150	2.7	82
EE198-207	EE198-213	91.8	97	1.6	106
EE271B-8 EE271B-31	EE271B-26 EE271B-24	90.6	260	1.6	92.85
EE268-22 EE268-6	EE268-26 EE268-15	90.8	230	1.4	106.5

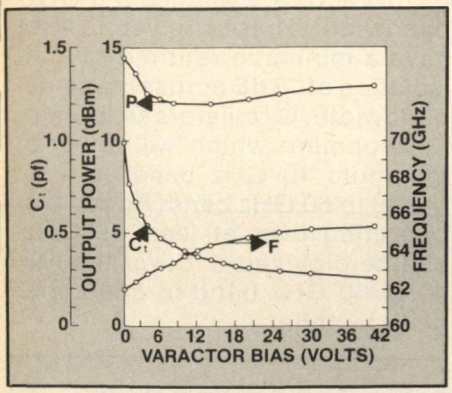

Fig. 3 Output power and frequency as a function of varactor bias voltage.

are 2 to 4 times the best available CW power per diode. Best pulse powers at 1% duty cycle with a 0.5 μsec pulse width are given in Table 4.

Millimeter Wave Low Noise and Medium Power Amplifiers

The initial effort in the development of InP Gunn diodes for amplifiers at millimeter waves was for low-noise applications. Specific designs were centered around the development of broad-band low-noise amplifiers for use above 26 GHz. A drop-in replacement for a low-noise traveling wave tube amplifier which operates over the entire 26.5 to 40 GHz frequency band has been developed using

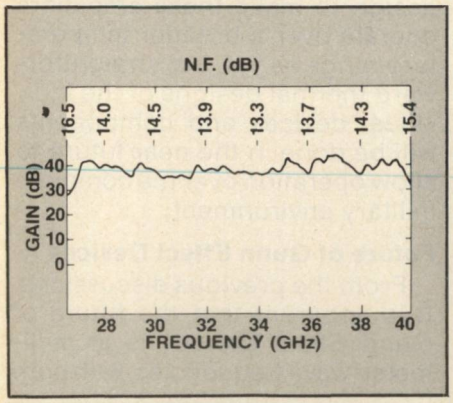

Fig. 4 Gain and noise figure of an all solid state amplifier replacement for a low-noise TWT.

InP Gunn diodes in all of the amplifier stages. This prototype TWT replacement was built as a demonstration of the capabilities of the InP Gunn diode with the results shown in Figure 4. The amplifier uses eight stages, with approximately 5 dB per stage, with each stage essentially covering the full bandwidth. The noise figures are also shown in Figure 4, and indicate that it is well within the 17 dB noise figure of the traveling wave tube. A program is now underway to reduce the overall noise figure to less than 10 dB.

The design of low-noise amplifiers using InP Gunn diodes was also extended to 60 GHz, with typical noise measures in the 9 to 12 dB range. A noise measure of 7.8 dB at 40 GHz is the best obtained to date with the n minus notch design. Characteristics of an amplifier which was developed to cover the 48 to 52 GHz band are shown in Figure 5. The typical noise figures were around 12 dB for this amplifier with an optimum noise figure of 10 dB at 50 GHz. A broad-band low-noise amplifier covering the complete 50 to 60 GHz band is now in the prototype

[Continued on page 146]

TABLE 4
InP DIODE RF EVALUATION
(BEST-TO-DATE, PULSED, 75-110 GHz)

DEVICE	FREQUENCY (GHz)	OUTPUT POWER (mW)	EFFICIENCY (%)
EE214	89.8	240	2.66
	92	215	
EE220	90	248	2.70
EE285	89.8	255	142
EE211	90.3	236	4.28
EE198	89.8	195	3.58
	93.7	155	3.25

TABLE 5
MEDIUM POWER AMPLIFIERS

OPERATING BANDWIDTH (GHz)	MINIMUM POWER OUTPUT (mW)	MINIMUM SS GAIN (dB)	NUMBER OF STAGES
27.0 to 35.0	100	20	3
33.5 to 36.5	200	25	3
42.0 to 46.0	100	30	3
54.0 to 58.0	100	25	3

stage. Work is continuing with the p notch design to further lower noise measures.

A number of amplifiers have been developed recently for medium-power applications requiring a minimum of 100 milliwatts of power output. These types of amplifiers are being used as the output transmitter of a short-range communications system or as a driver for a much higher power microwave tube. Some specific amplifiers which have been developed over the past year are described in Table 5, and their characteristics are shown in Figures 6, 7 and 8. A photograph of a 3-stage 60 GHz amplifier is shown in Figure 9. These amplifiers are similar in that they use standard reflection amplifier design with approximately 10 dB gain per stage. For the amplifiers in the 35 GHz range, GaAs diodes were used in the output stages. Higher power InP Gunn diodes will be developed for higher power output at these lower frequencies. In the design of these medium power amplifiers, flat profile InP Gunn diodes were used to furnish the highest power in the least number of stages. Even though specific low noise InP Gunn diodes were not used, the noise figures were typically in the 15 to 18 dB range. These types of low-noise figures were required for best system operation.

The development of amplifiers above 40 GHz for high gain and higher power operation has also required the development of circulators which has also been done at Varian. Circulators for operation up through 60 GHz have been developed with insertion loss of 0.3 dB across a minimum 6 GHz bandwidth. These circulators also have a minimum return loss and isolation of 15 dB across the same bandwidth. Circulators are now in development which will cover a minimum 10 GHz bandwidth in the 40 to 60 GHz band. Amplifiers operating over at least 10 GHz can be diplexed to cover the full 40 to 60 GHz band in one complete module.

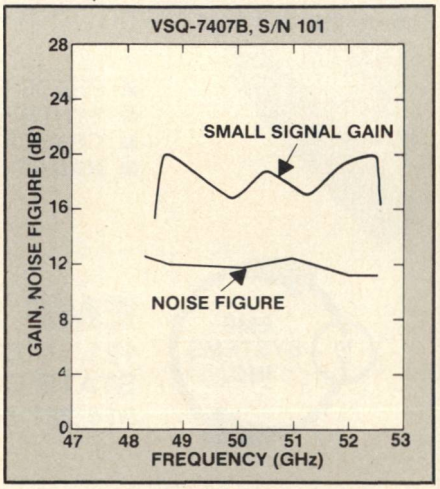

Fig. 5 Gain and noise figure of a two-stage InP Gunn amplifier with saturated power greater than 50 mW.

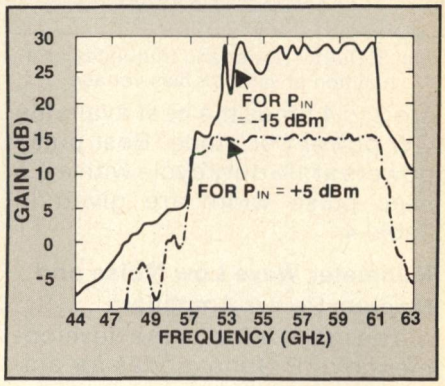

Fig. 6 Gain responses of three-stage amplifier at low and high drive levels.

These amplifiers are linear, up to the power level 10 dB below the "saturation" point, as shown by the transfer characteristics shown in Figure 8, and they are generally designed to operate over a temperature range of -10°C to +70°C. There has been no compensation design to make these amplifiers operate over a broader temperature range as yet, but straightforward thermal designs of the individual devices and components will be done in the near future to allow operation over the complete military environment.

Future of Gunn Effect Devices

From the previous discussions, it is apparent that the future of Gunn Effect devices is at millimeter-wave frequencies, with both

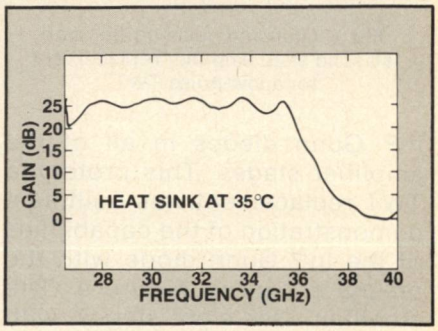

Fig. 7 Small-signal gain of a half band amplifier with saturated power greater than 100 mW.

oscillators and amplifiers being useful components. It is planned to develop the InP Gunn diodes and oscillators for low-noise, low-power applications up to 200 GHz. Power levels sufficient for local oscillator performance and for some short range radars should be possible with the InP Gunn diode over this frequency range. Peak pulse powers of one-half watt at 1% duty cycles up through 100 GHz should also be available with single diodes. Straightforward power combining techniques will increase both CW and pulse powers to at least four times typical single-diode values. Realistic values would probably be 300 mW of CW power and 1.0 watt of peak power in power-combined circuits at 100 GHz.

Perhaps the most popular usage of an InP Gunn diode is in low-noise and medium-power amplification. Low-noise amplifiers, with narrow and broadband performance, will be available to 100 GHz. Narrow-band noise measures less than 10 dB will be possible with the broad-band noise measure at less than 15 dB. The amplifier bandwidth will be limited primarily by circulator characteristics, but a 10 GHz bandwidth design should be available from 40 to 100 GHz.

Power levels of 100 mW will be typical of the broad-band medium power amplifiers and power levels of 0.25 W to 0.5 W may be available over bandwidths of a few percent. Although no pulsed amplifiers have been developed to date, power levels should be considerably higher than the CW power levels.

Below 30 GHz, Gunn effect devices have been used almost solely as oscillator devices, but above 30 GHz, the excellent low noise and broad-band properties of the InP diode have made the Gunn diode more versatile as an amplifier device as well as for oscillators. ■

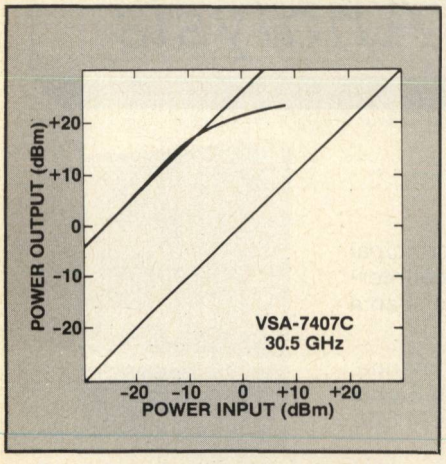

Fig. 8 Transfer characteristics of the three-stage half band amplifier.

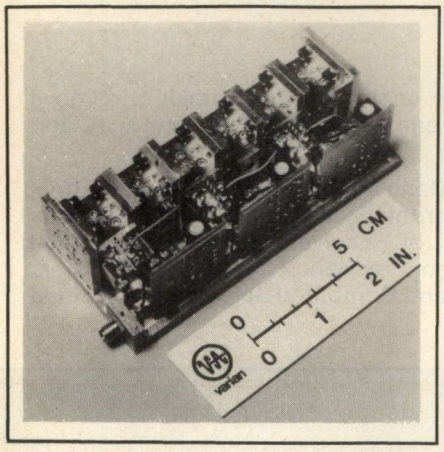

Fig. 9 V-band solid state amplifier.

Investigations on the Operating Modes of Millimetre Wave Gunn-Oscillators

Helmut Essen
Egon Wennerscheid

Introduction

After the mm-wave Gunn-oscillator had become a commercially available component including W-band (75-110 GHz) in recent years, a number of publications were dedicated to the explanation of the operating modes of this device[1-5]. While its operation at W-band frequencies was attributed to fundamental oscillations either in a hybrid mode or the quenched space charge mode in earlier publications[4,5], more recently the Gunn devices oscillating at W-band frequencies have been claimed to operate in a harmonic mode [1-3]

The experiments leading to this assumption up to now did not take advantage of electronic tuning of the Gunn-oscillator by means of the bias voltage with simultaneous observation of the spectral components of the output signal. They achieved the tuning strictly by mechanical means, possibly with a certain amount of load pulling.

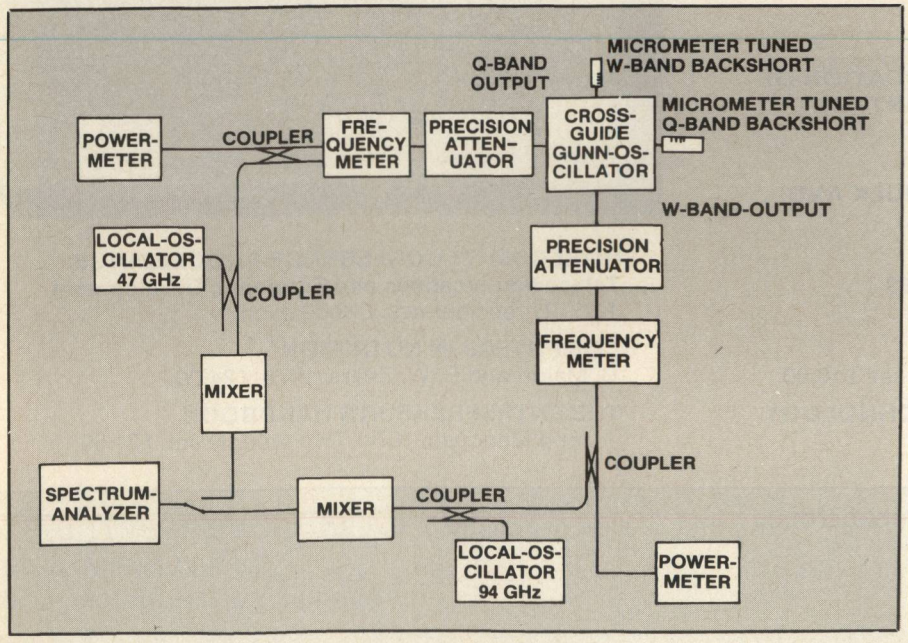

Fig. 1 Block-diagram of test set-up.

Experimental Set-Up

The test set-up, shown in Figure 1, tried to minimize the influence between the output channels during the tuning of the device. As shown in Figure 2, the device under test was mounted into a full height W-band waveguide with a tunable backshort. Above the diode-position, a crosswise Q-band waveguide including a tunable plunger was coupled to the diode by a circular hole with the bias-pin crossing both the Q-band and W-band waveguide. The Gunn-device was embedded into a disc-type resonator in a design employed usually[5,6]

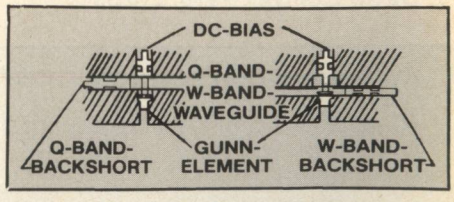

Fig. 2 Oscillator set-up.

PRINCIPLES OF ELECTROMAGNETIC COMPATIBILITY
Bernhard E. Keiser. 1979. £27.00

MICROWAVE TRANSMISSION LINE FILTERS
J. A. G. Malherbe. 1979. £21.50

ELECTRIC CHARACTERISTICS OF TRANSMISSION LINES
W. Hilberg. 1979. £24.00

UP TO 50% OFF OUR SELECTED BACKLIST!

25% OFF ON 2-4 TITLES

50% OFF ON 5 OR MORE TITLES

VARIABLE CAPACITANCE DIODES
Kenneth E. Mortenson. 1974. £18.00

ACTIVE FILTER DESIGN
Arthur B. Williams. 1975. £18.00

SPECTRUM ANALYZER THEORY AND APPLICATIONS
Morris Engelson and Fred Telewski. 1974. £18.00

MULTICONDUCTOR TRANSMISSION LINE ANALYSIS
Sidney Frankel. 1977. £18.00.

MICROWAVE DIODE CONTROL DEVICES
Robert V. Garver. 1976. £21.00

LASER APPLICATIONS
William Smith. 1970. £6.50

LOGARITHMIC VIDEO AMPLIFIERS
Richard Hughes. 1971. £7.50

DESIGN PERFORMANCE AND APPLICATION OF MICROWAVE SEMICONDUCTOR CONTROL COMPONENTS
K. E. Mortenson. 1972. £6.00

GALLIUM ARSENIDE MICROWAVE BULK AND TRANSIT TIME DEVICES
Lester Eastman. 1972. £13.00

AVALANCHE TRANSIT-TIME DEVICES
George Haddad. 1973. £9.00

FERRITE CONTROL COMPONENTS
Lawrence Whicker. 1974. Two volume set: £10.00

COMPOUND SEMICONDUCTOR TECHNOLOGY
David Colliver. 1976. £15.50

PHASED ARRAY ANTENNAS
A. Oliner and G. Knittel. 1972. £7.00

INFRARED-TO-MILLIMETER WAVELENGTH DETECTORS
Frank Arams. 1973. £6.00

SIGNIFICANT PHASED ARRAY PAPERS
R. C. Hansen. 1973. £7.00

RADAR SIGNAL SIMULATION
Richard Mitchell. 1976. £13.00

SYNTHETIC APERTURE RADAR
John Kovaly. 1976. £21.00

MTI RADARS
D. C. Schleher. 1978. £17.00

AUTOMATIC DETECTION AND RADAR DATA PROCESSING
D. C. Schleher. 1980. £31.50

RADAR DETECTION
J. B. DiFranco and W. C. Rubin. 1980. £27.00

PROBABILITY AND INFORMATION THEORY
P. M. Woodward. 1980. £12.00

THE COMPUTER BOOK
Fred Lee. 1978. £21.00

ADVANCED TECHNIQUES IN DATA COMMUNICATIONS
Ralph Glasgal. 1977. £18.00

MICROGRAPHICS HANDBOOK
Charles Smith. 1978. £21.00

TELEPHONE ORDER HOTLINE!

ORDER BY PHONE AND SAVE TIME!!!

CALL Jon at 01 - 222 - 0466 in our London Office.

Supply limited — available through Oct. 1, 1982.

INTELCOM '77 CONFERENCE PROCEEDINGS: Telecommunications and Economic Development
1977. Three volumes. £12.00 each

COMPUTERS IN NUTRITION
C. Maloff and R. W. Zears. 1979. £24.00

THE ENTREPRENEUR'S HANDBOOK
Joseph Mancuso. 1974. Two volume set: £21.50

In Western Europe, order Artech books from:

Please write all checks payable to Adtech in British currency.

ADTECH BOOK COMPANY, LTD.
25 Victoria Street
London, SW1H OEX, England

CIRCLE 107 ON READER SERVICE CARD

for W-band full height waveguide Gunn-Oscillators.

In both the Q-band and the W-band waveguides, the output-signals were down-converted and observed on a spectrum-analyzer used for precise IF-frequency-measurement.

From the IF-frequencies the oscillator's spectral outputs could be calculated from the known frequencies of the stable local oscillators. The use of broadband mixers allowed the observation of spectral components starting at the cut-off frequency of the Q-band waveguide at about 25 GHz to above 100 GHz at the W-band port.

Simultaneously, the output power in Q-band and W-band were monitored. The GaAs-Gunn-devices which were tested in the above set-up had active layer length of nominally 2.4 μm (vapour phase epitaxy)[7].

Experimental Results

In order to investigate the operating modes of the device, the oscillator was tuned electronically by variation of the applied bias voltage as well as mechanically by variation of the backshort-position in the Q-band or W-band waveguides. During the measurements it turned out that the operating mode of the device was strongly influenced by the position of the W-band plunger if it was in proximity of the resonator disc. This is due to the fact that the plunger acts as a tuning rod if it is sufficiently tight to the resonator disc.

In cases where the W-band backshort was sufficiently far away from the resonator disc, two spectral lines could be observed at the Q-band port, one at about 47.5 GHz and one at about 63.4 GHz. The corresponding spectral line at the W-band port was found at 94.0 GHz. The bias tuning characteristics of the observed spectral components were recorded simultaneously and are shown in Figure 3. It is apparent that in the case under consideration the tuning behavior of the 47.5 GHz and 94.0 GHz lines are practically identical while the gradient of the 63.4 GHz tuning curve differs considerably. Assuming harmonic operation of the device the relations $f_n = (n/m) \cdot f_m$ and $\Delta f_n = (n/m) \cdot \Delta f_m$ can be used for the determination of harmonic numbers. Under this supposition the harmonic number extracted from the Q-band and W-band spectral components is 1.5, indicating the 63.4 GHz line to be the first and the 94 GHz line to be the second harmonic of a 31.24 GHz oscillation. The first Q-band spectral line at 47 GHz observed simultaneously falls out of this scheme. Moreover a spectral component at 31.24 GHz could not be observed, though the set up was sufficiently broadband to allow observation of oscillations in this frequency region. This behavior makes the assumption of harmonic operation doubtful for the operation mode under consideration.

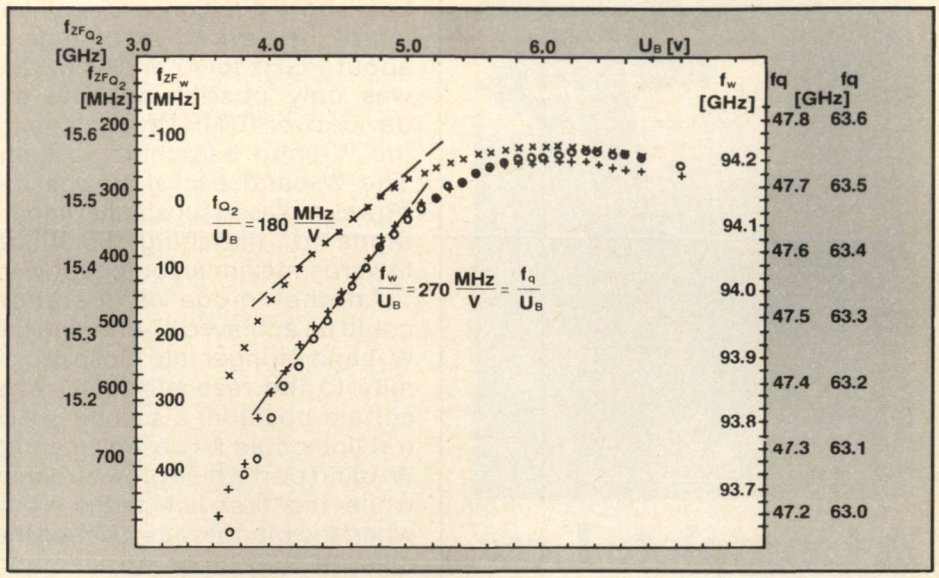

Fig. 3 Bias-tuning characteristic for the three spectral components near 47 GHz ($q_1 = t$), 64 GHz ($q_2 = x$) and 94 GHz ($w = 0$).

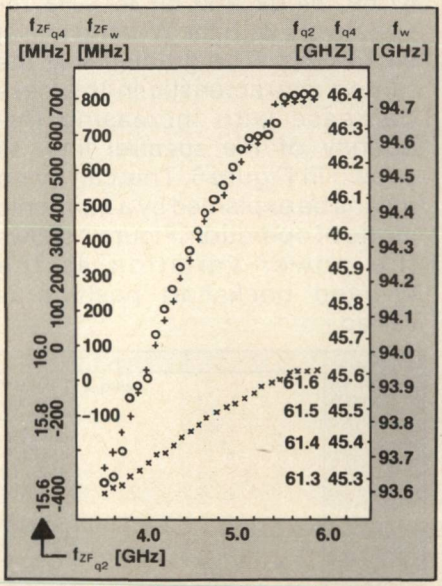

Fig. 4 Tuning by variation of the Q-band backshort position. Conditions otherwise unchanged compared to Fig. 3.

A similar behavior was observed during mechanical tuning of the device by variation of the position of the Q-band backshort under otherwise unchanged conditions. The 47.5 GHz and the 94 GHz line show the same gradient for the tuning characteristic while the gradient of the 63.4 GHz characteristic is smaller, leading again to a harmonic number of 1.5 between the 63.4 GHz and 94 GHz oscillation. Figure 4 shows the tuning characteristic for variation of the Q-band backshort-position; Figure 5, the output power when the short position is varied.

While variation of the Q-band

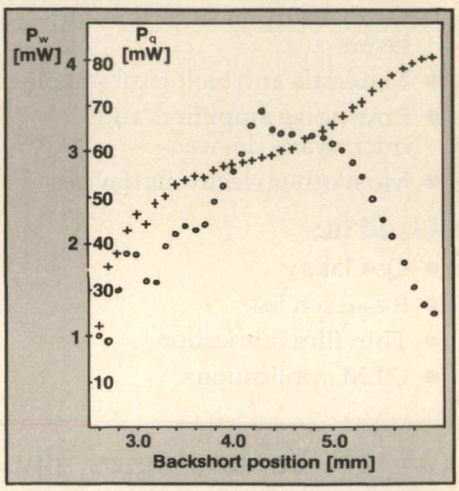

Fig. 5 Variation in output-power at Q-band and W-band and W-band port by changing at Q-band backshort position.

[Continued on page 152]

backshort position allowed tuning of the device over a range of about 1 GHz for 47 and 94 GHz, it was only possible to tune the device over 10 MHz by variation of the W-band backshort position. The W-band backshort-position however was of substantial importance for matching the diode towards maximum output power.

Another mode of operation could be achieved by bringing the W-band plunger into close proximity to the resonator disc. At a certain position, a second spectral line could be observed at the W-band port which grew stronger while the first line faded away when the plunger approached the disc. In that mode of operation three spectral components were observed at the Q-band port, at 47.69, 54.02 and 60.36 GHz respectively with the W-band line at 94.15 GHz. The gradients of the tuning characteristic in this case decrease with increasing frequency of the spectral line, as shown in Figure 6. This can by no means be explained by a harmonic mode of operation. Figure 7 shows the power variation as the W-band backshort position is varied.

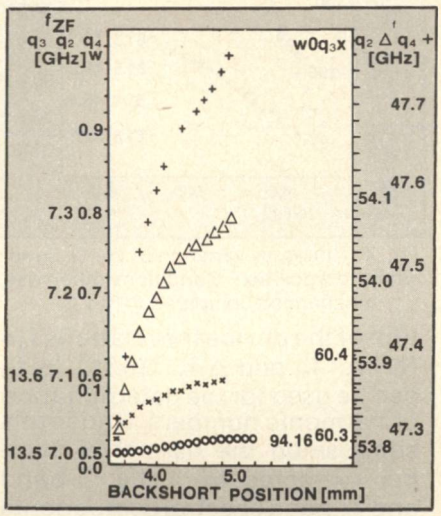

Fig. 6 Tuning characteristic of spectral components during variation of Q-band backshort position.

The results presented in this paper show that the W-band performance of Gunn devices can not alone be claimed to be based on harmonic operation, but other phenomena have also to be taken into account. As it was shown elsewhere, Gunn devices can deliver

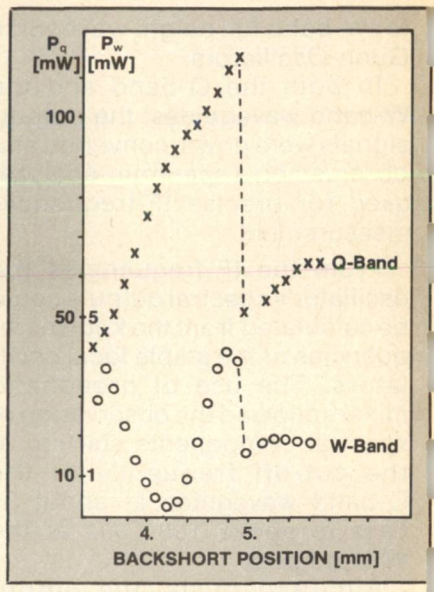

Fig. 7 Output power at Q-band and W-band parts during variation of W-band backshort position.

output power operating at harmonic modes, but in addition other operating modes which deliver substantial output power at W-band can appear when Gunn diodes originally designed for lower frequency operation are employed in W-band oscillators.

Acknowledgement

The authors wish to thank Dr. W. Haydl of the Institut für angewandte Festkörperphysik der Fraunhofergesellchaft, Freiburg, for his Gunn-diode support.

REFERENCES

1. Eddison, I.G., Brookbanks, D.M.: "Operating Modes of Millimetre Wave Transferred Electron Oscillators", *Electron. Lett.* 1981, 17, pp. 112-113
2. Haydl, W.H.: "Harmonic Operation of GaAs Millimetre Wave Transferred Electron Oscillators", *Electron. Lett.* 1981, 17, pp. 825-826
3. Barth, H.: "A Wideband Backshort-Tunable Second Harmonic W-Band Gunn-Oscillator", *MTT-1981 Symposium Digest*, pp. 334-337
4. Ruttan, T.G.: "Gunn Diode Oscillator at 95 GHz", *Electron. Lett. 1975*, 11, pp. 293-294
5. Ondria, J.: "Wide-band Mechanically Tunable and Dual In-Line Radial Mode W-Band (75-110 GHz) CW GaAs Gunn Diode Oscillators", 7th Biennial Conf. on active microwave semiconductor devices and circuits, Cornell University, Aug. 1979
6. Ondria, J.: "Wide-Band Mechanically Tunable W-Band CW Gunn Diode Oscillator", Agard Conference Proceedings No. 245 Millimeter and Submillimeter Wave propagation and Circuits, Reference Paper 12-1 thru 12-6, Munich, FRG, September 4-8, 1978
7. Gunn-Diodes fabricated by Institut fur angewandte Festkorperphysik der Fraunhofer Gesellschaft, Eckerstr. 4, D-7800 Freiburg, West Germany ■

Application Note

Simultaneous Transmission/Reflection Measurements Using the Hewlett-Packard 8410B*

D.E. Bradfield
Stable Energy Sources, Inc.
Lancaster, PA

Introduction

Network analyzer measurements play an important role in the characterization of microwave circuits, because they provide magnitude and phase information about a circuit at a particular frequency. The magnitude and phase information is derived by comparing two sources: the reflected wave and the transmitted wave. When a filter is characterized, it is advantageous to be able to monitor both the transmitted and the reflected waves simultaneously. A technique for monitoring both wavefronts in real time has been developed. This paper discusses this technique and a test system using the Hewlett-Packard microwave network analyzer (HP-8410B) and the transmission/reflection test unit (HP8743A).

Theory of Operation

The test system illustrated in Figure 1 consists of the HP-8410B network analyzer, the HP-8743A reflection/transmission test unit[1], and a sweep frequency generator. The sweep frequency generator output power is sampled by a 20-dB directional coupler. The sampled signal is the reference signal for the HP-8410B, and the other signal is applied to the unit under test (UUT). If the UUT does not have an input impedance equivalent to the system impedance (50 Ω), a reflected wave results. The signal at the output of the UUT is the transmitted wave. The operator selects the signal to be monitored from a switch on the front panel of the test set.

The technique for monitoring both the transmitted and the reflected waves is based on the ability to independently switch the two signals on and off. This operation can be accomplished by using two pulse modulators as shown in Figure 2. A 1-kHz clock signal is applied to a J-K flip-flop, which is connected so that the Q and $\overline{Q}$ outputs complement each time a clock pulse occurs. The Q output provides one modulator drive

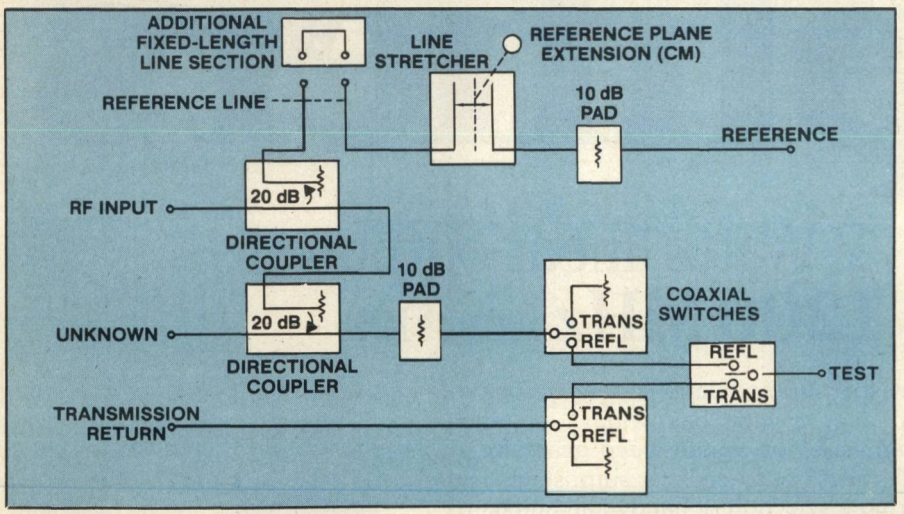

Fig. 1 Simplified RF schematic diagram of HP-8743A reflection/transmission test unit.

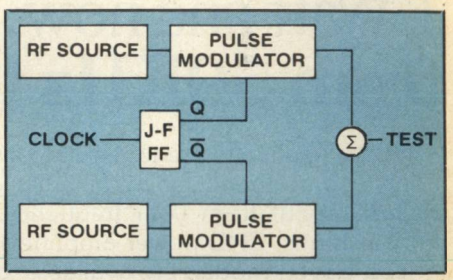

Fig. 2 RF switching circuit.

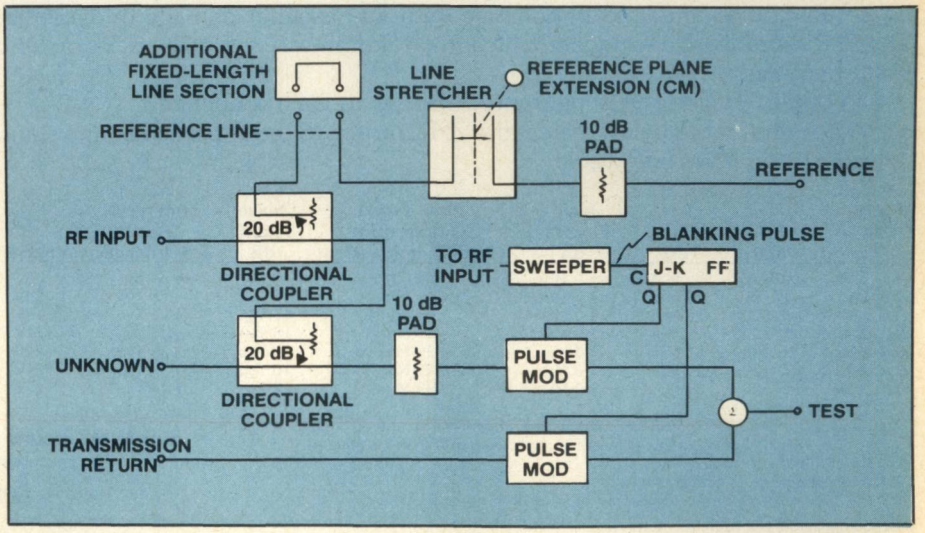

Fig. 3 Simplified RF schematic diagram of the modified network analyzer system.

*This paper is based upon work performed at COMSAT Laboratories under the sponsorship of the Communications Satellite Corporation.

signal while the $\overline{Q}$ output provides the other. Because the RF input to each modulator is from an independent radio frequency (RF) source, the output of each modulator is a time sample of that RF input. The summation of the two outputs results in a continuous waveform that contains an equal time sample of the two RF sources.

Figure 3 depicts the Hewlett-Packard measurement system using the technique described in the previous paragraph. The sweeper supplies a blanking pulse during the retrace, and this pulse is used to clock the flip-flop. Each time the pulse occurs, the outputs of the flip-flop complement. Because the RF input to the first modulator is the reflected wave, and the input to the second modulator is the transmitted wave, the summation of the two signals results in a time sample of the transmitted and reflected waves. The flip-flop is pulsed once each sweep; hence, the sample time of each wave is equivalent to the sweep time. Thus, the display alternates from reflection to transmission at the end of every odd number trace and from transmission to reflection at the end of every even number trace. If the sweep rate is high enough, the eye cannot detect the alternating pattern, and an effective simultaneous display of transmission and reflection information results.

Conclusion

A technique for an effective simultaneous real-time transmision/reflection measurement has been described that makes the tuning of filters easier because of its dual trace capability. This technique can be expanded to enable a greater number of traces. A pulse modulator must be added for each signal to be sampled, and the flip-flop must be replaced with a shift register having N bits, where N is the number of signals to be traced. As N increases, it may be advantageous to chop the signals rather than alternate them, because the sweep rate may not be high enough to prevent the eye from seeing each sweep of the sequential traces.

REFERENCE

1. Reflection-Transmission Test Unit, Operating and Service Manual, Hewlett-Packard Company, 1972. ■

Tunnel Diode Oscillators

Charles Blaine
Custom Components, Lebanon, NJ

The tunnel diode can be used as a microwave oscillator and can deliver output powers greater than 0.5mW up to frequencies as high as 30 GHz. Some tunnel diode oscillators have been operated at frequencies as high as 100 GHz.

Tunnel diode oscillators typically exhibit 20 to 30 dB lower noise than that achieved with either Gunn-effect or avalanche oscillators and they operate at high dc-to-R.F. efficiencies under low voltage (1.0 volts or less) dc power supply conditions. In addition, the GaAs tunnel diode oscillator has exhibited extremely long life at temperatures as high as 100°C and is particularly useful in those applications where *size, power drain,* and *long life* are *important.*

The equivalent circuit of a tunnel diode oscillator is shown in Figure 1.

In oscillator applications, the GaAs tunnel diode provides a voltage swing which is twice that available from germanium and produces four times the power output for a given negative resistance. The power output of a

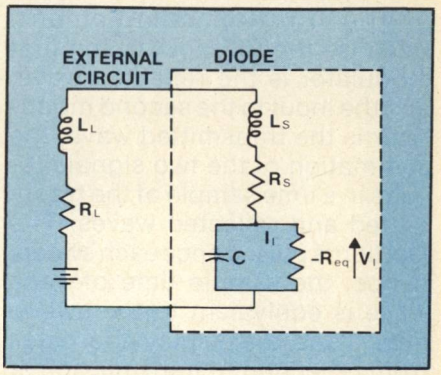

Fig. 1 Equivalent circuit of a tunnel diode oscillator.

GaAs tunnel diode oscillator is given by:

$$Po \approx 3/16\ (Ip - Iv) \bullet (Vv - Vp) \bullet \left(1 - \frac{fo^2}{fro^2}\right)$$

where: $f_{ro} = \frac{1}{2\pi\ |R_m|\ C_1} \bullet \left(\frac{R_m}{R_s} - 1\right)^{1/2}$ and

Rs = spreading resistance
Rm = minimum negative resistance
Cj = junction capacity
Vv = valley voltage
Vp = peak voltage

Power output versus frequency of typical tunnel diode oscillators is shown in Figure 2.

Because the tunnel diode exhibits a negative resistance, it is easily tuned over a broad range of frequency and generally has a linear frequency deviation versus temperature as indicated in Figure 3.

For extremely stable oscillator performance the tunnel diode is easily cavity-stabilized or can be clock locked to the harmonics of a low frequency crystal. Cavity stabilized oscillators at L band have exhibited a frequency stability better than 80 kHz over the temperature range from 20-100°C.

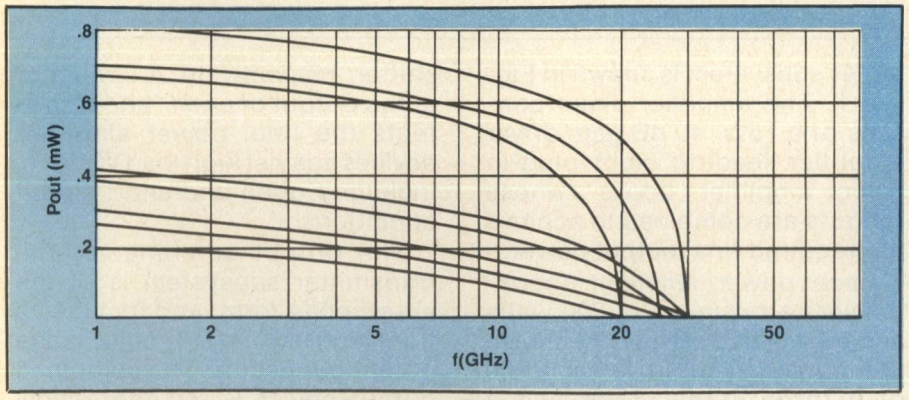

Fig. 2 Oscillator Output Power.

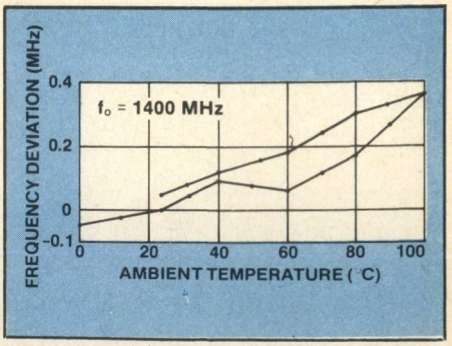

Fig. 3 Frequency deviation as a function of temperature for a GaAs tunnel-diode oscillator.

Main features of the tunnel diode oscillator are:

- low voltage operation
- low noise performance
- circuit simplicity
- immune to radiation exposure
- excellent frequency stability
- high dc-to-RF conversion efficiency
- capable of self oscillation from dc to 100 GHz
- operating temperature: -65° to 100°C ■

1kW Solid State L-Band Uplink Transmitter

M/A-COM MPD, Inc.
Hauppauge, NY

A fully solid state one kilowatt satellite uplink transmitter subsystem has been produced by M/A-Com Microwave Power Devices, Inc. Operating over the 1750-1850 MHz band, the mobile or fixed transmitter communicates to an orbiting satellite via frequency or phase-modulated signals. As part of the SGLS (Space Ground Link Systems) program, the transmitter subsystem can be used to control the satellite's propulsion system for orbital positioning, the transponder for data retrieval, and various other control functions.

The block diagram of the transmitter subsystem is shown in Figure 1. The amplifier chain consists of a 15W, 40 dB gain driver amplifier feeding eight plug-in power amplifier "books", whose outputs are combined to achieve the required final output power.

Each power amplifier "book" delivers a minimum of 200 watts and provides 23 dB gain. As shown in Figure 2, each "book" consists of a three stage driver and a balanced intermediate power amplifier module, followed by four balanced power amplifier modules operating in parallel. The four-way divider and combiner are isolated Wilkenson type couplers. The amplitude and phase of the output signal is adjustable by a regulator and an electronic phase shifter, respectively. A circulator at the output of each "book" protects the final power amplifier devices against high load VSWR's, including open and short circuit conditions.

The output combiner of the transmitter subsystem is of the air-stripline form, and includes a transition into a 1-5/8" coax flange output connector. The combined output power is fed thru a low pass filter for harmonic rejection, a dual directional coupler to monitor forward and reflected powers and, finally, a waveguide switch which selects the output load circuit, either the built-in dummy load or external antenna.

The loss from the PA "book" output to the main output of the

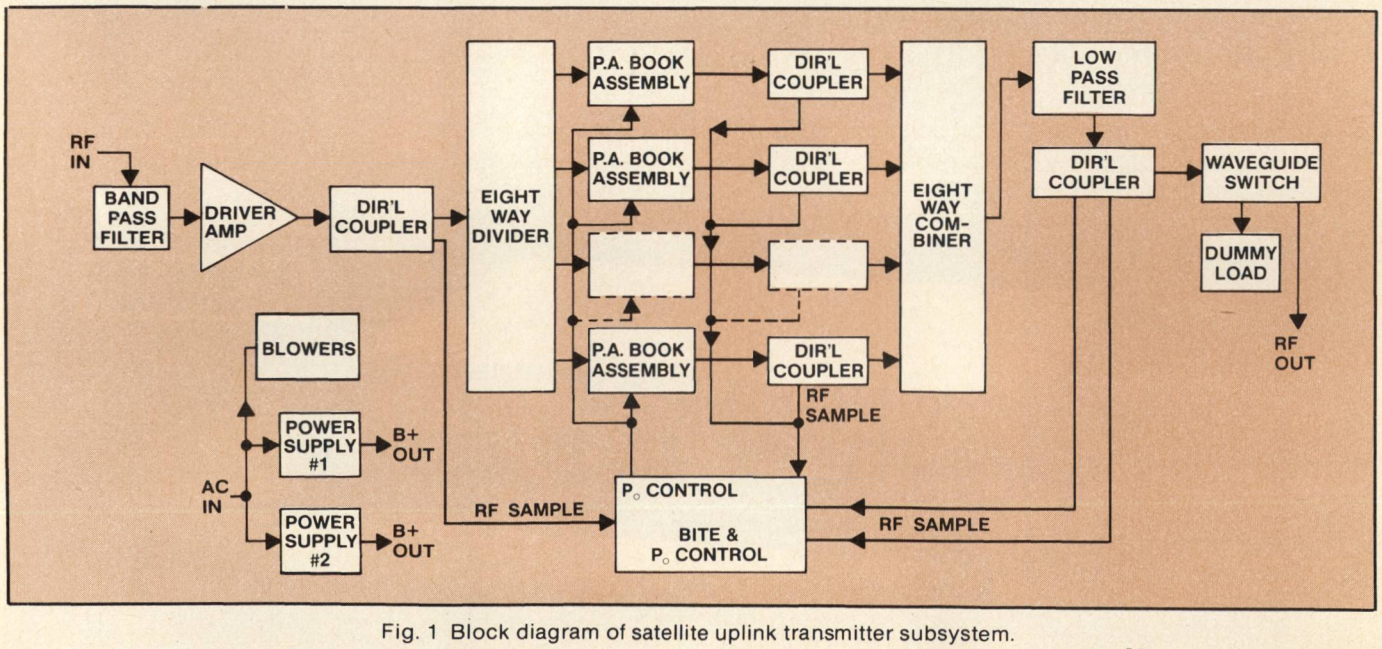

Fig. 1 Block diagram of satellite uplink transmitter subsystem.

[Continued on page 160]